AD-A032 407 LOCKHEED MISSILES AND SPACE CO INC PALO ALTO CALIF PA--ETC F/G 11/4
REINFORCEMENT MECHANISMS IN METAL-MATRIX COMPOSITES.(U)
JUL 74 R F KARLAK, F W CROSSMAN, J GRANT N62269-73-C-0576

UNCLASSIFIED LMSC-D403435 NL

1 OF 2
AD-A
032 407

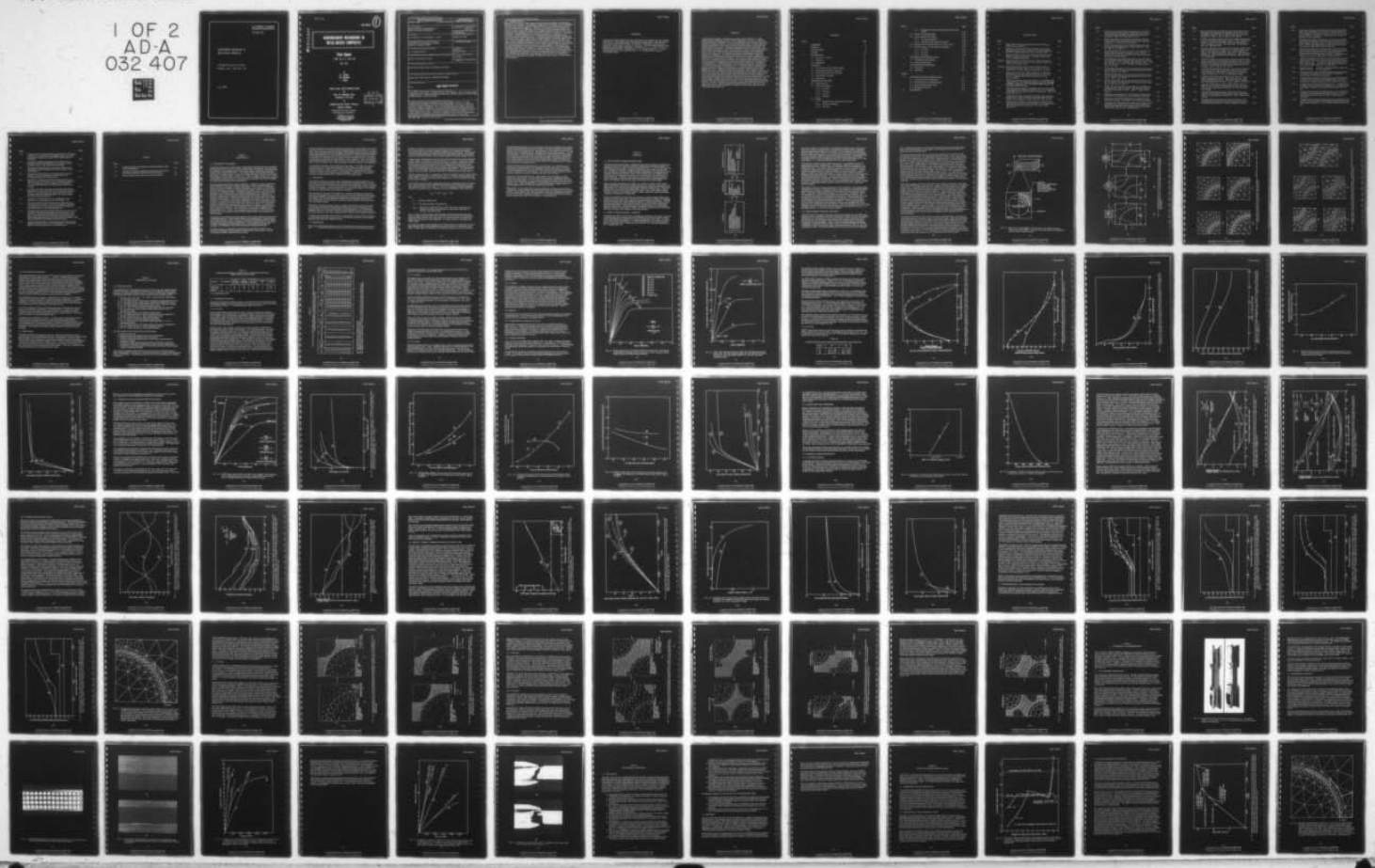

U.S. DEPARTMENT OF COMMERCE
National Technical Information Service

AD-A032 407

REINFORCEMENT MECHANISMS IN METAL-MATRIX COMPOSITES

LOCKHEED MISSILES AND SPACE COMPANY, INC., PALO ALTO, CA.

JULY 1974

334113

AD A032407

LMSC-D403435

REINFORCEMENT MECHANISMS IN METAL-MATRIX COMPOSITES

Final Report

1 JUNE 1973 to 1 JULY 1974

JULY 1974

by

R.F. KARLAK

F.W. CROSSMAN

J. GRANT

Prepared Under Contract N62269-73-C-0576

for

Naval Air Development Center

Department of the Navy

by

Lockheed Palo Alto Research Laboratory

Sunnyvale, California

APPROVED FOR PUBLIC RELEASE.
DISTRIBUTION UNLIMITED.

DDC
RECEIVED
NOV 20 1976
D

REPRODUCED BY
NATIONAL TECHNICAL
INFORMATION SERVICE
U. S. DEPARTMENT OF COMMERCE
SPRINGFIELD, VA. 22161

SECURITY CLASSIFICATION OF THIS PAGE *(When Data Entered)*

REPORT DOCUMENTATION PAGE		READ INSTRUCTIONS BEFORE COMPLETING FORM
1. REPORT NUMBER	2. GOVT ACCESSION NO.	3. RECIPIENT'S CATALOG NUMBER
4. TITLE *(and Subtitle)* REINFORCEMENT MECHANISMS IN METAL-MATRIX COMPOSITES		5. TYPE OF REPORT & PERIOD COVERED Final Report, 1 June 1973 to 1 July 1974 6. PERFORMING ORG. REPORT NUMBER LMSC-D403435
7. AUTHOR(s) R. F. Karlak, F. W. Crossman, J. Grant		8. CONTRACT OR GRANT NUMBER(s) N62269-73-C-0576
9. PERFORMING ORGANIZATION NAME AND ADDRESS Lockheed Palo Alto Research Laboratory Palo Alto, California 94304		10. PROGRAM ELEMENT, PROJECT, TASK AREA & WORK UNIT NUMBERS
11. CONTROLLING OFFICE NAME AND ADDRESS A. R. Fletcher (302P)		12. REPORT DATE July 1974 13. NUMBER OF PAGES 96
14. MONITORING AGENCY NAME & ADDRESS*(if different from Controlling Office)* Naval Air Development Center		15. SECURITY CLASS. *(of this report)* Unclassified 15a. DECLASSIFICATION/DOWNGRADING SCHEDULE

16. DISTRIBUTION STATEMENT *(of this Report)*

Approved for Public Release, Distribution Unlimited

17. DISTRIBUTION STATEMENT *(of the abstract entered in Block 20, if different from Report)*

Approved for Public Release, Distribution Unlimited

18. SUPPLEMENTARY NOTES

None

PRICES SUBJECT TO CHANGE

19. KEY WORDS *(Continue on reverse side if necessary and identify by block number)*

Composites, metal-matrix, interface stresses, local stresses, micro mechanics, finite element analysis, transverse mechanical properties, yielding, plastic flow, deformation, residual stresses, thermal stresses.

20. ABSTRACT *(Continue on reverse side if necessary and identify by block number)*

A finite-element program, developed in part under contract N00019-71-C-0289 "Reinforcement Mechanisms in Metal-Matrix Composites," for the U.S. Naval Air Systems Command, Washington, D.C., was modified and used to analyze the macro- and micro-mechanical behavior of several unidirectional boron-aluminum (6061-T6) composites subject to plane-strain transverse-normal tension in the elastic and plastic plastic ranges of the matrix. Mechanical properties were found to depend on: the reinforcement concentration, the packing arrangement of the circular reinforcements, the direction of the applied transverse-normal stress relative to the packing

DD FORM 1 JAN 73 1473 EDITION OF 1 NOV 65 IS OBSOLETE

SECURITY CLASSIFICATION OF THIS PAGE *(When Data Entered)*

20. ABSTRACT (Cont.)
symmetry, the extent of reinforcement-matrix interface debonding, and the thermal history of the composite. Two packing arrangements were studied – square and hexagonal; the applied tensile stress was parallel to lines of nearest neighbors or parallel to lines of next-nearest neighbors. The effect of reinforcement concentrations from 20 to 70 volume percent was analyzed for the square arrays stressed parallel to the lines of nearest neighbors; for that array stressed parallel to the lines of next-nearest neighbors, concentrations from 30 to 60 volume percent were considered. The hexagonal array, stressed parallel to both directions separately, was analyzed for the 50-volume percent concentration only. Progressive interface debonding was analyzed for the 30-volume percent square array stressed parallel to the nearest neighbor direction. Residual stresses induced during a -250°F change to room temperature, and their effect on subsequent transverse normal loading, were analyzed for a 50-volume percent reinforcement concentration in the two square-packing cases and for the hexagonal packing stressed parallel to the lines of nearest neighbors. Macromechanical properties included the determination of stress-strain curves into the plastic range, including elastic modulus, transverse-transverse Poisson ratio, and yield strength; the micromechanical analysis was used to determine interface-normal stresses, interface-tangential shear-stresses, local stress concentration factors, and plastic zone growth. Specially prepared tungsten-aluminum (6061-T6 and -0), unidirectional, square-array composites were tested in transverse-normal tension to verify theoretical predictions.

FOREWORD

This report is a description of the work performed at the Lockheed Palo Alto Research Laboratory on "Basic Reinforcement Mechanisms in Metal Matrix Composite" for the U.S. Naval Air Development Center, Warminster, Pennsylvania, under Contract N62269-73-C-0576, from 1 June 1973 to 1 July 1974. The work was performed in the Metallurgy and Composites organization, managed by Dr. T. E. Tietz, with Mr. R. F. Karlak the program leader, assisted by Dr. F. W. Crossman and Mr. J. J. Grant. The technical project was monitored by Mr. A. R. Fletcher (302A), Naval Air Development Center.

ABSTRACT

A finite-element program, developed in part under contract N00019-71-C-0289 "Reinforcement Mechanisms in Metal-Matrix Composites," for the U.S. Naval Air Systems Command, Washington, D.C., was modified and used to analyze the macro- and micro-mechanical behavior of several unidirectional boron-aluminum (6061-T6) composites subjected to plane-strain transverse-normal tension in the elastic and plastic ranges of the matrix. Mechanical properties were found to depend on: the reinforcement concentration, the packing arrangement of the circular reinforcements, the direction of the applied transverse-normal stress relative to the packing symmetry, the extent of reinforcement-matrix interface debonding, and the thermal history of the composite. Two packing arrangements were studied – square and hexagonal; the applied tensile stress was parallel to lines of nearest neighbors or parallel to lines of next-nearest neighbors. The effect of reinforcement concentrations from 20 to 70 volume percent was analyzed for the square arrays stressed parallel to the lines of nearest neighbors; for that array stressed parallel to the lines of next-nearest neighbors, concentrations from 30 to 60 volume percent were considered. The hexagonal array, stressed parallel to both directions separately, was analyzed for the 50 volume percent concentration only. Progressive interface debonding was analyzed for the 30-volume percent square array stressed parallel to the nearest neighbor direction. Residual stresses induced during a -250° F change to room temperature, and their effect on subsequent transverse normal loading, were analyzed for a 50-volume percent reinforcement concentration in the two square-packing cases and for the hexagonal packing stressed parallel to the lines of nearest neighbors. Macromechanical properties included the determination of stress-strain curves into the plastic range, including elastic modulus, transverse-transverse Poisson ratio, and yield strength; the micromechanical analysis was used to determine interface-normal stresses, interface-tangential shear-stresses, local stress concentration factors, and plastic zone growth. Specially prepared tungsten-aluminum (6061-T6 and -0), unidirectional, square-array composites were tested in transverse-normal tension to verify theoretical predictions.

CONTENTS

ILLUSTRATIONS

TABLES

Section 1
INTRODUCTION

1.1 STATEMENT OF PROBLEM

Advanced composites are a unique class of materials of particular interest to aerospace engineering by virtue of their low density, high stiffness, and strength, and because they are amenable to custom design that can provide an optimal combination of the component properties for specific requirements. The reinforcement, whether boron filaments, beryllium rods, graphite fibers, or any of a variety of glasses, contribute high strength and stiffness, while the matrix, whether it is a metal, an organic polymer, or in certain cases graphite or some other form of carbon, serves to transfer the load to the reinforcements and maintain their spacing, while imparting the necessary compressive strength by restricting the buckling of the reinforcement.

Mechanical properties of metal-matrix composites, in addition to being a combination of the constituents' properties, depend on the latter's relative chemical affinity (or tendency to react chemically) at elevated temperatures, on the relative coefficients of thermal expansivity, on the concentration of reinforcement, and for each case on the direction of the applied stresses. The applied stress directions for which the various parameters most strongly affect the mechanical properties is the transverse-normal direction, the direction normal to the parallel reinforcement axes. Although it is possible to design certain composite structural members such that loads are directed along the reinforcements, in most cases extraneous service loads may occur in other directions. Furthermore, the optimum arrangement may contain cross-plies, some of which will be stressed normal to the reinforcement. For a 50 volume percent boron-aluminum composite, 50 vol % B/Al (6061-T6), the onset of plastic flow in the matrix occurs at a transverse-normal tensile strain of about 0.15 percent, or at about one-fourth the strain-to-failure of the reinforcement if it has a typical strength of 400 ksi and a modulus of 60×10^6 psi. Thus, the matrix will be subject to plastic strains during service even if a factor of 2 is assigned to the structure, in which case a substantial portion of the matrix ($\sim 40\%$) will have yielded and thus may be subjected to service fatigue.

The quality of the reinforcement matrix interface will clearly influence the transverse composite properties. Some chemical affinity of the constituents is essential to produce a second interfacial bond. However, excessive chemical interaction can degrade the interface strength if excessive quantities of a weak compound form, if any of the interfaces separate because the products have a lower specific volume than the reactants, or if diffusion occurs with the formation of Kirkendahl porosity.

For these reasons it is essential to understand the mechanisms of failure in unidirectional composites under transverse normal tension, and how they are related to the various possible conditions that may obtain.

During a preceding study entitled "Reinforcing Mechanisms in Metal-Matrix Composites" performed for the U.S. Naval Air Systems Command under contract N00019-71-C-0289 (Ref. 1) the finite element method was used to theoretically analyze the micro- and macro-stress-strain behavior of 50 vol % B/Al(6061) and Be/Ti (6 Al-4V) unidirectional square-array composites stressed in transverse normal tension. Interface failure, caused by normal stresses at the interface, was found to occur catastrophically once such failure was initiated, in essentially the same manner for each composite. Also, the predicted ultimate strengths and strains, based on failure of the matrix where the local octahedral shear stress is greatest, were considerably higher than those reported in the literature.

A continuation of previous work is presented in this report. It includes the results of analyzing many more cases than previously with the computer program modified to increase efficiency, to improve the predictions of failure, and to provide a better analysis of residual thermal stresses. The specific cases analyzed include variations of volume fraction, reinforcement packing arrangement, and direction of the applied transverse-normal stress relative to directions in the packing array.

1.2 OBJECTIVES

The general objective of this study was to investigate the strength-limiting factors in metal-matrix composites related to fiber-matrix interface characteristics, the cross-sectional shape of the reinforcements and their packing arrangement, and the constituent mechanical properties. To achieve this objective, an available finite element computer program was refined to improve predictions of the mechanical behavior, and to expand the range of composite types and loadings to be analyzed.

More specifically, the goal of the program was to analyze the influence of reinforcement packing arrangement and the volume concentration of the reinforcements on gross mechanical properties of unidirectional composites, the distribution of stresses within the composite, the way they influence the plastic flow of the ductile matrix as well as the distribution of normal stresses at the fiber-matrix interface, and the way these can in turn lead to failure.

Refinement of the finite element computer program consisted of improving the quality of the results after detailed examination of predictions on the basis of their reasonableness and by introducing suitable additions and modifications. The modifications included activation of a program to analyze residual thermal stresses induced during fabrication and/or service, and to determine their influence in the composite properties.

To obtain some verification of the validity or applicability of the theoretical predictions, an experimental-precision composite was to be fabricated and tested, and the results analyzed in the light of the computer results.

1.3 BACKGROUND

Some of the fundamental background work for this program has already been described (Ref. 1). Several additional pertinent articles and reports have subsequently been

published or discovered, and these are briefly reviewed below to show the relevance of the present work to the areas of general interest in the composites community, and to provide the reader with references to additional related material. The research reviewed includes experimental measurements of mechanical properties to theoretical analyses of stresses and plastic flow, and determination of thermal residual stresses.

A large amount of mechanical test data on boron-aluminum and boron (Borsic)-titanium by Toth, Menke, and Scheirer can be found in Refs. 2, 3, and 4. Transverse-normal tensile moduli, ultimate tensile strength, and strains-to-failure measured for several volume fractions of reinforcement are used for comparison with the present work. The ultimate strengths and strains are not valid for theoretical comparison since they usually occurred prematurely because of diametral fiber fracture. For unidirectional (UD) 50 vol % B/Al (6061), elastic modulus values ranged from 15.4×10^6 to 18.3×10^6 psi in one report (Ref. 3) to 22.9×10^6 psi in a work about 2 years latter (Ref. 4).

Swanson and Hancock (Ref. 5) measured the Uniaxial Transverse-Normal Tensile (UTNT) elastic modulus for UD 30 vol % B/Al (7075) to be 11.5×10^6 psi, while Alexander and Carlson (Ref. 6) measured the TNT elastic modulus of 50 vol % B/Al (2024) in the range of 20.5 to 21.9×10^6 psi.

A very useful rule-of-mixtures relationship relating the longitudinal transverse Poisson ratio of UD composites to the constitutent Poisson ratios was developed and verified experimentally by Allred et al. (Ref. 7). For a UD composite stressed longitudinally in tension, the negative ratio of transverse-normal to longitudinal strain is given by

$$\nu_{TL} = \nu_f V_f + \nu_{mp} (1 - V_f)$$

where

ν_f = the fiber Poisson ratio

V_f = the volume fraction of reinforcement

ν_{mp} = the elastic or plastic Poisson's ratio of the matrix, depending upon whether or not the matrix undergoes stresses only elastically or entirely in the plastic range

Lin et al. (Ref. 8) used the finite element method to analyze the plastic flow of the matrix in square array (S) UD 50 vol % B/Al (6061-T6) composites under longitudinal tension and observed that, after initial yield, a 1-percent increase in applied stress caused the entire matrix to flow plastically. No report, however, was made of the Poisson effect.

Two separate studies of crack propagation in UTNT stressed UD composites have been made using the finite element method with appropriate routines to account for local failure. Adams (Ref. 9) composed a finite element program in which crack initiation

and subsequent propagation occur as the result of the local octahedral shear stresses. Using an incremental loading, iterative scheme, whereby the properties of any finite element to fail are suitably altered when necessary, it was possible to show that true failure occurs macroscopically, as evidenced by the stress-strain behavior, in a predictable fashion. Buyukozturk (Ref. 10) performed a similar finite element analysis for a composite masonry structure in transverse-normal compression, and showed remarkable agreement between the theoretical predictions and experimental observation. Unlike Adams, Buyukozturk used the Coulomb-Mohr criterion for failure as the material tested was very weak in tension and failed in compression as a combination of cohesive and frictional stress.

Analytical mathematical expressions have been derived by Yu and Sendickyj for interacting circular inclusions in an homogeneous elastic matrix (Refs. 11 and 12). The ultimate equations are in series form that can be solved numerically to obtain interface tangential and normal stresses. For a specific case the magnitude of these stresses in general is inversely related to the fiber volume fraction.

Dvorak et al. has analyzed the initial yield surface for UD composites in biaxial transverse-normal tension, using the finite element method, including the effect of temperature changes (Ref. 13). For hexagonal packing of circular fibers, the initial uniaxial yield is essentially independent of the applied stress direction relative to the packing. Also, matrix yielding that occurred for temperature changes of only 72°F caused yielding in 30 vol % B/Al with a matrix yield of 10 ksi.

Hoffman (Ref. 14) also analyzed the effect of temperature changes on the stresses in composites by an approximate shear-lag method by which the constituents are assumed to have the same Poisson ratio, and the stresses within each constituent are uniform. From an approximate elastic-plastic analysis, it is concluded that strains under temperature excursions to 2000°F are sufficient to cause plastic flow.

Section 2
APPROACH

2.1 USE OF FINITE ELEMENT METHOD (FEM)

The finite element method (FEM) is undoubtedly the most practical and versatile from among the theoretical techniques available for analyzing the mechanical behavior of composites on both the macro- and micromechanical scales. As in any numerical solution, including the evaluation of analytical relationships expressible in series form only, the degree of precision possible depends on the quantity of calculation performed to achieve adequate convergence. Thus, a series solution may be truncated at any arbitrary term if retention of additional terms is determined to not influence the results significantly. Similarly, the fineness of a finite element grid can be made as large (or small) as necessary to give the required precision, or interpolation functions can be assigned with whatever degree will produce the desired results.

There are specific advantages to the FEM – for example, the ease by which elastoplastic deformations and thermal residual stresses can be included to give gross composite properties as well as quasi-continuously following changes in local deformations and stresses, for virtually any possible applied loadings or displacements. Several examples are summarized in the introduction section. Also, once a basic program has been composed, it is possible to perform easily a parametric study that includes virtually any combination of constituents.

Figure 2-1 summarizes some of the major features of a finite element program such as that used in the present work. That is not to imply that this program is completely general and that any case can be analyzed simply by altering a few numbers. Although this type of program has obvious desirable qualities, it would require extensive computer storage and such a large amount of time to compile that its use would require extensive justification. The actual program developed for this work is sufficiently general to permit a large number of cases to be studied requiring at most a new Finite Element Grid (FEG), and changing of material properties.

2.2 FINITE ELEMENT METHOD – SUMMARY

A complete description of the FEM is too lengthy for inclusion in this report. However, a brief account of the principles involved is presented to provide the reader with sufficient understanding to appreciate the range of applicability of the method, as well as some of its virtues and limitations. A complete development of the subject has been made by Zienkiewicz (Ref. 15) and Desai and Abel (Ref. 16), and a good summary by W. C. Paulsen (Ref. 17).

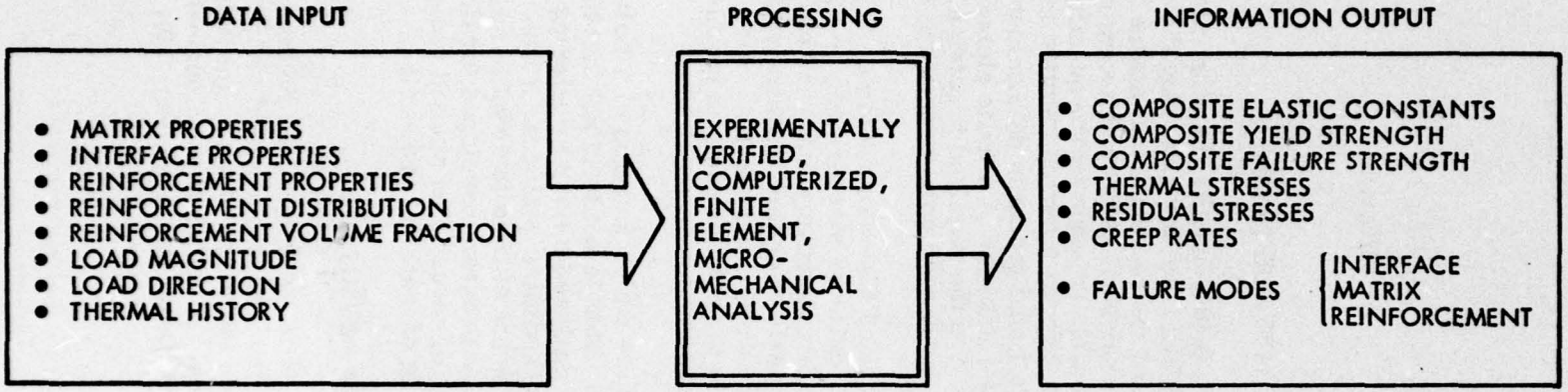

Fig. 2-1 Finite Element Analysis of Reinforcement Mechanisms in Metal-Matrix Composites

As its name implies, the FEM differs from traditional methods to the extent that the object to be analyzed is regarded as an assemblage of discrete (finite), contiguous, interconnected elements instead of a continuum. It is convenient to consider plane-strain (or plane-stress) cases to limit the calculations to essentially two dimensions, thereby reducing the complexity of the program and calculations. This approximation is in fact a realistic model for plastic flow in transversely loaded unidirectional composites since the rigid reinforcement effectively limits deformations to the transverse plane, i.e., in the plane perpendicular to the reinforcement axes.

The model for a unidirectional composite consists of a representative portion of a cross section normal to the fiber axes. This portion, called the repeating cell, is subdivided into an FEG, usually composed of triangles with common boundaries and corners call nodes. The FEG is superimposed over a coordinate system to permit a systematic identification of the nodes eventually used in the calculation. Progress toward a solution is made by using basic stress and strain equations to compute displacements in each element produced by a simple system of forces from neighboring elements acting through the nodes. The nodal displacements result in strain taken to be constant within each element, and these directly determine stresses through the mechanical properties of each element. Since the elements are all interconnected (as a system of springs), strains develop in each element until forces balance through a number of simultaneous equations easily solvable in matrix form on high-speed digital computers.

The method conforms to a strict requirement of solid mechanics – strain compatibility. Displacements of interior and boundary points of each element are determined through equations in the coordinate variables to ensure continuity between adjacent element sides. When linear interpolation functions are used as here, this approach imposes an approximation in that no strain gradients can exist within any element. The error thereby introduced can be made arbitrarily small by choosing sufficiently small elements in regions where steep gradients are anticipated. As the element sizes are decreased, the mechanical properties calculated by FEM do in fact converge to those calculated using closed-form continuum methods. A second approximation lies in the linear boundaries of the elements as this requires modeling real curved boundaries by connected straight-line segments. Again, the resulting error can be made negligibly small by increasing the number of segments representing the curve, i.e., decreasing the element size on the curved boundary.

2.3 FINITE ELEMENT MODELING AND GRIDS

The distribution of filaments in practical unidirectional composites is not sufficiently uniform to permit application of the FEM to composites directly since the large number of filaments in a representative region and the limited capacity of computers would preclude the use of a finite element grid (FEG) of the fineness needed to properly take account of stress gradients. This is avoided by considering the composites as consisting of an idealized uniformly spaced array of filaments imbedded in a matrix, so that only a small representative region, bounded by symmetry lines, is used as the computational model. Two such distributions are the square array and the hexagonal

array. Adams and Tsai (Ref. 18) showed that the square array provides better agreement with measured values than the hexagonal array though it may be necessary to employ the latter in specific cases.

The idealized doubly periodic square array and the repeating cell on which the FEG is formed are shown in Fig. 2-2. Symmetry about the X and Y axes of the repeating unit allows the calculations to be made in the first quadrant which is the repeating cell. Because of the relatively high stiffness of the composite parallel to the fiber direction, the Poisson strains in that direction induced by transverse stresses are expected to be small, and a state of plane-strain can be reasonably assumed to simplify the calculations and to predict plastic behavior. The effects of this restriction are considered in the discussion. It is clear that a slight overestimation of the transverse composite modulus and transverse-transverse Poisson ratio will result. However, correct values can be calculated from the computed results. The FEG is formed by subdividing the repeating cell into triangular elements such as shown in Fig. 2-2. The number of elements used and their sizes are determined by the minimum required for convergence of the calculated properties or by the nature of the analysis; smaller elements are used if microstresses are desired in regions of steep gradients or in small regions where materials with distinct properties exist, such as a thin interfacial layer of intermetallic compound.

Three basic repeating cells were used in this work to analyze the behavior under plane-strain (PS) UTNT of square-array (S) and hexagonal-array (H) composites, as designated in this report. These have been referred to elsewhere as special cases of rectangular packing, but the terminology used here is preferred as it is in keeping with crystallographic convention familiar to materials engineers. The repeating cells for these arrangements are shown schematically in Fig. 2-3, together with their relationship to the unidirectional packing of the circular reinforcements. The simple-square array (S1) is related to the diagonal-square array (S2) in that the packing of the filaments is the same but the direction of the applied stress is rotated 45 deg, so that instead of being parallel (or perpendicular) to the lines connected to the first neighbor centers, as in S1, it is parallel (or perpendicular) to the lines connecting the centers of next-nearest neighbors. Similarly, the array and loading directions studied can be defined for the hexagonal packing. As shown in Fig. 2-3, the load is applied parallel to the lines joining the centers of nearest neighbors to give what will be designated as the H1 arrangement. When the applied stress is rotated 90 deg relative to this orientation, it becomes parallel to the line of next-nearest neighbor centers and is designated by H2. Other possibilities exist, but they require repeating cells too complicated for the present program.

The specific FEGs used to study the various arrays, stress directions, and reinforcement concentrations, are shown in Figs. 2-4(a) through 2-4(k). High stress gradients occurring in the vicinity of the reinforcement-matrix interface dictated the use of FEG with the smallest elements in that region. Also, since some properties such as yield strength depend on the element size, as will be shown in a later section, the size of elements bordering on the interface were kept as nearly constant as possible. For the cases of 20- and 30 vol % S1, the size of these elements was increased somewhat to permit the use of not-too-large elements elsewhere without changing the total number of elements in the matrix, i.e., 74. The effect of not using identical interface elements will be seen also in the results for the S2 arrangement to be presented later.

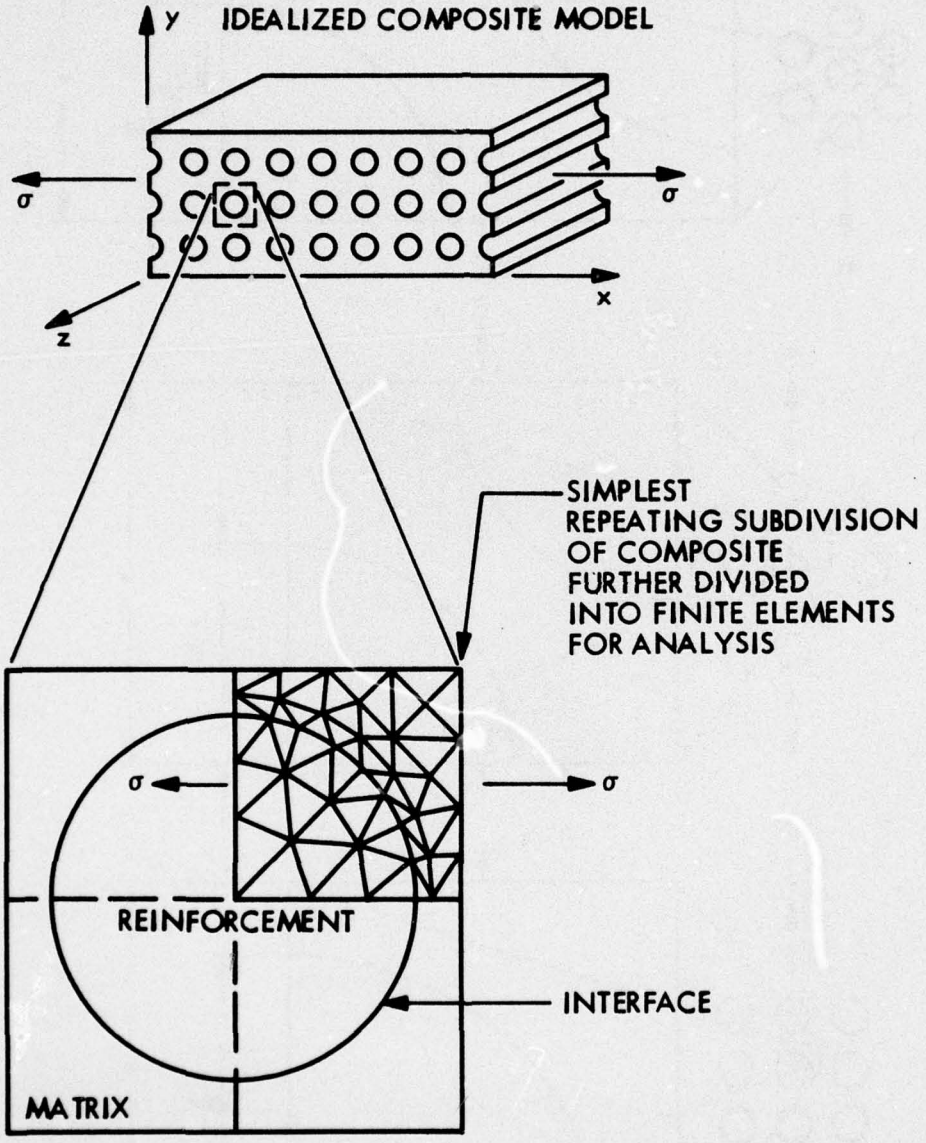

Fig. 2-2 Reduction of Unidirectional (UD) Composite, With Doubly-Repeating Reinforcement Periodicity, to Simplest Repeating Subdivision (Repeating Cell) for Finite Element Analysis

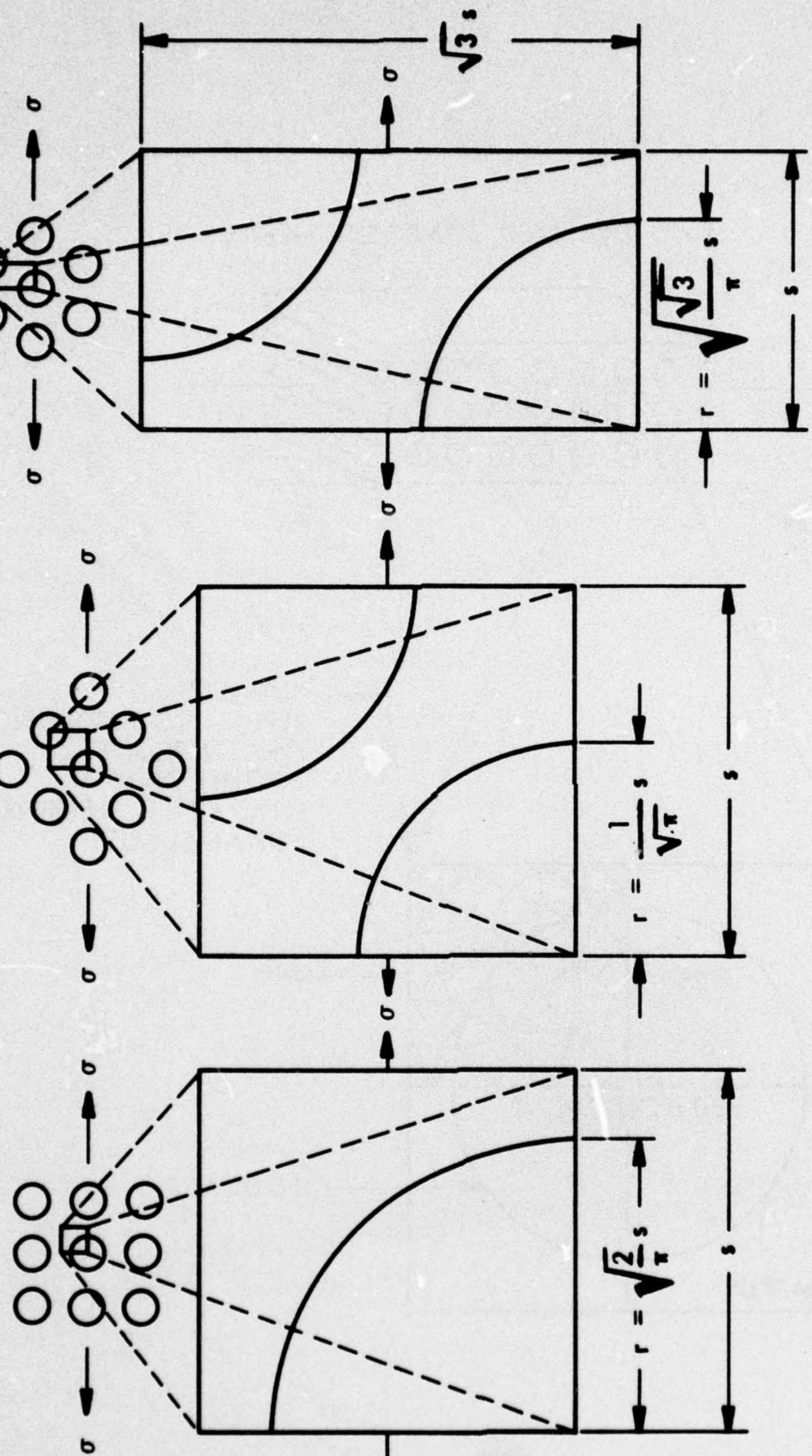

Fig. 2-3 Repeating Cells for 50-Percent UD Arrays Analyzed in This Report: (a) Simple Square (S1), (b) Diagonal Square (S2), and (c) Hexagonal (H1 and H2)

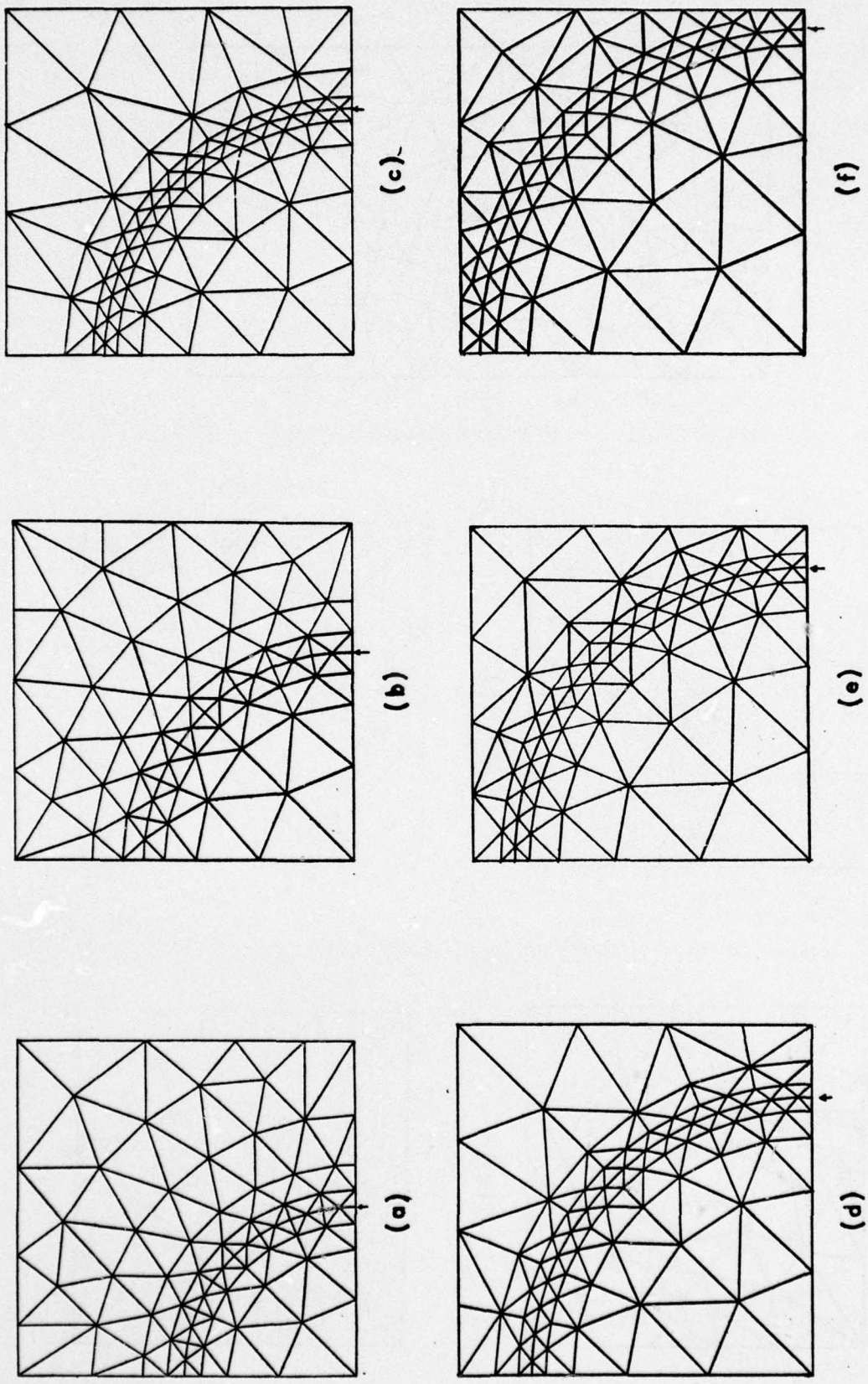

Fig. 2-4 Finite Element Grids Used to Analyze UDS1 Composites in PSTNT: (a) 20 vol %, (b) 30 vol %, (c) 40 vol %, (d) 50 vol %, (e) 60 vol %, and (f) 70 vol %

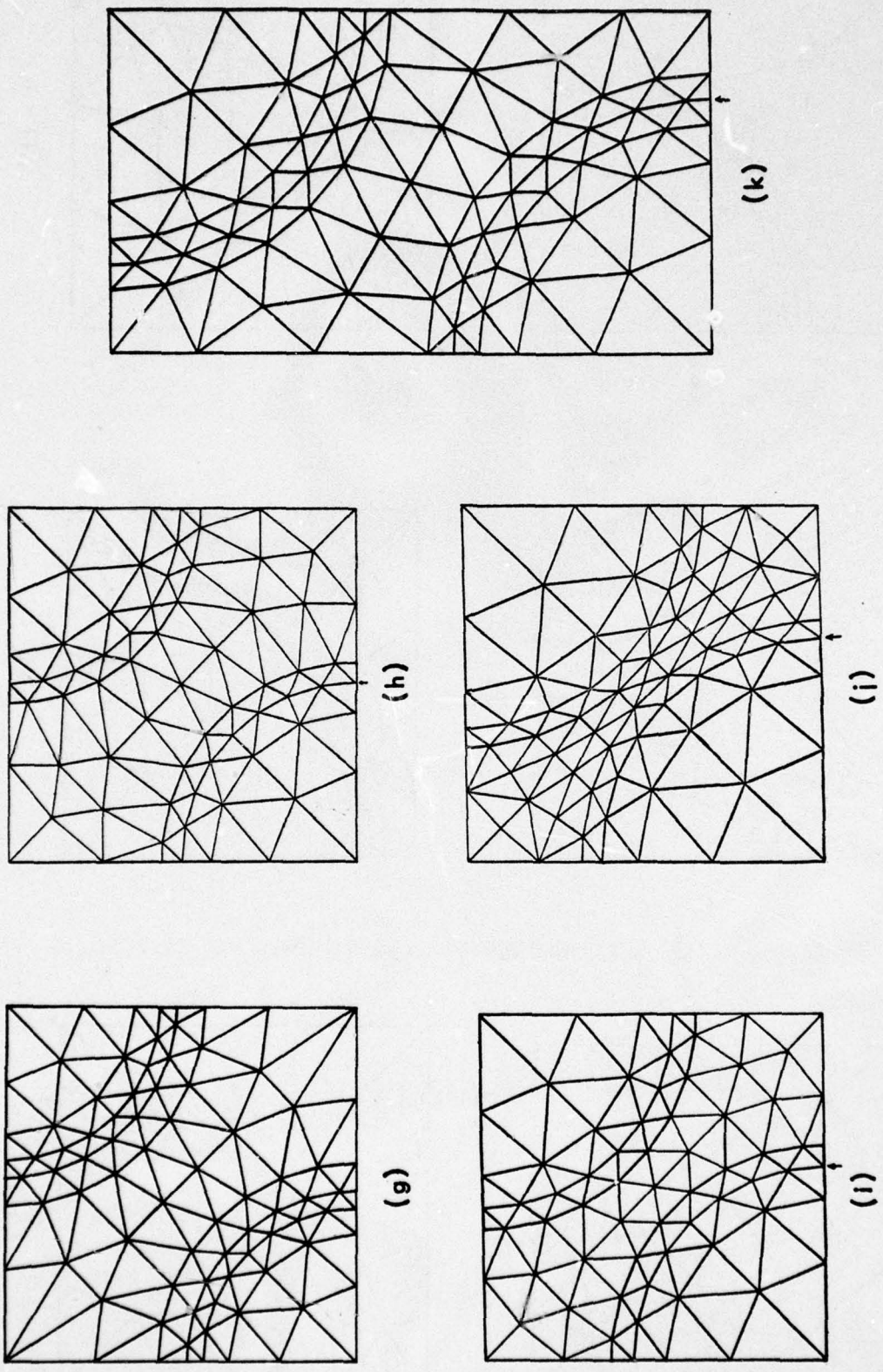

Fig. 2-4 Finite Element Grids Used to Analyze UDS2 and UDH1, 2 Composites in PSTNT: (g) S2, 30 vol %, (h) S2, 40 vol %, (i) S2, 50 vol %, (j) S2, 60 vol %, and (k) H1, 2, 50 vol %

2.4 THE COMPUTER PROGRAM

The computer program used at the start of this study was essentially the same as that employed for the work reported in Ref. 1. However, detailed analyses of local stress changes indicated that failure predictions were not being made properly because of the rapid change of slope that occurs between the elastic and the plastic portion of the bilinear stress-strain curve representation as described in Appendix A of this report. At least a partial solution was found by using a 5-segment piecewise linear representation in conjunction with a scheme to limit the maximum stress change experience by any element during each load increment. Also, some computing economy was achieved by considering the transverse-transverse contraction constraint as an initial boundary condition instead of superimposing two orthogonal displacements. One time-consuming stiffness matrix inversion per load increment iteration was thereby eliminated while the matrix size was increased only slightly.

Three additional computer program modifications were made in order to expedite calculation of specific cases and to broaden the analytical capabilities. A section was included to calculate the influence of thermal contraction differences between the constituents a residual thermal stresses and the way they in turn affect the plastic flow of the matrix and the composite stress-strain curves.

A few other efficiency schemes were tried and discarded when they were found to have no real advantage; for example, asymmetric S2 and H grids were tried to economize on the total number of elements and nodes by increasing the number around one reinforcement quadrant and decreasing it around the other. The results were too disparate to warrant continued usage.

Debonding was accomplished as in Ref. 1 by using the node-superposition method over progressively longer portions of the interface starting with the point of interaction of the interface and a stress-line through the reinforcement center. As a final modification of the computer program, the interface normal (radial) stresses and tangential shear stresses previously calculated on a programmable desk-top calculator were included in the major computer program to improve the overall efficiency.

2.5 LIMITATIONS

Prediction of ultimate tensile failure when any elemental octahedral shear stress becomes equal to the corresponding stress for a uniaxial test of the pure matrix at failure does not appear to be valid for several reasons. In particular, it does not permit failure for any value of hydrostatic tension (triaxial tension) where local decohesion and void formation leading to failure is likely to occur. There are other factors that also contribute to inaccuracies in failure predictions, such as the size of the element to fail or the size of load increment used on each iteration. As a result, ultimate tensile strength predictions are not attempted in this report.

Section 3
THEORETICAL ANALYSIS

3.1 CASES ANALYZED

Only aluminum (6061-T6) reinforced with circular boron rods was studied because previous work (Ref. 1) indicated that titanium (6 Al-4V) reinforced with beryllium behaved in a qualitatively similar manner. Of the four reinforcement arrangements described in the previous section, the following cases were analyzed in detail:

- S1 – 20- , 30- , 40- , 50- , 60- , and 70- volume percent reinforcement well bonded to the matrix
- S1 – 30-volume percent reinforcement progressively debonding from matrix
- S1 – 50-volume percent reinforcement completely debonded from matrix
- S1 – 50-volume percent reinforcement after a -250° F temperature change
- S1 – 50-volume percent reinforcement applied stress
- S2 – 30- , 50-, 60-volume percent reinforcement well-bonded to matrix
- S2 – 50-volume percent well-bonded reinforcement after a -250° F temperature change
- S2 – 50-volume percent fully debonded reinforcement
- S2 – 50-volume percent well-bonded reinforcement with an applied TNT stress to 42,667 psi after a -250° F temperature change
- H1 – 50-volume percent well-bonded reinforcement
- H1 – 50-volume percent fully debonded reinforcement
- H1 – 50-volume percent well-bonded reinforcement after a -250° F temperature change
- H1 – 50-volume percent well-bonded reinforcement with an applied TNT stress to 42,667 psi after a -250° F temperature change
- H2 – 50 -volume percent well-bonded reinforcement

For most of these cases, the following were determined:

- Stress-strain curves
- Interface normal and tangential shear-stress distribution
- Maximum stress concentration factor at interface
- Growth of plastically deformed zone in matrix with increased bond or temperature change
- Variation of elastic-modulus yield strength and transverse-transverse Poisson ratio with extent of debonding or volume fraction reinforcement
- Distribution of principal stresses in reinforcement and matrix under applied stress or temperature change

Some of these composite characteristics were analyzed using the bilinear stress-strain representation for the matrix. The elastic properties or early-plastic properties were nearly identical. Constituent properties used for the calculations are presented in Table 3-1.

Table 3-1

TENSILE PROPERTIES OF CONSTITUENT COMPOSITE MATERIALS USED IN FEM CALCULATIONS

Material	Condition	Elastic Modulus (10^6 psi)	Yield Strength[a] (10^3 psi)	Fracture Strength (10^3 psi)	Elongation (%)	Poisson Ratio
Boron (B)	–	60	400	400	–	0.20
Aluminum (6061)	T6	10	36	45	16	0.33

(a) Proportional Limit.

3.2 PRELIMINARY RESULTS

Elastoplastic properties calculated initially, with the bilinear stress-strain representation (yield strength of Al-6061-T6 matrix of 38.2 ksi), and only a portion of the arrays are presented in Table 3-2. The following observations were made.

3.2.1 S1 Array

Increasing the filament content for the S1 case is seen to increase the transverse elastic modulus, the yield strength, the ultimate strength, and the load concentration factor (which, when multiplied by the applied load, gives the greatest stress normal to the filament matrix interface) occurring in the loading direction when no interface debonding is present, and otherwise at the tip of the debonded region. In contrast, the transverse-transverse Poisson's ratio and the strain-to-failure vary inversely with reinforcement content; the former at 60 volume percent is only 71 percent of the value at 30 volume percent.

Entries 2 and 3, and 4 through 7 for the S1 array show the effect of element size and distribution in the vicinity of the interface. For 30 volume percent, increasing the number of interface elements by 1/3 results in a change of less than 1 percent in modulus and Poisson ratio, but a 6-percent decrease in yield strength and a decrease of nearly 2 percent in the ultimate strength. These findings occur because steep stress concentration gradients exist near the interface that are more closely approximated with smaller elements; the constant stress over each is a closer approximation to the true continuum case. Thus, yielding and failure can be determined more accurately with the smaller elements. Entries 6 and 7 of Table 3-2 are calculated for a grid identical to that shown in Fig. 2-4 (c) but with elements in the filament adjacent to the interface near lower boundary made successively finer to determine the effect on the stress concentration factor. The initial subdivision caused an increase of less than 1 percent and the second had an undetectable effect though a slightly larger decrease in F_{YT} and F_{UT} occurred in the second case.

Table 3-2

CALCULATED TRANSVERSE MECHANICAL PROPERTIES OF VARIOUS UNIDIRECTIONAL COMPOSITES WITH WELD-BONDED INTERFACES

Array	Vol % Boron	Elements	Nodes	$\Delta\sigma$ [a] (10^3 psi)	E_T (10^6 psi)	ν_{TT} [b]	F_{YT} (psi)	F_{UT} (psi)	ϵ_{UT} (%)	ϕ [c]	θ [d] $\sigma_\theta = 0$ (deg)
1. S1	20	132	79	1.20	14.7	0.451	34,373	42,773	0.307	1.396	69.5
2. S1	30	120	72	1.20	17.2	0.420	35,498	45,098	0.285	1.412	69.5
3. S1	30	152	89	1.20	17.34	0.416	33,488	44,288	0.274	1.487	68.6
4. S1	40	152	89	1.20	20.50	0.381	37,419	44,619	0.228	1.47	69.5
5. S1	40	152	89	1.20	20.43	0.383	37,525	45,925	0.240	1.43	69.5
6. S1	40	154	90	1.20	20.43	0.383	37,526	45,926	0.240	1.44	69.5
7. S1	40	157	92	1.20	20.43	0.383	37,509	45,909	0.240	1.44	69.5
8. S1	44.1	157	89	1.10	22.0	0.367	38,794	49,794	0.249	1.50	68.9
9. S1	50	152	89	1.10	24.4	0.347	40,197	54,497	0.251	1.53	71.7
10. S1	60	146	85	1.60	29.21	0.316	41,644	59,244	0.219	1.58	69.5
11. S2	50	158	94	1.10	20.18	0.458	39,246	49,146	0.363	1.00	~90.
12. S2	50	158	94	1.10	20.12	0.460	38,598	48,498	0.348	1.00	84.5
13. S2	50	120	73	1.20	20.20	0.458	38,784	49,584	0.364	0.995	90
14. S2	50	130	78	1.20	17.2	0.420	35,498	45,098	0.285	1.005	90
15. H1	50	144	87	1.10	22.10	0.406	37,113	51,413	0.289	1.493	min at 90

(a) Load increment per computer iteration.
(b) Transverse-transverse Poisson ratio.
(c) Maximum ratio of interface – normal stress to applied stress (parallel to applied load).
(d) Angular position of zero interface – normal stress measured from applied-load direction.

LOCKHEED PALO ALTO RESEARCH LABORATORY
LOCKHEED MISSILES & SPACE COMPANY, INC.
A SUBSIDIARY OF LOCKHEED AIRCRAFT CORPORATION

Of the properties listed, only the angular position for zero normal stress at the interface is insensitive to the filament content.

3.2.2 S2 Array

The diagonal square array (S2) is the same doubly periodic square filament array above but with the load applied parallel to the line of next-nearest neighbors as shown in Fig. 2-3(b). It is a case of interest since real composites are practically never loaded in the S1 configuration and the change in geometrical factors caused by rotating the loading direction should alter the macro- and micro-mechanical behavior because of the change produced in filament-filament interaction. Indeed, comparison of entry number 9 of Table 3-2 with entries 11 and 13 shows a drop in modulus of about 17 percent from 24.4×10^6 psi to an average of 20.17×10^6 psi. Also, there are a slight decrease in yield strength, a decrease of nearly 10 percent in the ultimate transverse tensile strength, and an increase in strain-to-failure of 44 percent.

Another remarkable difference between S1 and S2 loading occurs at the interface. The stress concentration factor for the former is 1.50, whereas it is only 1.00 for the latter, indicating that filament-matrix debonding is more likely to occur when S1 conditions prevail.

The difference between entries 11 and 12 for S2 loading is that in the latter the interface was bounded by larger elements on one side and smaller ones on the other; in entry 11, on the other hand, the grid was modified so as to place the interface between the two bands of nearly equal-size elements. The effect of this difference is reflected by a small change in all properties, but there is essentially no difference in the sequence of element yielding in the matrix along the boundary.

Entry 13 of Table 3-2 gives the results of using a simpler S2 array for the purpose of reducing the total number of elements and nodes in the FEG and permit analyses of interface debonding without exceeding the computer capacity, since new nodes must be introduced for this purpose. The gross properties are sufficiently unaffected, as were the local stresses along the interface bounded by finer elements, to permit the use of such an FEG for interface debonding studies.

Reducing the FEG dimensions was tested also by an asymmetrical division with respect to the diagonal within the matrix. The results shown as entry 14, are not as good as those for the previous case in which the number of elements and nodes are greater by 10 and 5, respectively. Therefore, the asymmetrical grid will not be used unless the reduced symmetrical grid displays anomalies in later more detailed analyses.

3.2.3 H1 Array

Hexagonal packing is similar to the diagonal square with the repeating cell dimensions altered as shown in Fig. 2-3(c). Loading is along the line of nearest neighbors in this case, although loading at 30 deg to this direction along the line of second-nearest neighbors is of interest also and will be examined subsequently. All gross properties in this case (50 volume percent) occur essentially midway between the S1 and S2 values,

except that as in the S2 case the interface-normal stress never becomes zero but reaches a minimum at 90 deg to the applied stress direction. It seems that the interface stress behavior in this case is similar to the S1 array in the loading direction (concentration factor 1.5) because filament proximity is similar in this direction, while at 90 deg to the load the interface surrounding more closely resembles the S2 case.

3.2.4 Fracture

The progression of yielding to fracture has been studied in detail for several cases; it was found that the current computer program contains features incorporated for economic reasons that predict unrealistic failure loads and strains. Specifically, the matrix (6061-T6) stress strain curve is a bilinear approximation. This is reasonably accurate but introduces problems as follows. As the applied load is incrementally increased at each program iteration, some of the elements enter the plastic range with too high a stress and then experience a steady unloading during subsequent iterations until at some point the load on one of them drops below the material yield stress. The subsequent load increment calculates the stress on that particular element for the completely elastic material and results in failure because of the steep slope of the elastic curve relative to the plastic portion for adjacent elements. Thus, the failure strength and strains are somewhat under-estimated. They are analyzed more completely in Appendix A.

3.3 RESULTS

The results of analysis performed with the improved computer program are presented in this subsection. Every case previously described was reanalyzed except for the modified FEGs that provided no advantage initially.

3.3.1 Reinforcement Concentration (S1 Case)

Stress-strain curves calculated for the S1 case with a well-bonded interface are shown in Fig. 3-1 together with the data for pure boron and for the pure aluminum (6061-T6) matrix. The extent of plastic flow varies with each concentration only because of the limit imposed on the number of applied load increments that are predetermined for each computer run required to generate the data for one curve. Experimental data obtained during that study and by others seldom show a transverse tensile elongation exceeding 0.3 percent.

3.3.2 Interface Debonding

An S1 UD 50 vol % B/Al (6061-T6) composite with a very weak, or absent, interfacial bond has a much lower TNT elastic modulus (4.2×10^6 versus 24.4×10^6 psi), and a much lower yield strength (4.7 versus 24.4 ksi), as shown in Fig. 3-2. As the debonded case approaches a perforated material, the properties are much inferior to the pure matrix.

The influence of a change in reinforcement concentration for the S1 case is shown in Figs. 3-3 through 3-8 where various significant quantities for 30-volume percent S1 are compared with those for 50-volume percent S1 obtained from Ref. 1.

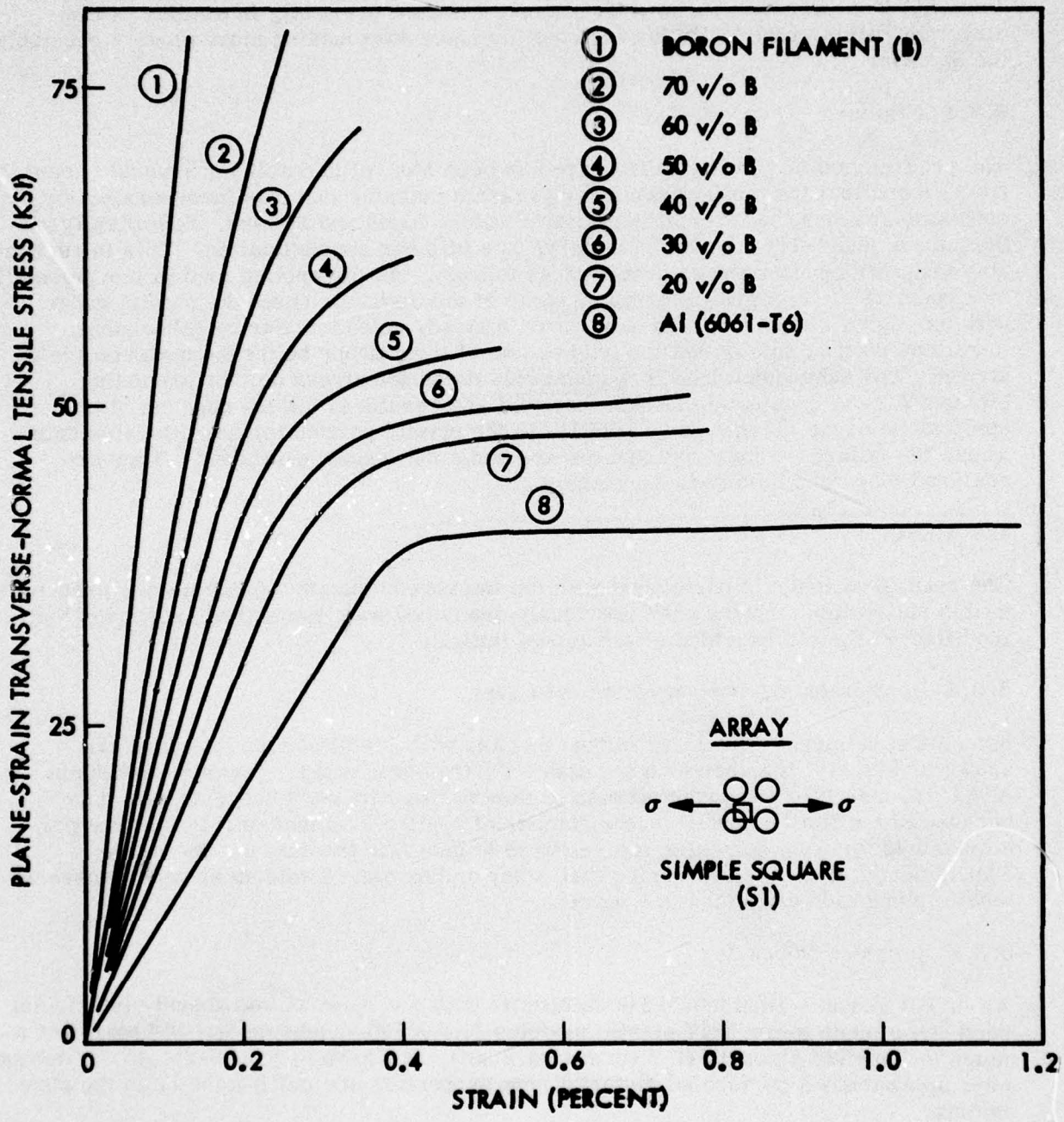

Fig. 3-1 Stress-Strain Curves for UDSS B/Al(6061-T6) Composites, With Several Concentrations of Reinforcement From 20 to 70 vol %, Loaded in Plane-Strain Transverse-Normal Tension (PSTNT)

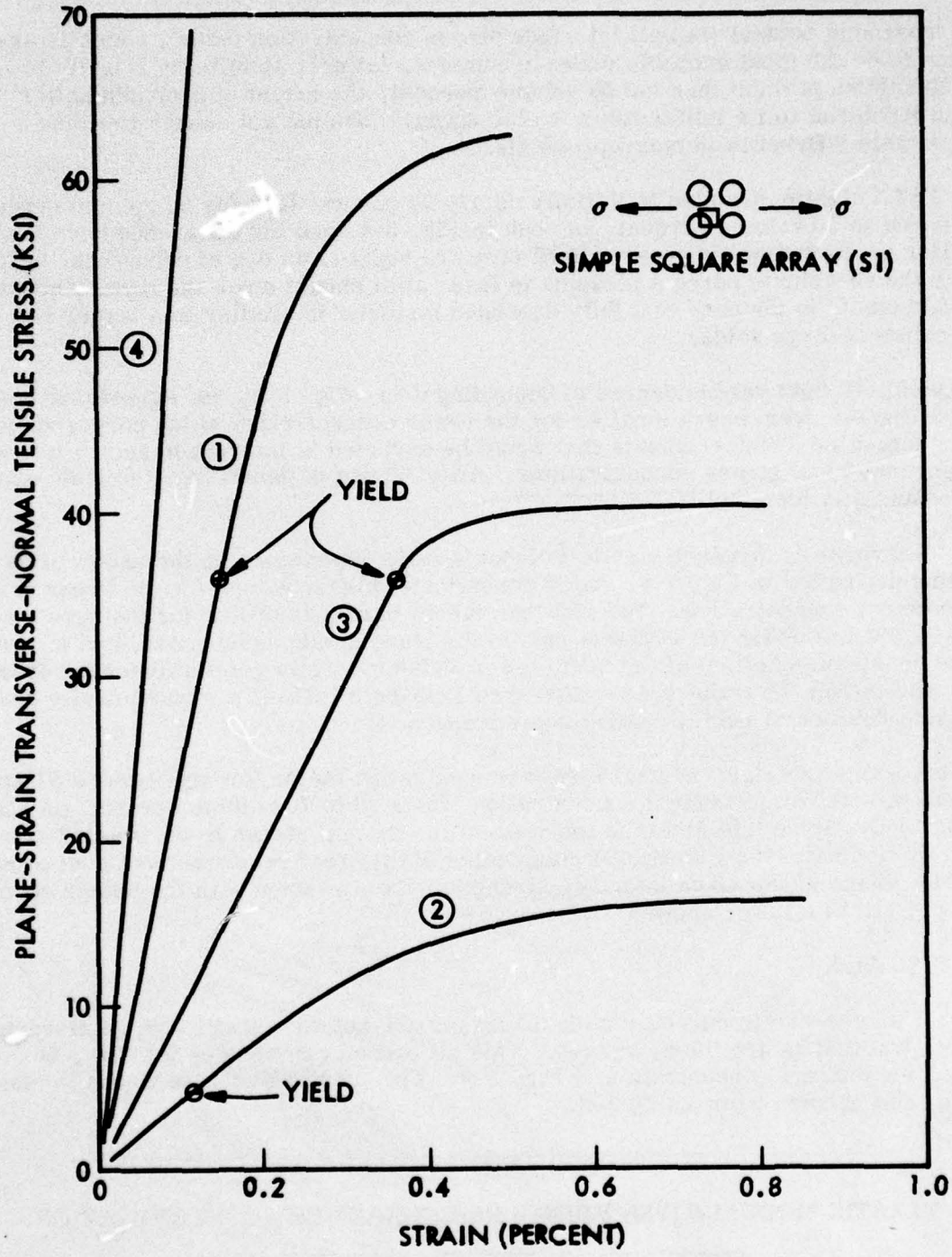

Fig. 3-2 PSTNT Stress-Strain Curves for UDSI 50 vol % B/Al(6061-T6) Composite With: (1) Well-Bonded Interface and (2) Debonded Interface, Compared to (3) Pure Matrix Al(6061-T6) and (4) Pure Reinforcement (Boron)

The maximum normal (radial) interface stress concentration factor, which is assumed to be the most probable cause of interface failure, is initially slightly lower for 30 volume percent than for 50 volume percent; the extent of debonding after which it returns to its initial value is also slightly less but not enough to cause a measurable difference in macroproperties.

The PSTN elastic modulus is initially nearly 30 percent less for 30 volume percent compared to 50 volume percent, as seen in Fig. 3-4, and the difference becomes smaller as debonding progresses until they are equal at 45 deg of debonding, beyond which the 50-volume percent modulus is less, as it should since the layer amount of reinforcement in the case of a fully debonded material is similar to a larger concentration of large voids.

The yield strength versus degree of debonding data (Fig. 3-5) is surprising in that the values are everywhere smaller for the lower concentration which corresponds to more separated reinforcements that would be expected to interact in such a way as to decrease local stress concentrations. After 60 deg of debonding, the yield stresses are essentially identical.

The transverse-transverse elastic Poisson's ratio dependence on the extent of debonding presented in Fig. 3-6, shows consistently higher values for the lower reinforcement concentration. The fact that values in excess of that for the pure matrix ($\upsilon = 0.33$) are predicted is due in part to the plane strain assumption, and in part to the constraining effect of the stiff, lower Poisson's ratio reinforcements. It is later shown that the transverse-transverse Poisson's ratio is a monotonically decreasing function of reinforcement concentration.

The maximum interface-normal stress concentration factor for well-bonded S1 arrays increases with reinforcement concentration, from 20 to 70 volume percent, as shown in Fig. 3-7. Since this factor is the ratio of the normal stress to the applied stress, the trend indicates that, for two S1 composites of different reinforcement concentration but with identical interface interface strengths, the specimen with the higher concentration will fail at a lower applied TNT load.

3.3.3 S2 Array

PSTNT stress-strain curves for the S2 arrays are not as sensitive to reinforcement volume fraction as are the S1 arrays. This difference can be seen for 30- , 50- , and 60-volume percent concentration in Fig. 3-8. The quantitative differences in elastic moduli can be seen from Table 3-3.

Table 3-3

ELASTIC MODULUS (PSI) VERSUS REINFORCEMENT CONCENTRATION

Vol %	S1	S2
30	17.2×10^6	15.7×10^6
50	24.4×10^6	20.3×10^6
60	29.2×10^6	23.6×10^6

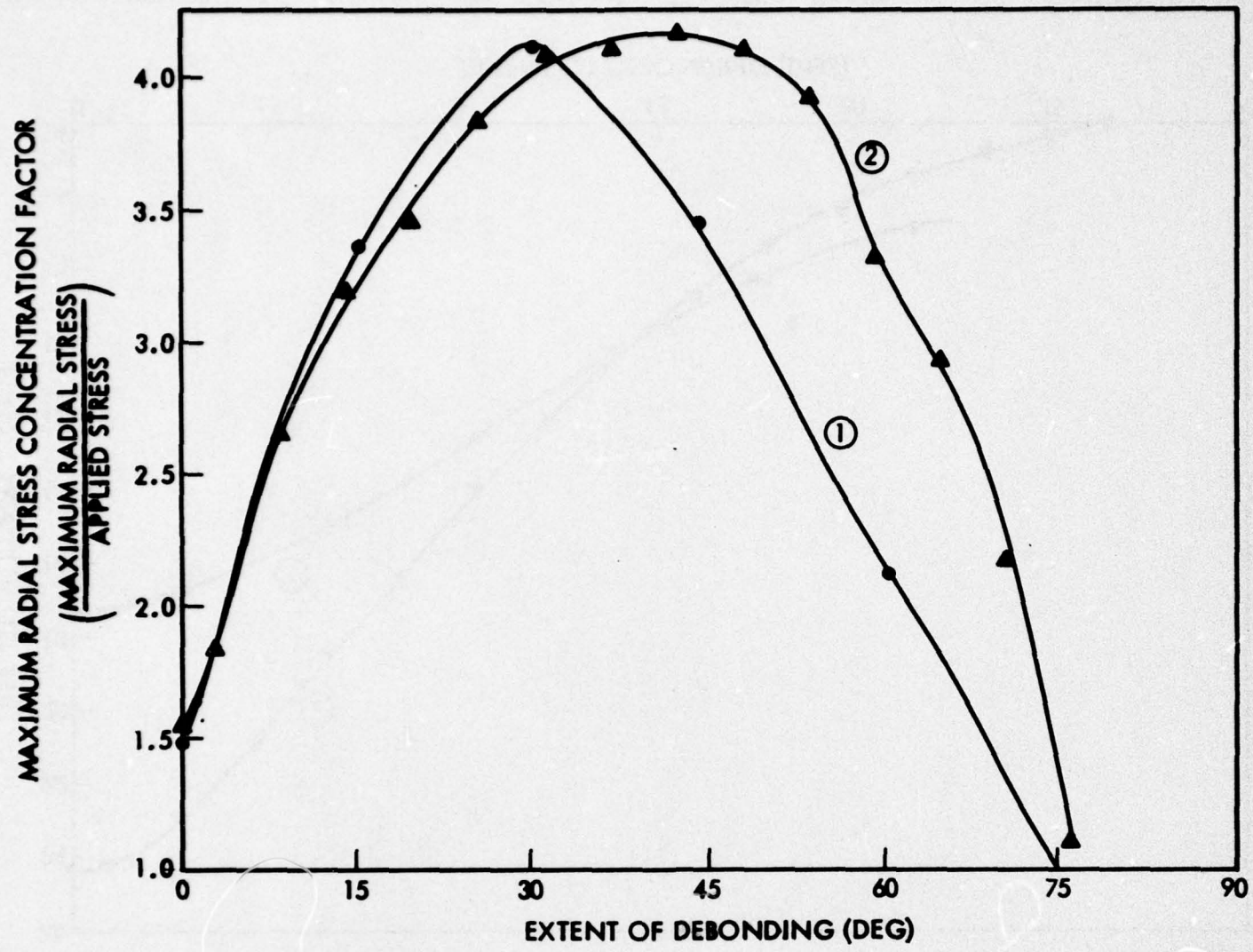

Fig. 3-3 Maximum Interface Stress-Concentration Factor Versus Extent of Debonding From Direction of Applied TNT Load in B/Al(6061) Composites With Two Reinforcement Concentrations: ① 30 vol % and ② 50 vol %

LOCKHEED PALO ALTO RESEARCH LABORATORY
LOCKHEED MISSILES & SPACE COMPANY, INC.
A SUBSIDIARY OF LOCKHEED AIRCRAFT CORPORATION

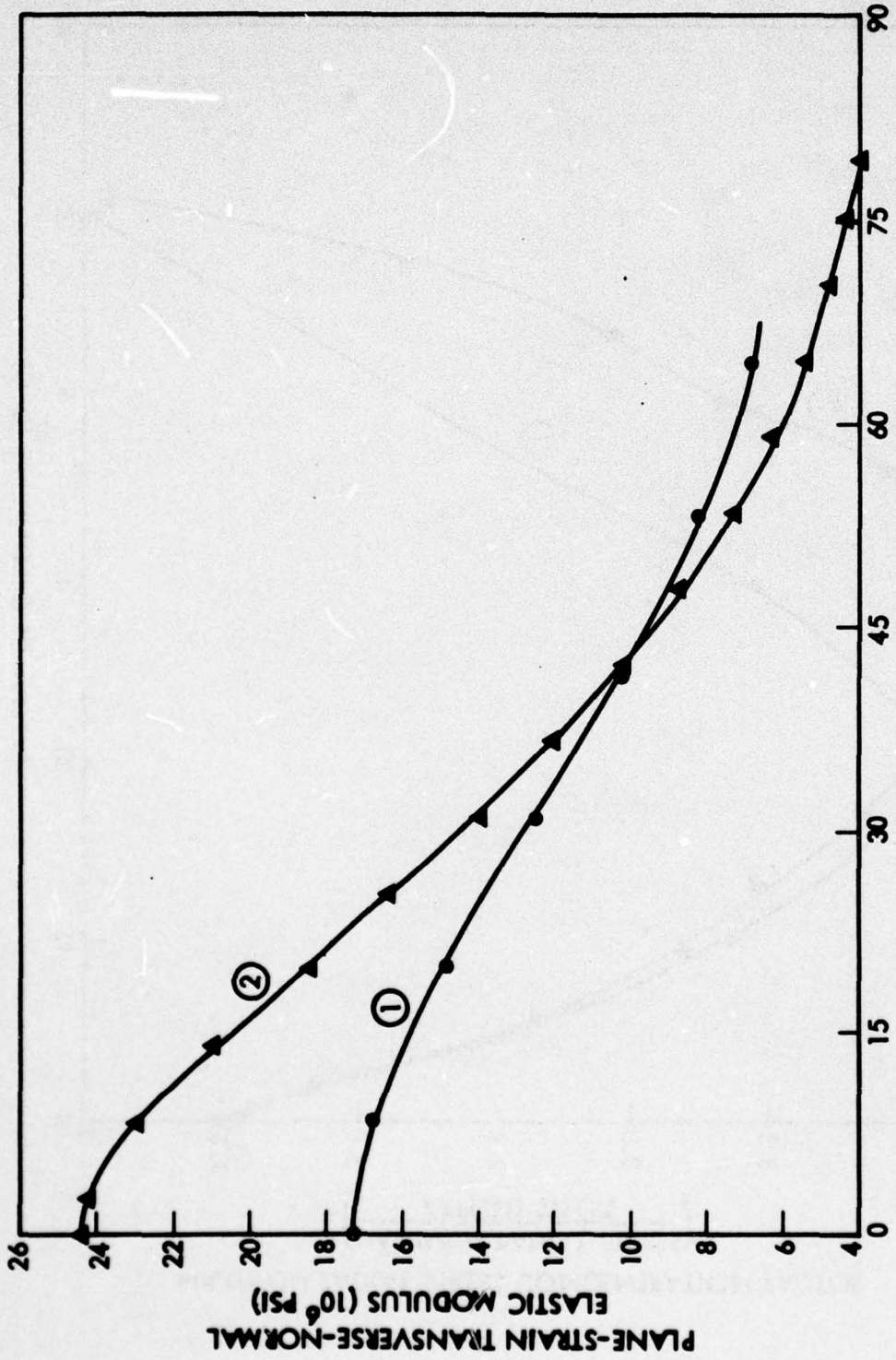

Fig. 3-4 PSTNT Modulus Versus Extent of Debonding From Direction of Applied Load in UDS1 B/Al(6061) Composites With Two Reinforcement Concentrations: ① 30 vol % and ② 50 vol %

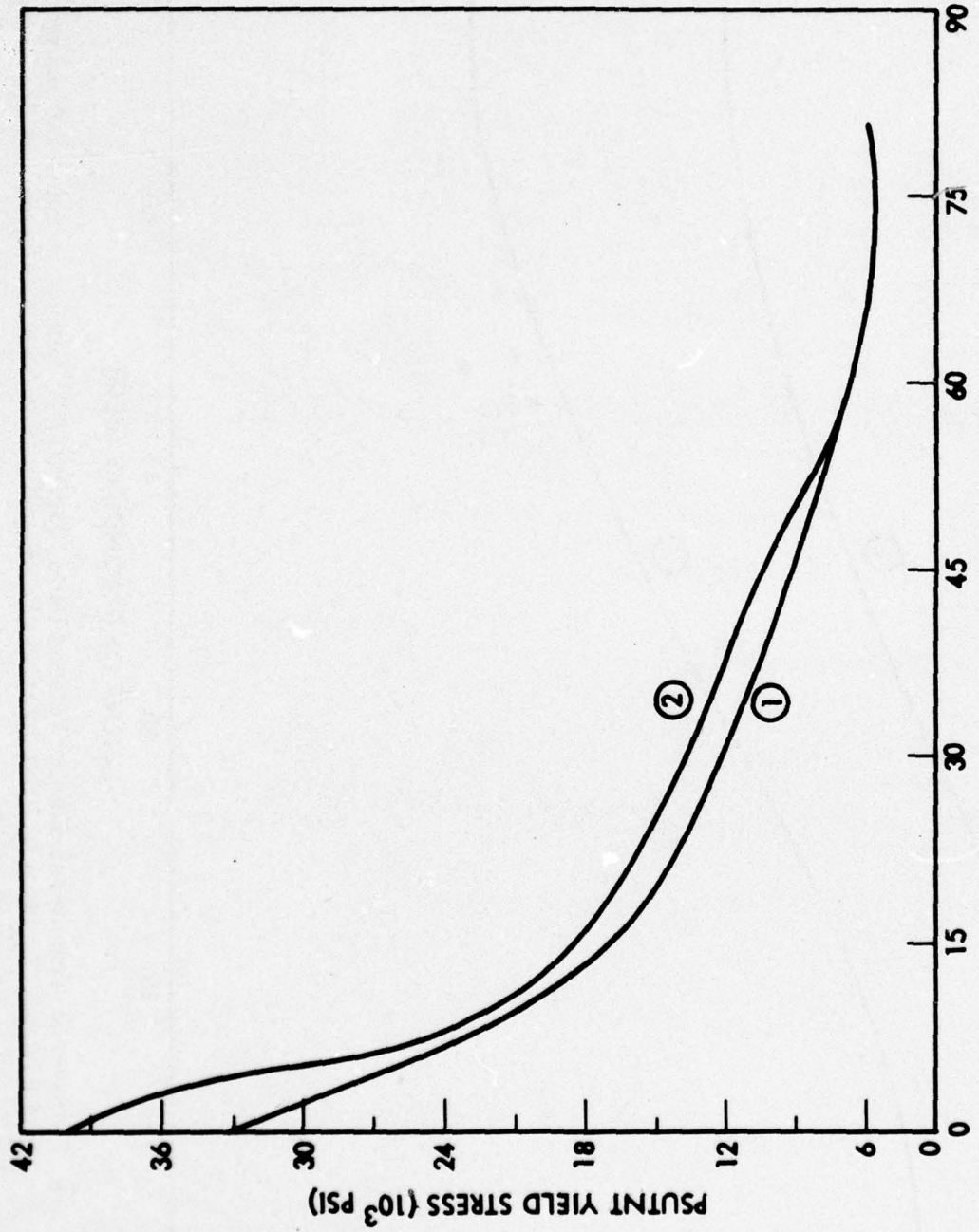

Fig. 3-5 PSTNT Initial Yield Stress Versus Extent of Debonding From Applied Load Direction in UDSi B/Al(6061-T6) Composite With Two Reinforcement Concentrations: ① 30 vol % and ② 50 vol %

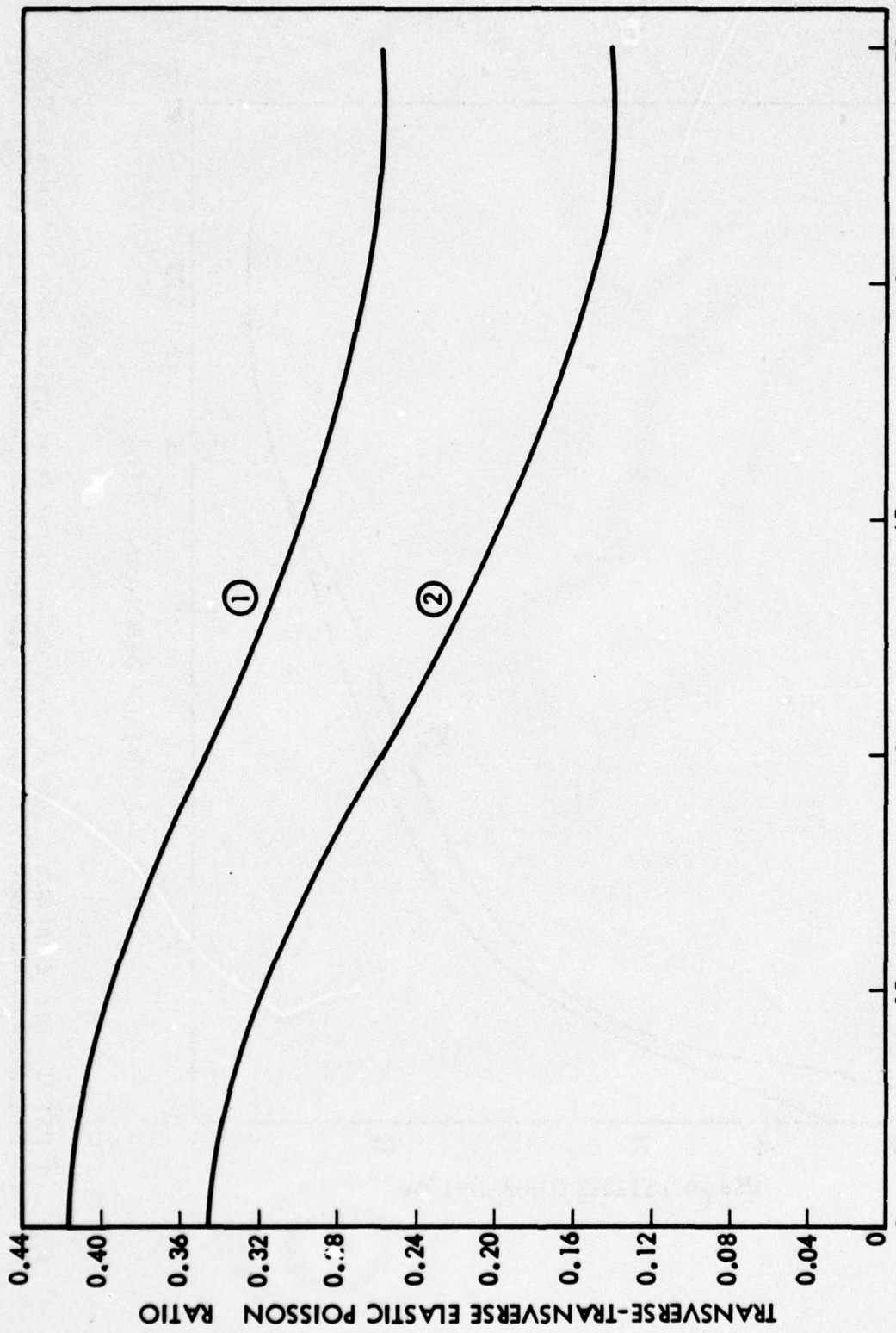

Fig. 3-6 Transverse-Transverse Elastic Poisson Ratio, for PSTNT, Versus Extent of Debonding From Applied Load Direction in UDS1 B/Al(6061) Composite With Two Reinforcement Concentrations: ① 30 vol % and ② 50 vol %

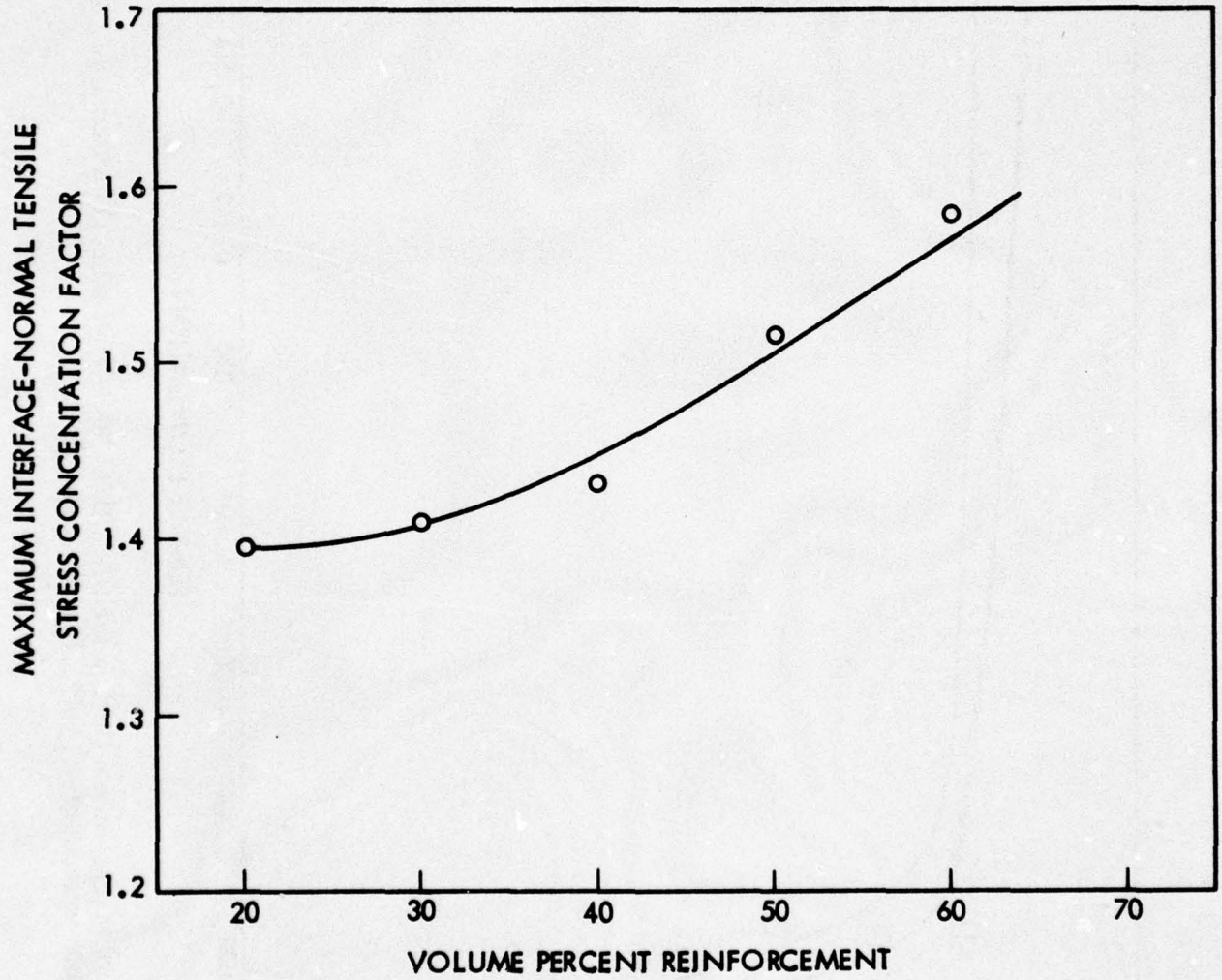

Fig. 3-7 Maximum Interface-Normal Stress-Concentration Factors Versus Volume-Percent Reinforcement for UDS1 B/Al(6061) Composites in Transverse-Normal Tension

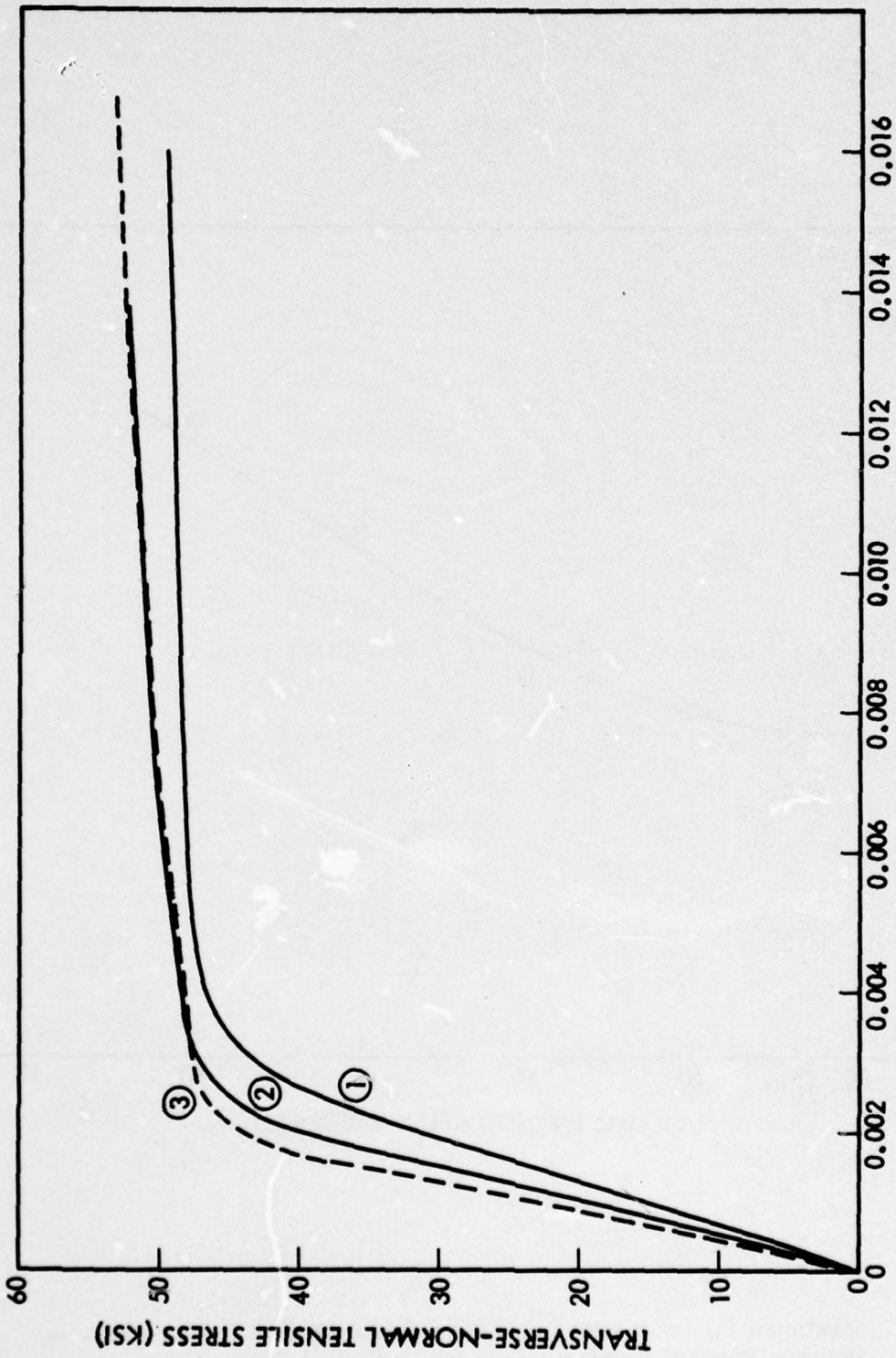

Fig. 3-8 PSTNT Stress-Strain Curves for UDS2 B/Al(6061-T6) Composites Containing Reinforcement Volume Percent of: ① 30, ② 50, and ③ 60

However, the values for corresponding concentrations are always lower for the S2 case, and these are also somewhat less sensitive to concentration.

3.3.4 Hexagonal Arrays and Comparison With Previous Cases

The hexagonal arrays H1 and H2 show a PSTNT stress-strain behavior intermediate to the cases S1 and S2, as can be seen from Fig. 3-9 for 50 vol % B/Al (6061-T6). The elastic moduli for the two hexagonal arrays are virtually the same (22.2×10^6 psi for H1, and 22.1×10^6 psi for H2); the < 1/2-percent difference is possibly caused by the slightly different matrix element deformation due to their nonequilateral form. However, the yield strength varies more noticeably, with the H1 value at 33.4 ksi compared to 34.8 ksi for H2. It is remarkable that, for these four cases, the yield strengths of the composites are little different from that of the pure matrix. It should be remembered that the yield strength as defined here is a microyield or true micro-proportional limit, as can be seen in Fig. 3-9 by the fact that there is no perceptible change of slope at the points marked "yield."

Differences between the curves of Fig. 3-9 become more apparent when the data are replotted as applied TNT stress versus plane plastic tensile strain (Fig. 3-10). The relative positions of the curves are the same except in the region of small deformations where S1 and H2 coincide and S2 and H1 are reversed to show that the former initially work hardens faster but soon becomes softer than the latter. The differences observed in the plastic behavior are a consequence of the complex, array-dependent, stress distribution existing in the matrix when under applied stress, as will be discussed subsequently.

The dependence of PS TNT modulus, yield strength, and Poisson's ratio on concentration of reinforcement for cases S1, S2, and H1 are shown in Figs. 3-11, 3-12, and 3-13, respectively. As shown previously, the dependence of elastic modulus is greater for S1 arrays than for S2, particularly at the higher concentrations. The single value for H1 packing is intermediate to S1 and S2 at 50 volume percent.

Yield strength depends strongly on reinforcement concentration for the S1 arrays and in a slightly reverse manner for the S2 (Fig. 3-12). The latter situation may be an artifact caused by the sensitivity of predicted yield strength to the size of the element that yields, as will be discussed in subsection 3.4.

Poisson ratio variations with reinforcement concentration for S1 and S2 are presented in Fig. 3-13 together with a single point for H1. Again, the S1 condition produces a greater sensitivity to concentration than does the S2. Since Poisson's ratio, unlike yield strength, is a macro-property, i.e., relatively insensitive to FEG differences, the predicted behavior is genuine. As with the modulus, the H1 value lies intermediate to the S1 and S2.

The influence of total interface debonding for the three cases of S1, S2, and H1 with 50-volume percent reinforcement is seen in Fig. 3-14, where the stress-strain curves are presented for the well-bonded and completely debonded cases. The curves

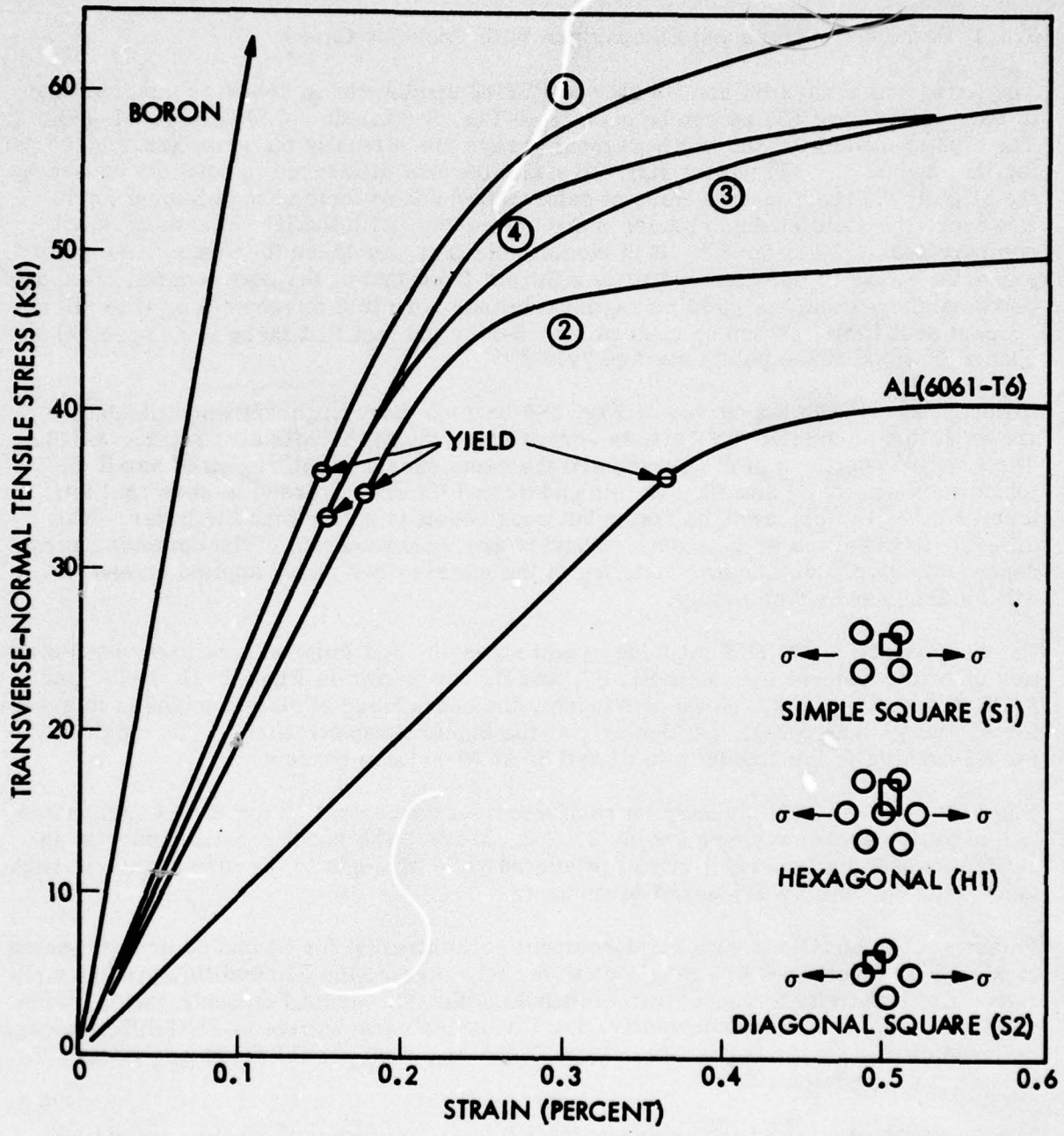

Fig. 3-9 PSTNT Stress-Strain Curves for UD 50 vol % B/Al(6061-T6) Composites With Arrays as Indicated in Inset: (1) S1, (2) S2, (3) H1 (stressed as shown), and (4) H2 (stressed at 90 deg to direction shown)

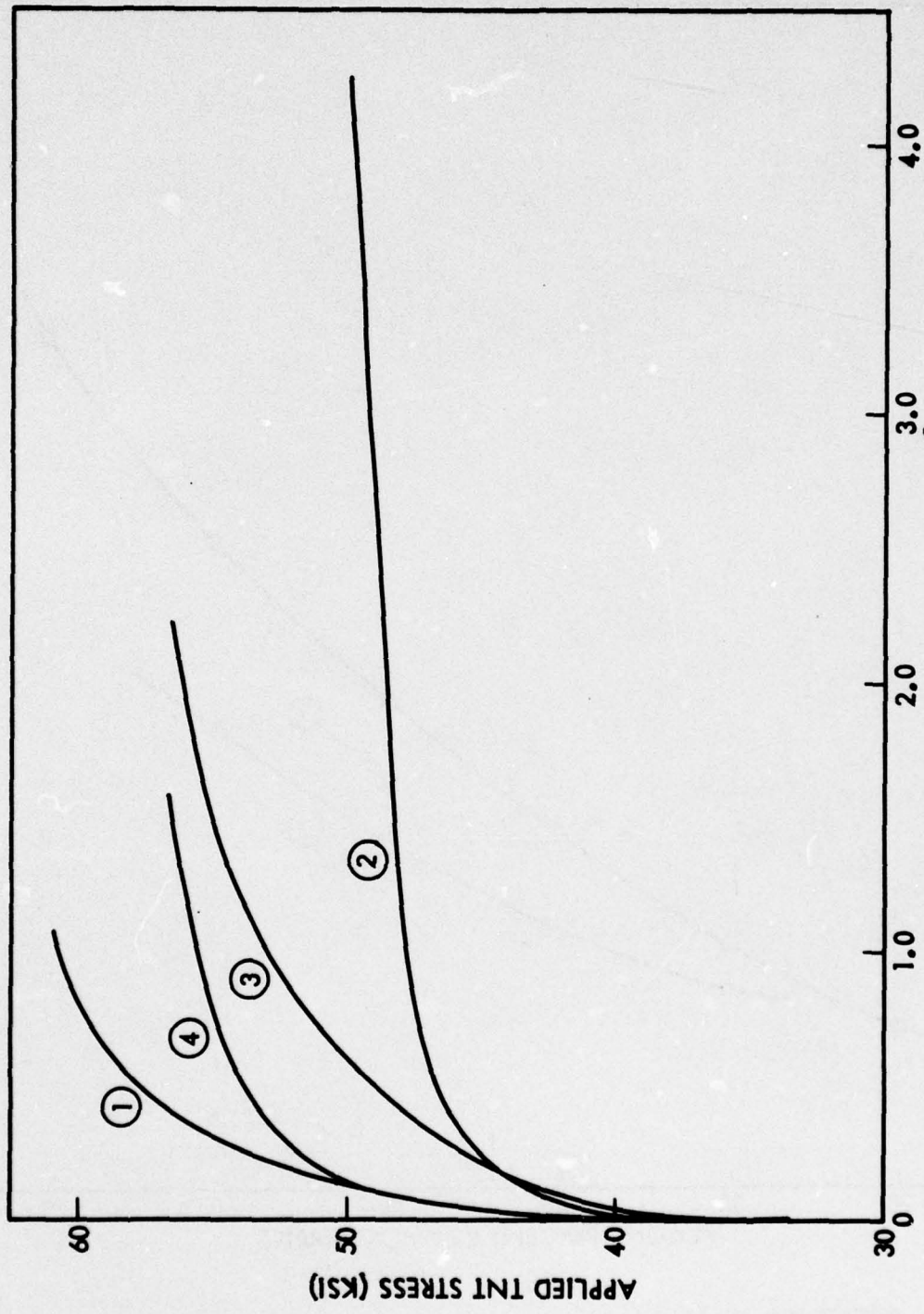

Fig. 3-10 PSTNT Stress Versus Plane Plastic Strain Curves for UD 50 vol % B/Al(6061-T6) With Reinforcement Arranged as Follows: (1) S1 (E_{TN} = 24.32 × 10^6 psi), (2) S2 (E_{TN} = 20.18 × 10^6 psi), (3) H1 (E_{TN} = 22.09 × 10^6 psi), and (4) H2 (E_{TN} = 22.08 × 10^6 psi)

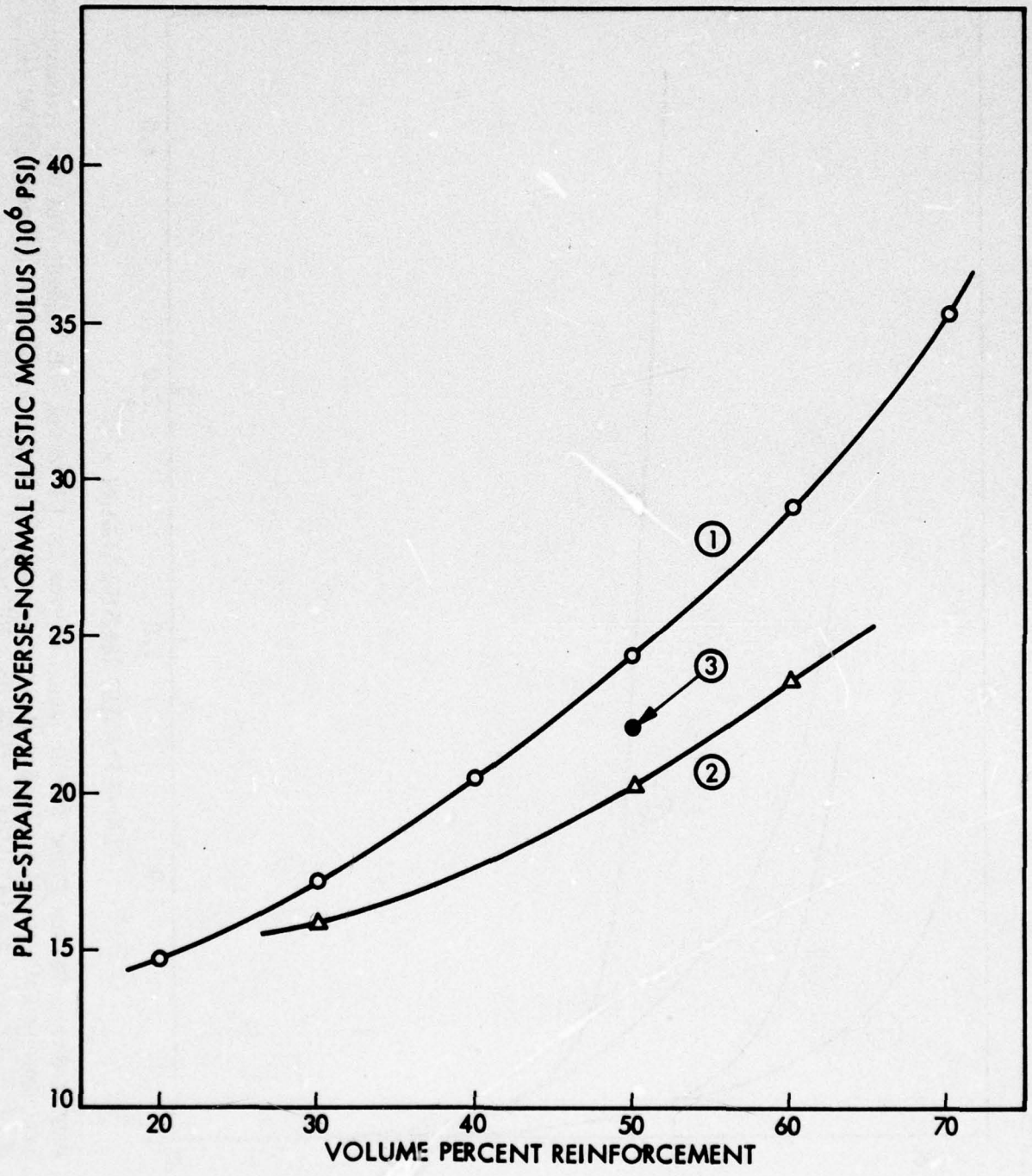

Fig. 3-11 PSTNT Elastic Modulus Versus Volume Percent Reinforcement for UD B/Al(6061-T6) Composites With Reinforcement Arrays: ① S1, ② S2, and ③ H1

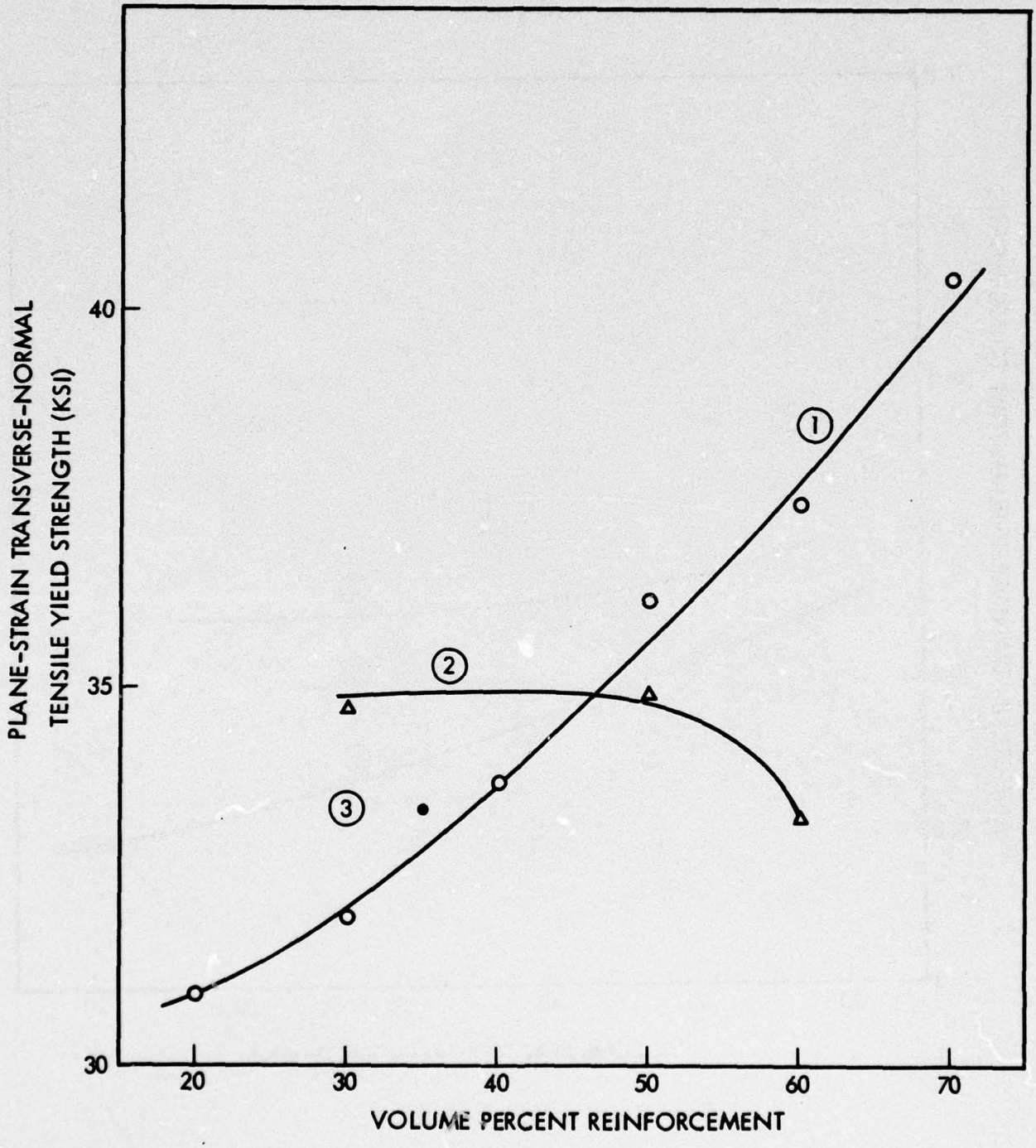

Fig. 3-12 PSTNT Yield Strength Versus Volume Percent Reinforcement for UD B/Al(6061-T6) Composites With Reinforcement Arrays: (1) S1, (2) S2, and (3) H1

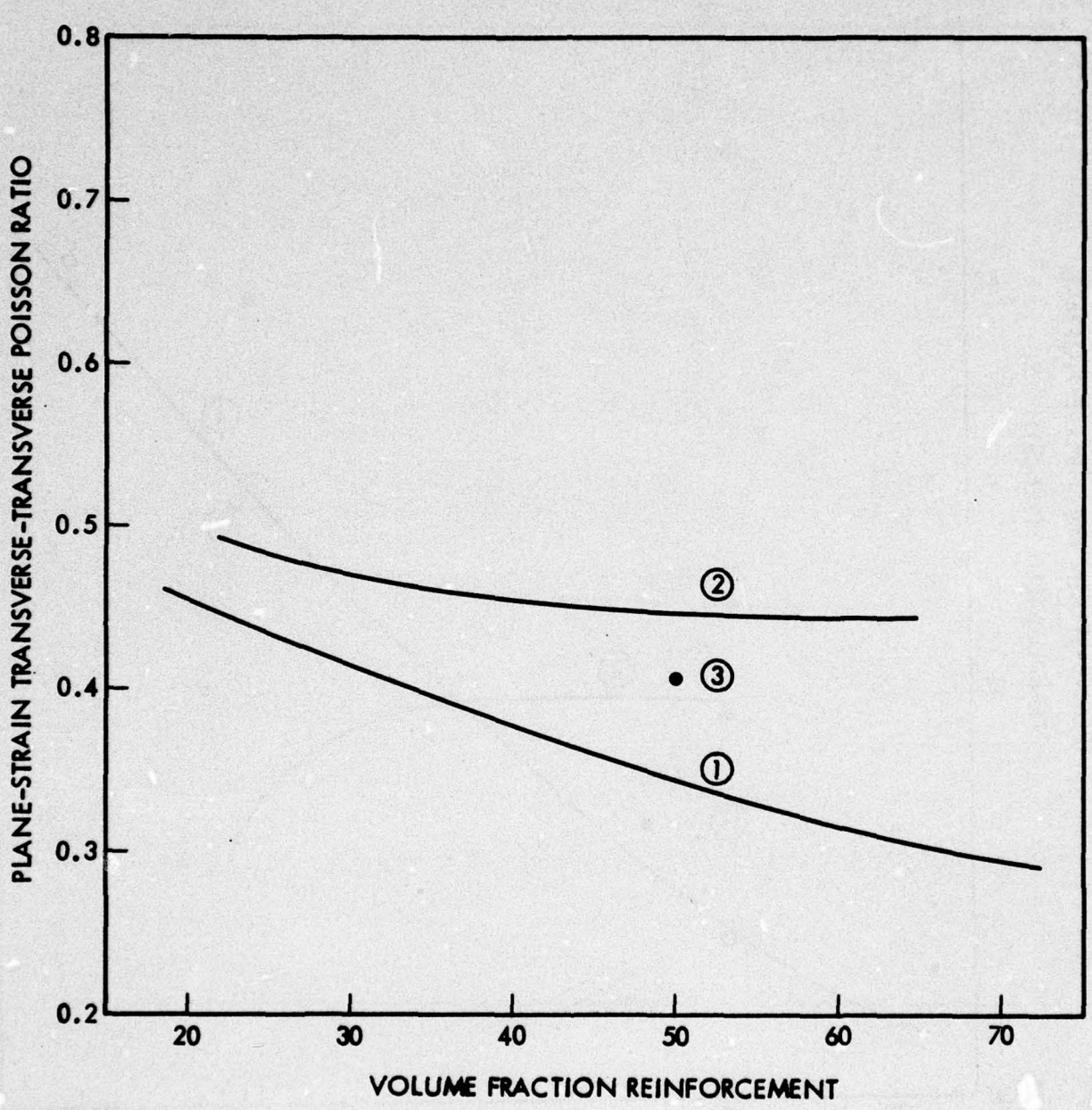

Fig. 3-13 PSTNT Poisson Ratio Versus Volume Percent Reinforcement for UD B/Al(6061-T6) Composites With Reinforcement Arrays: ① S1, ② S2, and ③ H1

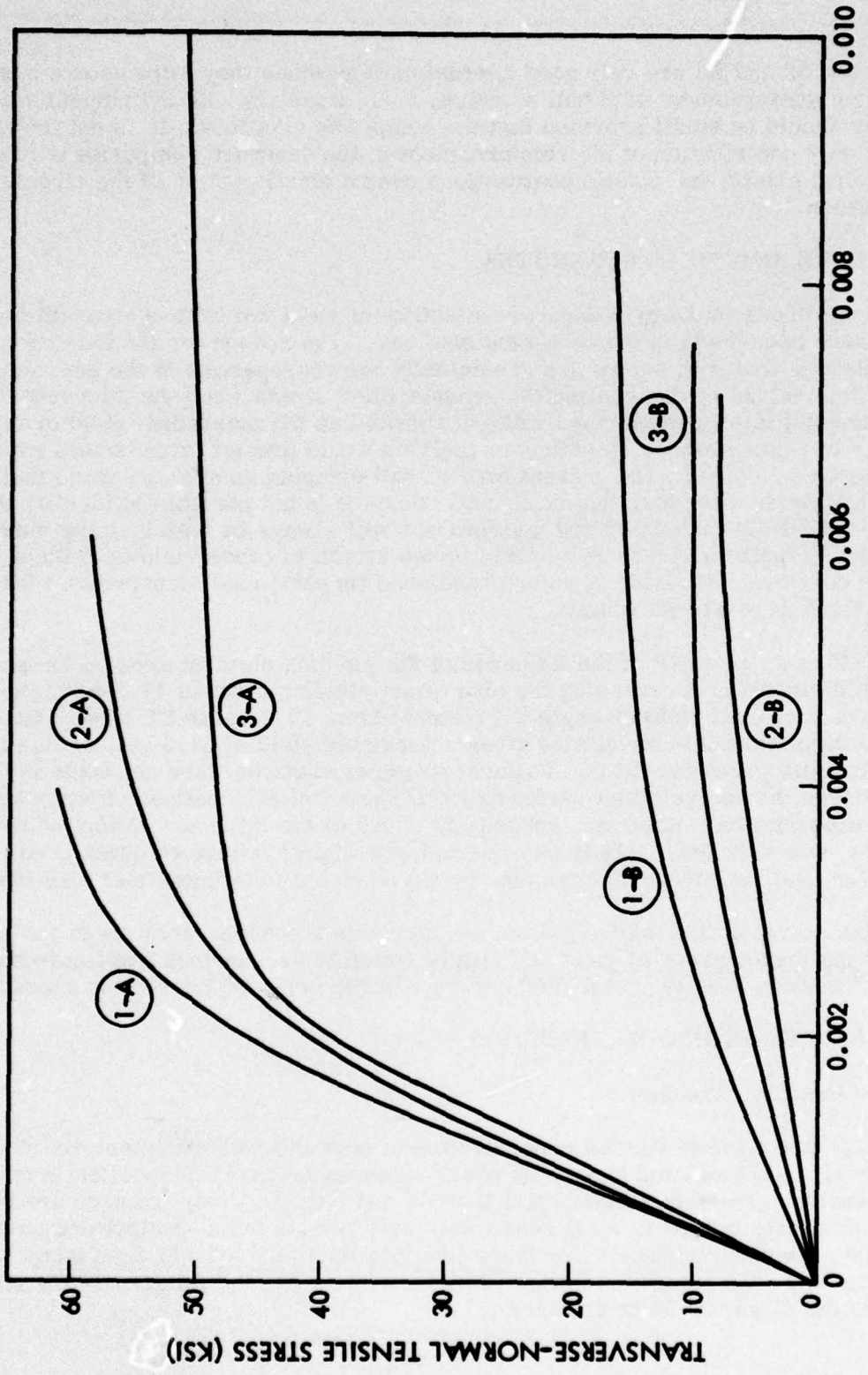

Fig. 3-14 PSTNT Stress-Strain Curves for UD 50 vol % B/Al(6061-T6) Composites With (-A) and Without (-B) Interface Bonding for Three Reinforcement Arrays: (1-) S1, (2-) S2, and (3-) HT

for debonded S2 and H1 are only good approximations since they were determined by assuming a reinforcement with null modulus, i.e., a matrix with cylindrical voids. The error should be small provided that the composite plastic strain is not too large, since the only contribution of the reinforcement in the debonded composite is to constrain lateral elastic and plastic contractions over a small portion of the circular cross section.

3.4 FAILURE AND YIELD STRENGTHS

Several references to the questionable reliability of yield and failure strength predictions have been made in the foregoing sections. The reason for the existence of a problem is that both properties are actually microproperties in the sense that they are determined by designating the gross applied stress when the microstress in some element attains a prescribed value designated as the octahedral yield or ultimate strength. In regions where a continuum analysis would predict large-stress gradients within one finite element, the present method will compute an average value that may be significantly smaller than the maximum. Since it is not possible to identify these a priori in the FEM, the predicted microvalues will always be less than the maximum, and this will require a larger-than-real applied stress to cause yield or failure. Also, failure is currently predicted at some prescribed (in part) load increment so that an error in the failure-stress results.

Figure 3-15 is an example of the influence of the yielding element area on the predicted yield strength. Decreasing the size of the yielding element 16 percent decreased the predicted yield strength 2.5 percent from 40.2 ksi to 39.2 ksi. Extrapolating to infinitesimal element size gives a predicted yield of 34.5 ksi, or 86 percent of the originally predicted value. Failure-stress predictions were not made in these cases because the analysis was performed with the unreliable belinear matrix stress-strain representation. However, subsequent check of the influence of applied load increment shown in Fig. 3-16 is as expected,with higher failure strength predicted for smaller load increment that can also be extrapolated to infinitesimal load increments.

Each of the extrapolation methods described above is a possible solution to the problem of improving the accuracy of yield and failure predictions, but they are time-consuming and can at best be used to give a good estimate of the error or correction needed.

3.5 INTERFACE STRESS DISTRIBUTION

3.5.1 No Residual Stresses

An analysis was made of volume concentration effects and reinforcement distribution on the interface-normal and tangential shear stresses for B/Al composites in transverse-normal tension. The interface-normal (tensile and compressive) stresses are believed to dominate failure in most reasonably well-bonded metal-matrix composites; in contrast, the shear stresses are more likely to dominate in weak interfaces when predominantely compressive interface forces are present and failure occurs according to the Coulomb-Mohr criterion.

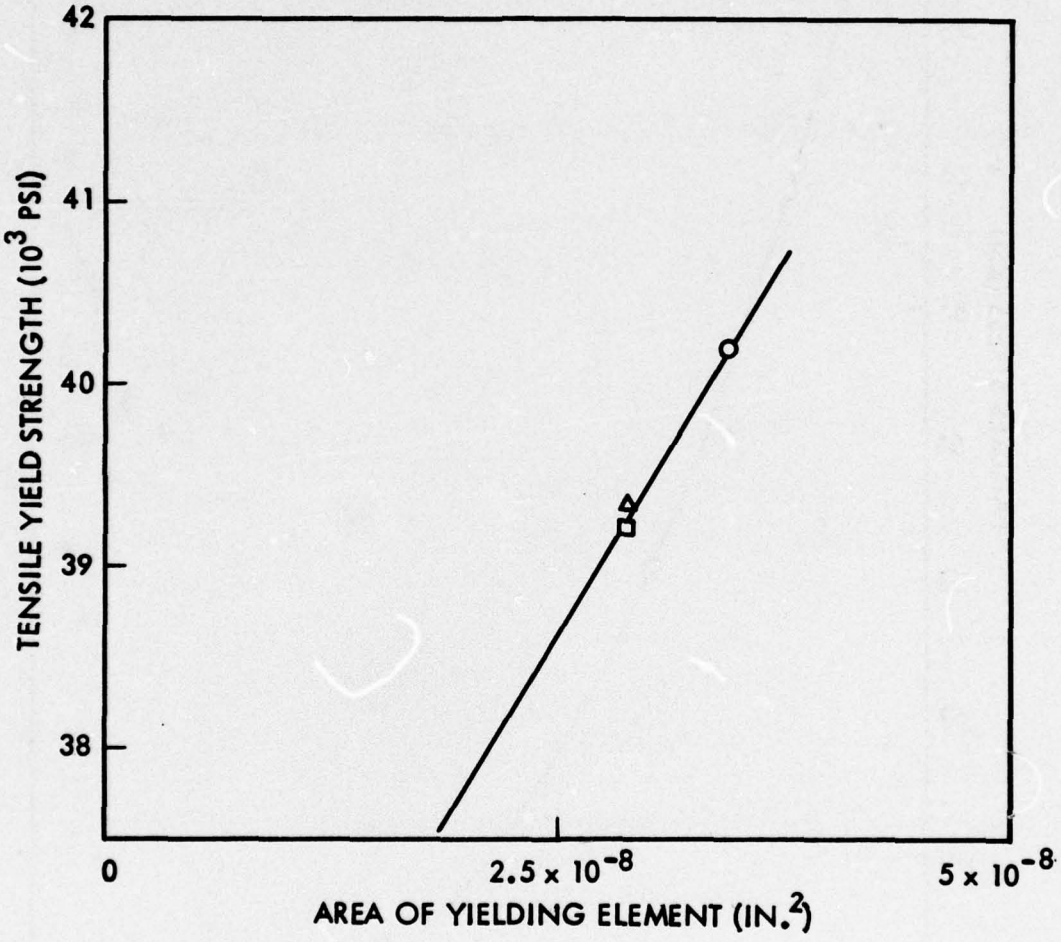

Fig. 3-15 Dependence of Predicted TNT Yield Strength on Size of First Finite Element to Experience Local Octahedral Yield Stress

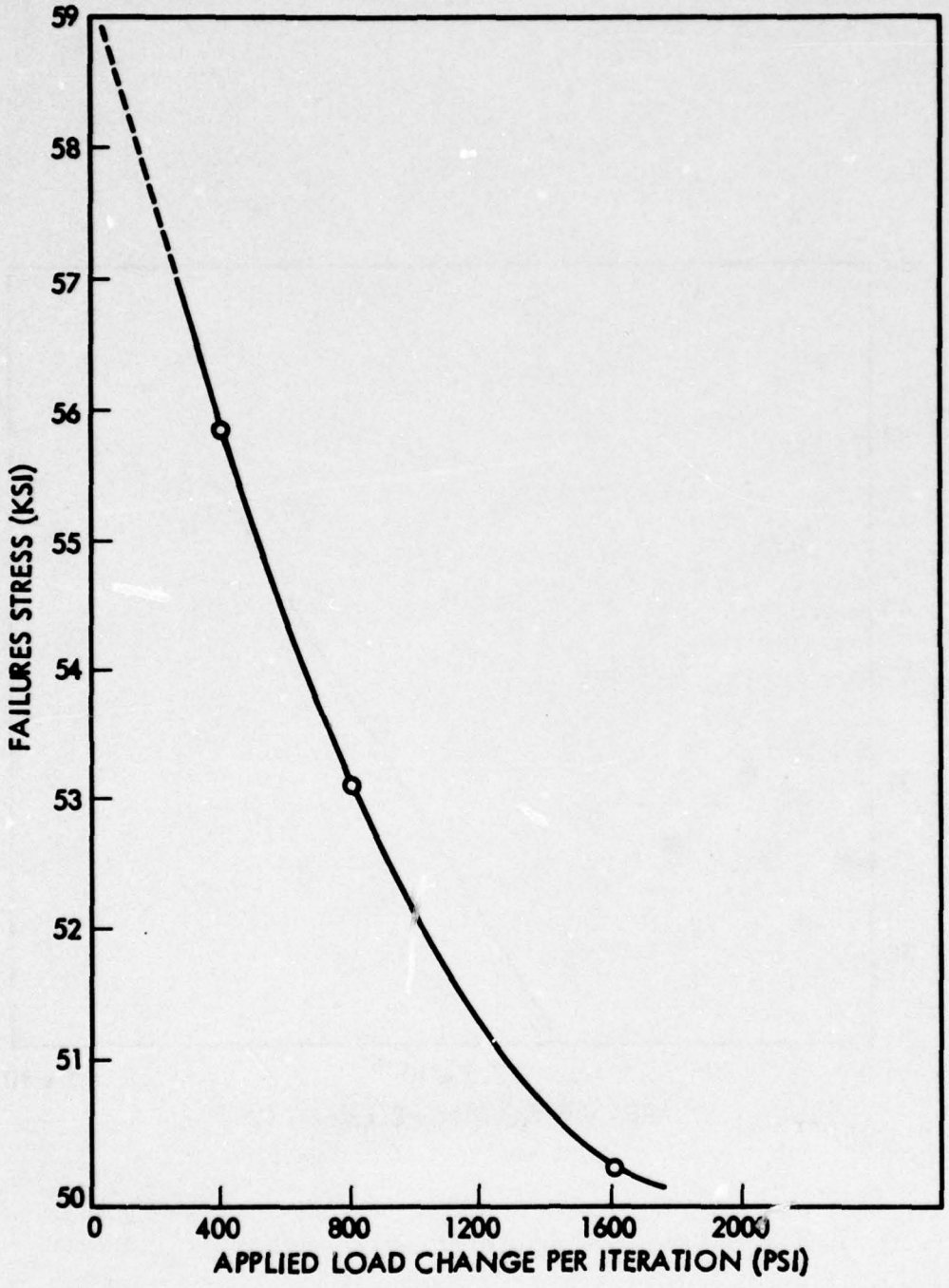

Fig. 3-16 Dependence of Predicted Failure Stress on Applied Load Increment Per Iteration and Evidence of Possible Extrapolation

The variations after two interface stresses with angular position from the loading direction for UD S1 B/Al with 20- , 50- , and 60-vol % reinforcement are presented in Fig. 3-17. Minor changes are produced by increasing the reinforcement concentration from 20 to 60 vol % with the greatest change at 0 deg, where the stress-concentration factor increases from about 1.4 to nearly 1.6, indicating that for a specified interface tensile strength, failure would occur for a slightly lower applied tensile stress for the higher volume fraction. The crossover point, where the interface-normal stress is zero, is virtually unaffected by the reinforcement concentration, so the interface failure is therefore expected to be equally catastrophic in either extreme of volume fraction. The shear stresses appear too small to contribute significantly to failure in the compressive normal-stress region. It is interesting to note that the stress distribution for a square array of fibers given by Ing-Wu Yu and Sendeckyj (Ref. 12) are qualitatively the same as those presented except that there is no interchange of relative position for the curves at approximately 13 deg; no negative values (compressive normal stresses) are predicted in the vicinity of 90 deg, and the referenced curves are reversed in order at 0 deg. These differences are probably the result of the different specific materials properties used in each analysis; i.e., the matrix and fiber Poisson's ratio used in the reference were 0 and 0.5, respectively. In the present analysis, however, values of 0.33 and 0.20 have been used.

A similar plot is presented in Fig. 3-18 to show how the interface stress distribution varies depending on the reinforcement packing arrangement and the relative applied stress direction for UD 50-vol % B/Al (6061) in an initially stress-free condition as were all previously described cases. A much greater qualitative as well as quantitative difference occurs as a result of varying arrays than does from concentration variations. The S2 configuration, for example, results in a 0-deg stress-concentration factor with only 2/3 the value of that for the S1 array. An even larger difference is apparent for H2 compared to either H1 or S1; H1 is only 0.6 of the S1. Also noteworthy is that neither the S2 nor the H1 array produces a compressive normal stress in the vicinity of the interface at 90 deg to the applied stress direction. This finding suggests that debonding failure in such cases might continue until the entire interface is debonded rather than the failure arresting around 70 deg as observed previously for case S1 (Ref. 1). The third significant difference is noted in the H2 array, which has a peak stress-concentration factor at about 30 deg from the applied bend direction instead of the customary 0 deg. In such a case, failure would initiate at four points around a typical filament (one in each quadrant), and the interface crack formed would propagate in opposite directions from each point until debonding extended around the entire portion of each reinforcement where the normal stresses are tensile in the well-bonded case. As before, the interface tangential shear stresses, distribution, though significantly different for each array, are not of sufficient magnitude to merit consideration, as mentioned above in the analysis of concentration effects.

When no residual stresses are present initially in a composite, before transverse-normal loading, there is little change in the interface stress distribution pattern or stress concentration factor, as the external load is increased beyond initial yield. Thus, the concentration factors and the analysis presented for the figures described above are generally applicable to any state of uniaxial TNT stress.

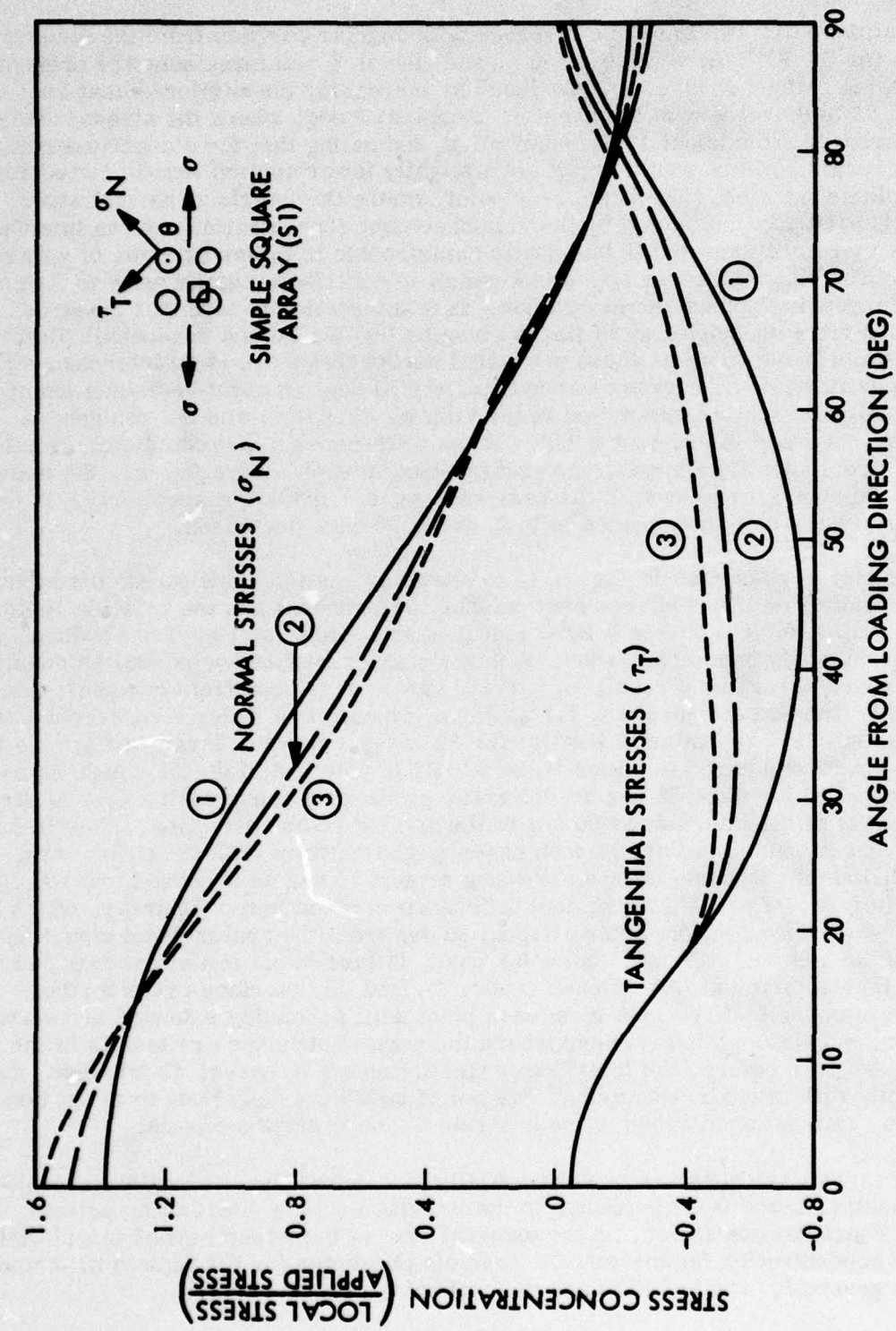

Fig. 3-17 Theoretical Variation of Interface Stress Concentration Factors With Angle From Applied TNT Load Direction in UDSS B/Al(6061) Composites With Three Reinforcement Concentrations: ① 20 vol %, ② 50 vol %, and ③ 60 vol %

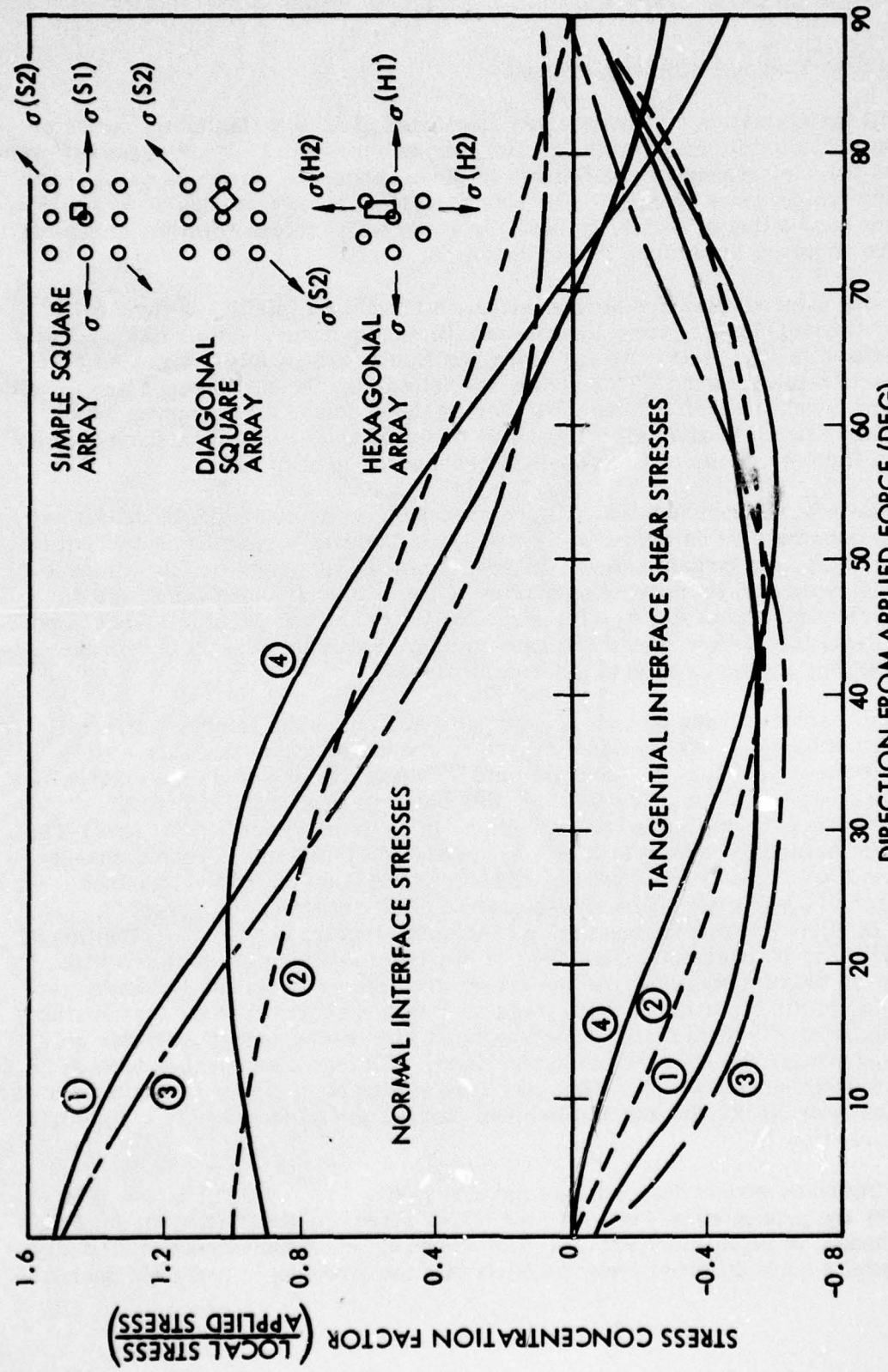

Fig. 3-18 Theoretical Variation of Interface Stress Concentration Factors With Angle From Applied TNT Load Direction for UD 50 vol % B/Al(6061) Composite With Two Reinforcement Arrays and Two Orientations: ① S1, ② S2, ③ H1, and ④ H2

3.5.2 Residual Thermal Stresses Present

Virtually all metal-matrix composites are fabricated at an elevated temperature or they will be subjected to temperature cycling during service. Because of the difference between the thermal expansion coefficients of the constituents, stresses will be induced during temperature changes. For this analysis a change of -250° F was selected to represent the cooling of aluminum (6061) to room temperature from the annealing temperature required to produce the T6 condition.

The thermally induced interface normal stresses for S1, S2, and H1 arrays in UD 50 vol % B/Al (6061) cooling from the T6 annealing temperature are plotted against angular position in Fig. 3-19. As the 0-deg position is arbitrarily designated here as that direction in which the UTNT stress is applied, the S1 and S2 cases are identical with the curves relatively displaced by 45 deg on the abscissa. The curves do not coincide exactly because of small differences in actual values resulting from the use of interface finite elements of somewhat different sizes in each case.

The interface-normal residual-thermal stresses induced on cooling B/Al (6061) are everywhere compressive as indicated by the larger thermal expansion coefficient of the matrix. Also, the largest values of stress occur at the points on the reinforcement surface closest to its nearest neighbors, i.e., at 0 and 90 deg for S1 (or 45 and 135 deg for S2), and at 0, 60, 120, etc., for the hexagonal packing. As will be shown in a section to follow, these stresses greatly modify the plastic flow of the matrix on subsequent application of external stresses.

The residual thermal stress state in a composite influences the interface-normal stress distribution also. As would be expected, the distribution transforms progressively to the case where residual thermal stresses are absent as the external stress is increased. The manner in which this occurs is shown in Fig. 3-20, where the interface-normal stress distribution, in a UD S2 50 vol % B/Al (6061-T6) composite, is plotted for a temperature change of -171° F and an additional change of -79° F for a total change of -250° F, and after the application of a UTNT load in three steps to 22,667 psi. The stresses are initially radially compressive, increasing in intensity with the magnitude of the temperature change. Application of a small UTNT stress causes the compressive stresses to decrease slightly, with little change in the distribution. As the external stress is increased, much larger changes occur in the direction of that stress such that it approaches the distribution for the initially stress-free state. The maximum stress-concentration factor only gradually approaches the nonresidual stress case, with the value equal to 0.88 at 22,667 psi applied UTNT instead of 1.0. Also, the zero stress point shifts quite slowly toward 90 deg so that even at 22,667 psi applied load most of the interface is in a state of radial compression.

The radial interface stress distributions for arrays S1, S2, and H1 of 50 vol % B/Al (6061-T6) are presented in Fig. 3-21 for UTNT stressing to 22,667 psi, following a -250° F change to room temperature. The S2 and H1 conditions produce virtually identical results quite different from the S1 in that the stresses in that case decrease

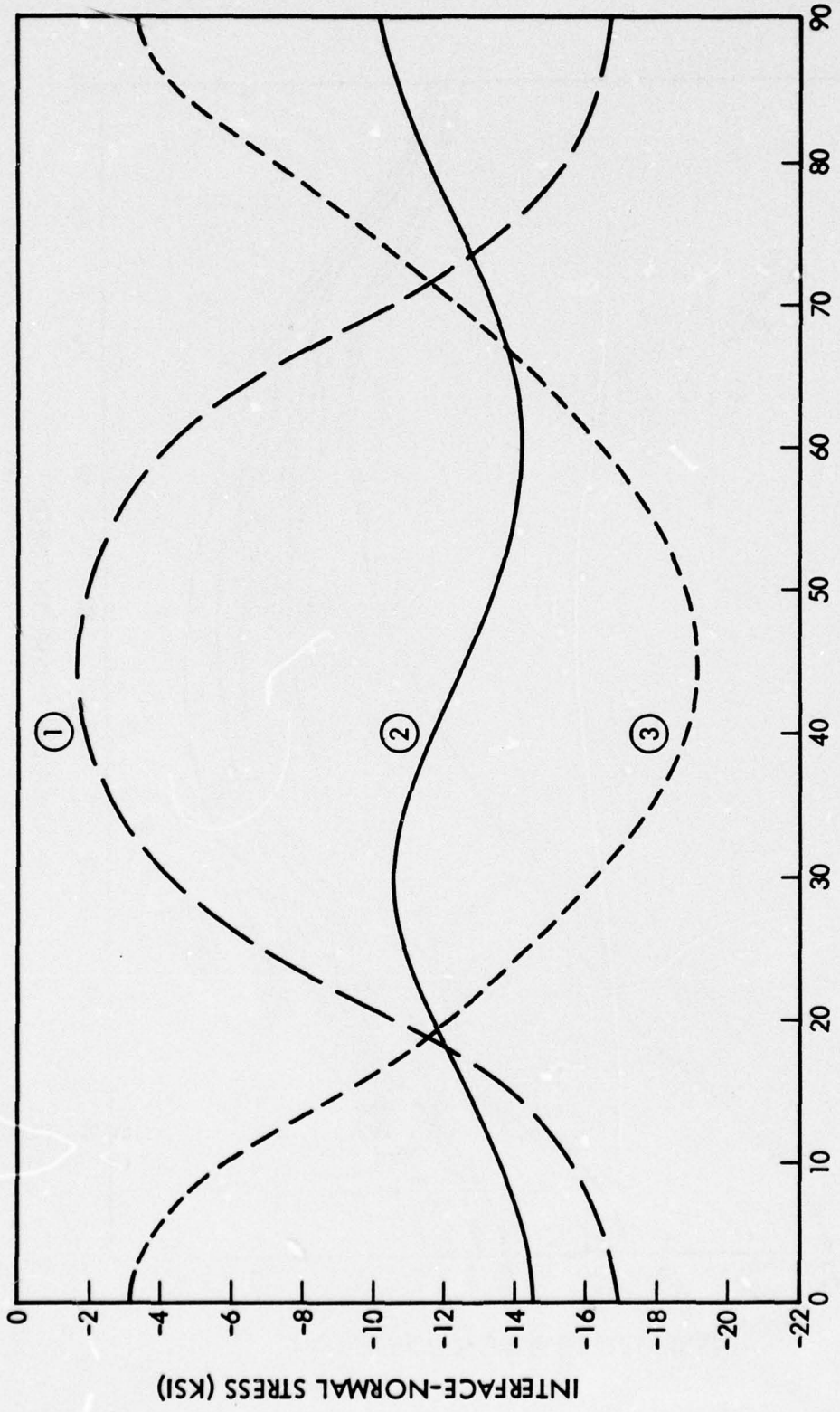

Fig. 3-19 Variation of Interface-Normal Stress With Angular Position From Transverse-Transverse Direction, After a -250°F Temperature Change in UD 50 vol % B/Al(6061) Composites With Reinforcements Arranged as Follows: ① Square (S1), ② Hexagonal (H1), and ③ Square (S2)

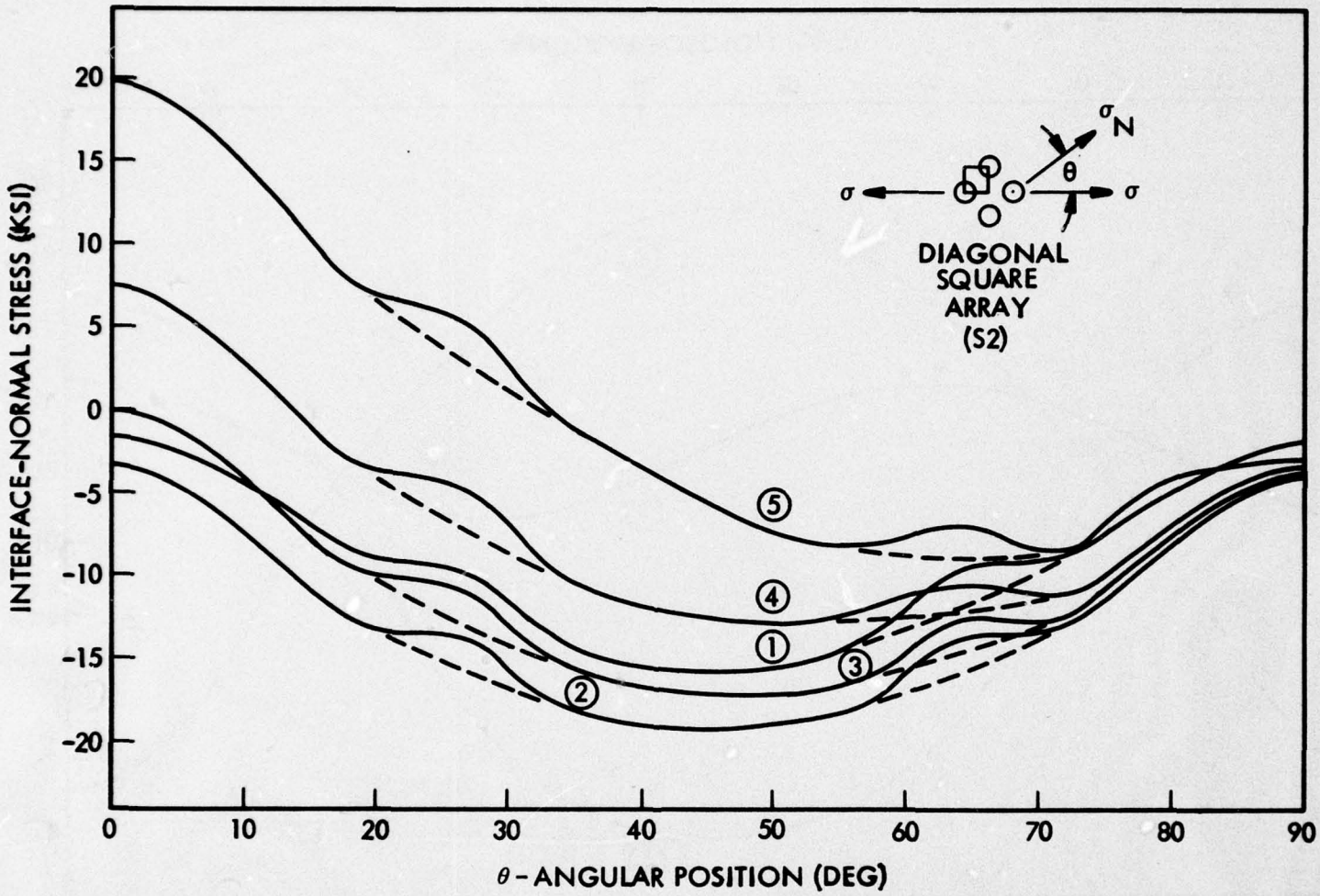

Fig. 3-20 Variation of Interface-Normal Stress With Angular Position From Applied Stress Direction in UDS1 50 vol % B/Al Composite After ① -171°F Temperature Change, ② -250°F Temperature Change, ③ -250°F Temperature Change Plus a 346-psi Applied TNT Stress, ④ Same With 10,667-psi Stress, ⑤ Same With 22,667-psi Stress

LOCKHEED PALO ALTO RESEARCH LABORATORY
LOCKHEED MISSILES & SPACE COMPANY, INC.
A SUBSIDIARY OF LOCKHEED AIRCRAFT CORPORATION

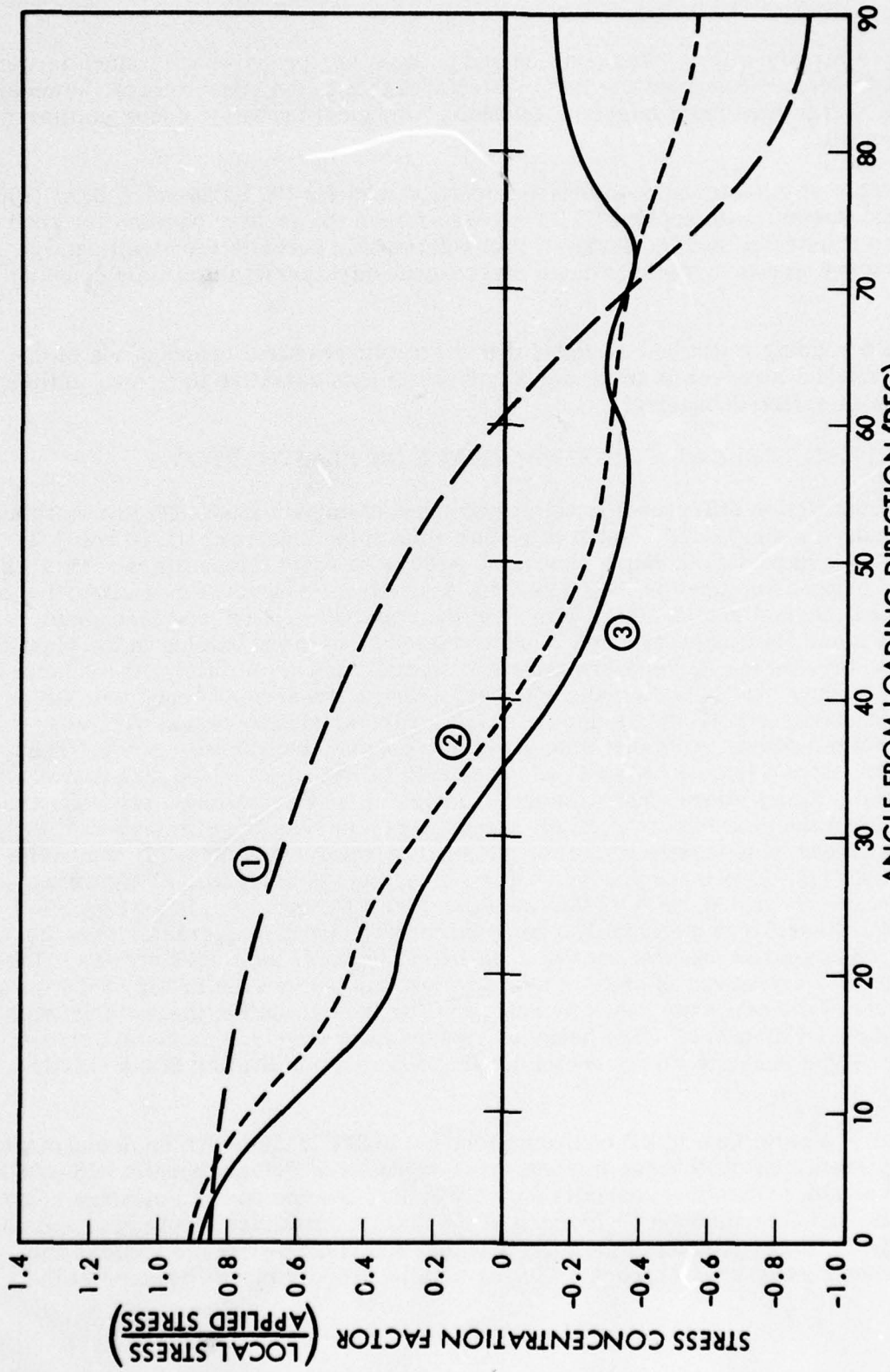

Fig. 3-21 Variation of Interface-Normal Stress Concentration Factor With Angular Position From Applied Stress Direction, After a -250° F Temperature Change and an Applied TNT Stress of 22,667 psi on UD 50 vol % B/Al(6061) Composites With Following Arrays and Loadings: ① S1, ② H1, and ③ S2

much more rapidly with angular position and become compressive at a much larger angle. The stress-concentration factor is comparable to the other arrays, however, indicating that failure from interface debonding will most probably occur similarly for each case.

The variation of the maximum interface normal stress for UD S1 50 vol % B/Al (6061-T6) varies linearly with applied UTNT stress as does the angular position for zero stress, as illustrated in Fig. 3-22. If this relationship persists for significantly higher applied stresses, the maximum stress-concentration would remain constant at 0.88.

From the foregoing it can be concluded that the major practical consequence of the thermal residual stresses is to render a composite less sensitive to failure initiation from interface debonding.

3.6 RESIDUAL THERMAL STRESS INFLUENCE ON PLASTIC FLOW

Thermal contraction differences between boron and aluminum (6061-T6) are sufficiently large to induce a singificant amount of plastic flow in the matrix of UD 50 vol % B/Al (6061-T6) composites during a change of -250° F to room temperature. This will produce a noticeable affect on the transverse mechanical behavior since alteration of the residual thermal stress state, with even the smallest applied load increment, will cause some local unloading and in other regions increased loading in the plastic range such that the micro yield strength is essentially zero. Actually, the volume of matrix loading plastically and the changing internal stresses are such that the theoretical stress-strain curves appear to have a linear elastic region with an apparent elastic modulus somewhat smaller than the same, but initially stress-free composites, except for the S2 case, as illustrated in Fig. 3-23. The differences between the initially stress-free case and the case of residual thermal stresses are accented when the elastic portion of the stress-strain curves are eliminated to produce a stress/plastic-strain plot for each UD 50 vol % B/Al(6061-T6) composite array as in Figs. 3-24 through 3-26. Of the three arrays analyzed, S1 shows the greatest work-hardening, with S2 the lowest and H1 intermediate. In every case the initially stress-free material has an apparent work hardening greater than the material with residual thermal stresses, at least for small total TNT strains. There appears to be a crossover at greater total strains as can be seen in Fig. 3-26 for case H1 and in the other two cases by extrapolating the curves for the material with residual thermal stresses. This behavior results from the complex matrix stress interactions that result in concurrent unloading (elastic) and loading in the elastic and plastic ranges.

The extent of plastic flow in UD composites under UTNT loading can be demonstrated clearly by examining the change in transverse-transverse Poisson's ratio with applied stress or strain. When the matrix is entirely elastic the composite Poisson's ratio is also elastic and determined as a function of the elastic constituent properties. As a progressively larger portion of the matrix enters the plastic state the value of the total Poisson's ratio will approach unity, or a value slightly larger because of the

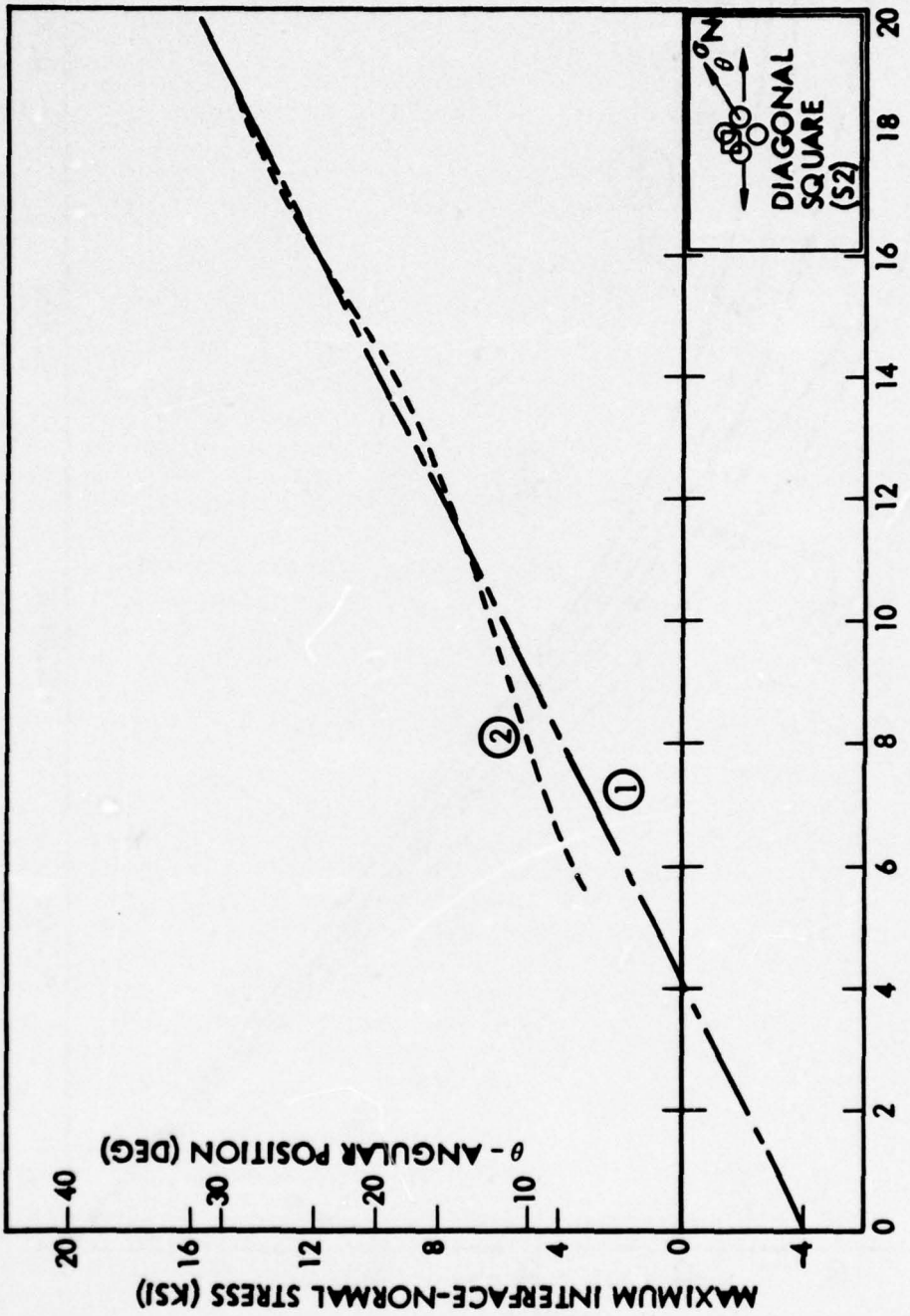

Fig. 3-22 Variation With Applied TNT Stress of: ① Maximum Interface Normal Stress and ② Angular Position for Zero Interface Normal Stress, in a UDS2 50 vol % B/Al(6061-T6) Composite Loaded in PSTNT After a -250°F Temperature Change

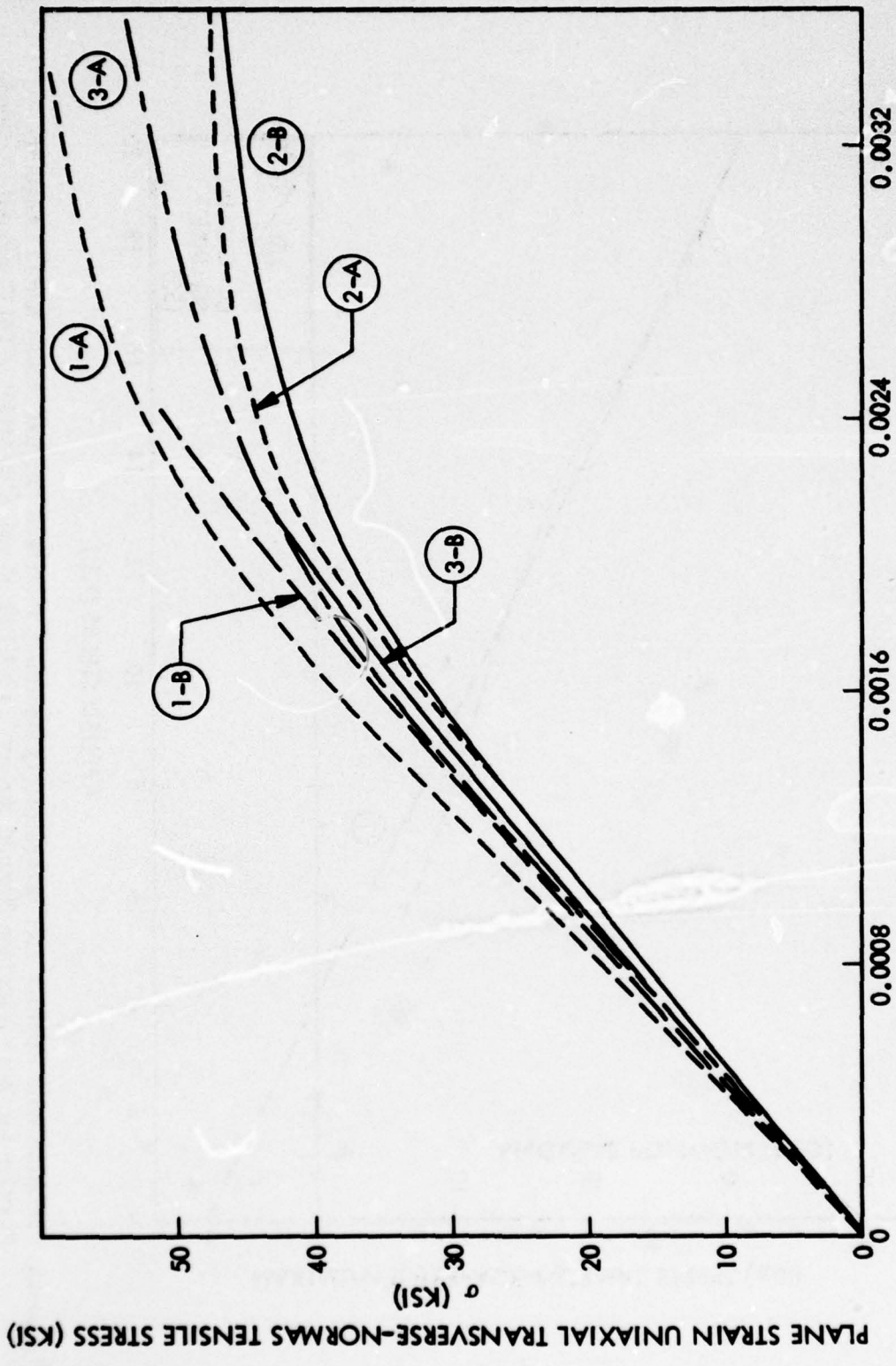

Fig. 3-23 Calculated PSTNT Stress-Strain Curves for UD 50 vol % B/Al(6061-T6) Composite Initially (-A) Stress-Free and (-B) With Residual Stresses From a -250°F Temperature Change, and Three Reinforcement Arrays: (1) S1, (2) S2, and (3) H1

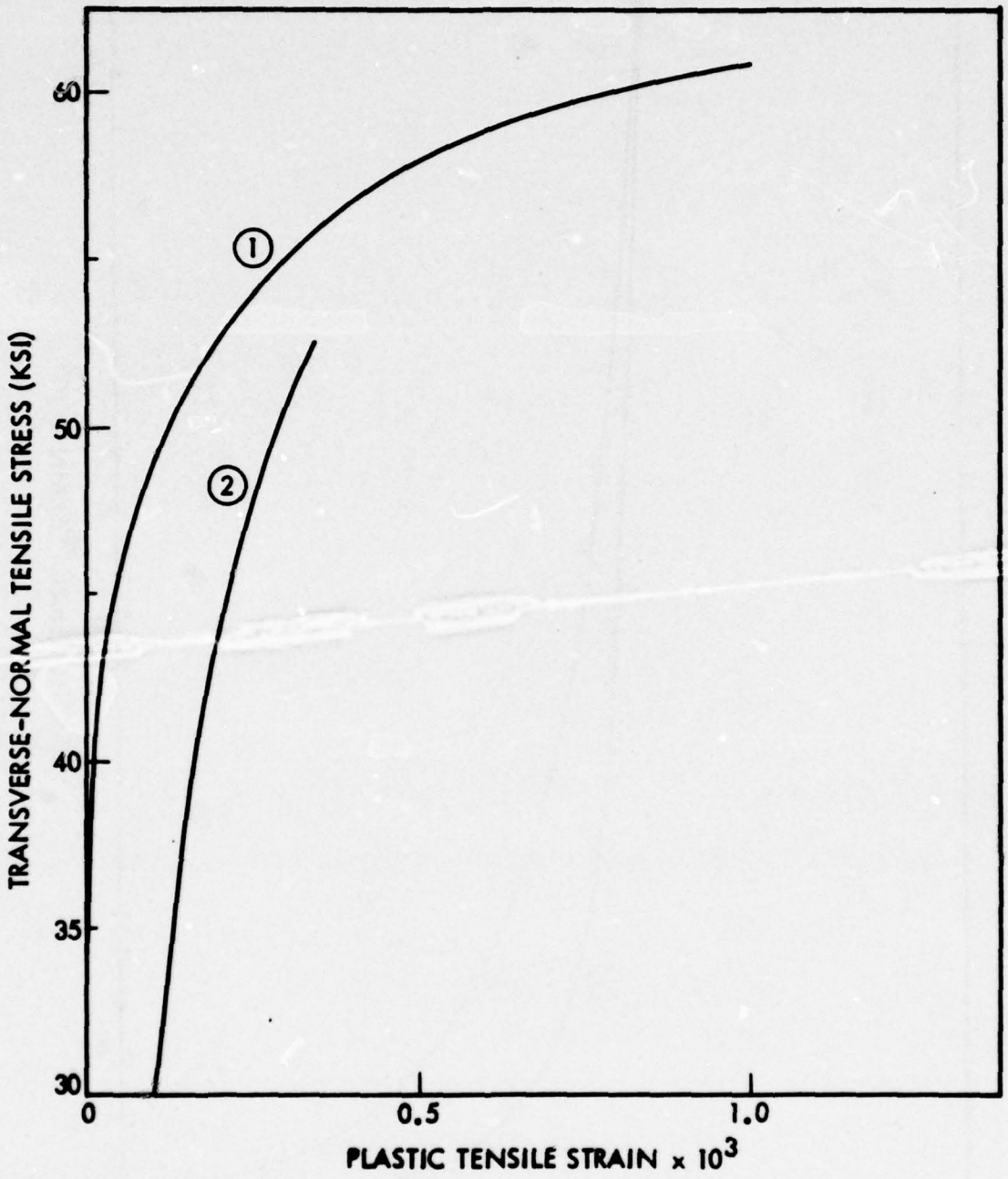

Fig. 3-24 Calculated PSTNT Stress-Plastic Tensile Strain Curves for UDS1 50 vol % B/Al(6061-T6) Composite; Initially (1) Stress-Free and (2) With Residual Stresses From -250°F Temperature Change

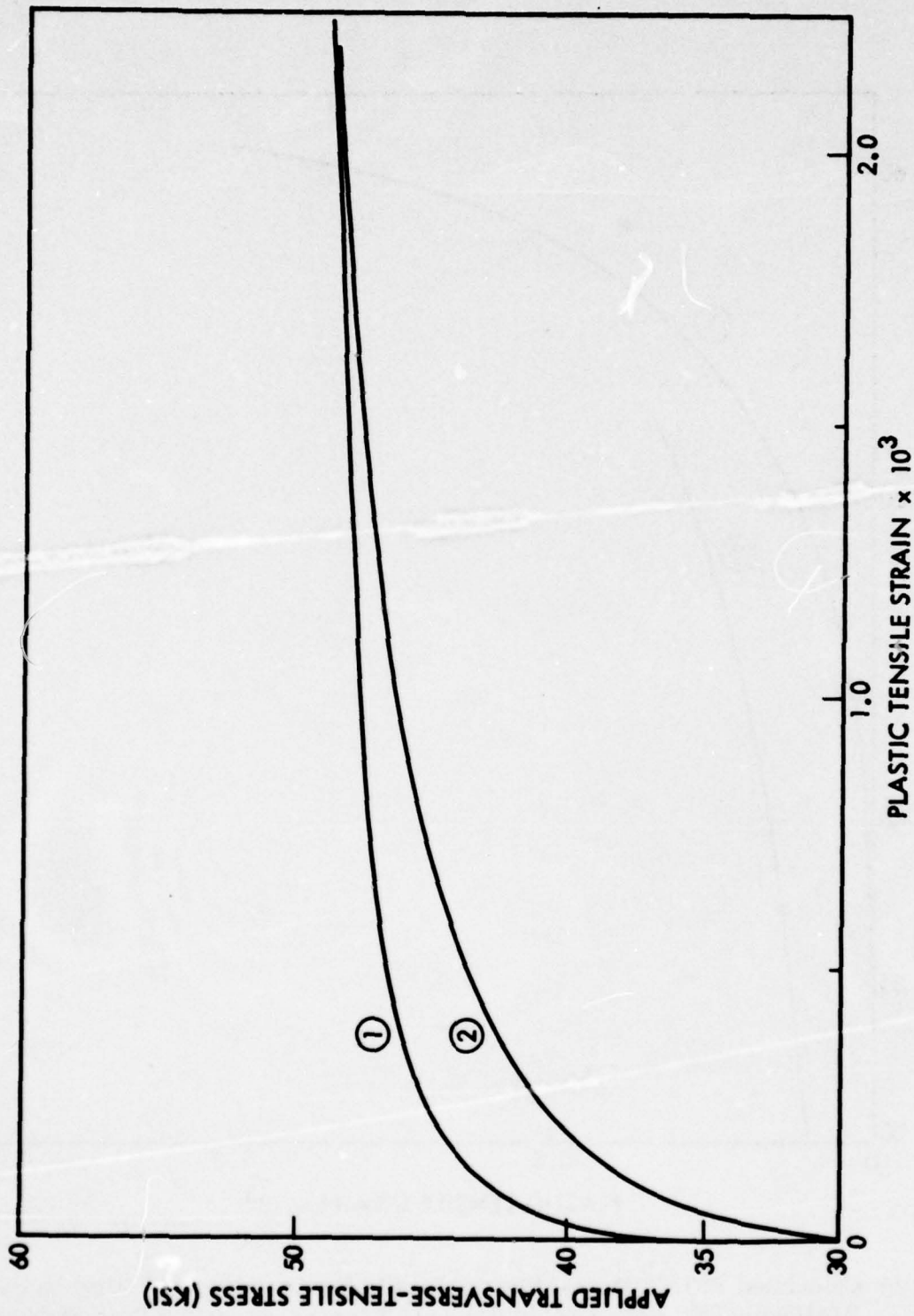

Fig. 3-25 Calculated PSTNT Stress-Plastic Tensile Strain Curves for UDS2 50 vol % B/Al(6061-T6) Composite; Initially ① Stress-Free and ② With Residual Stress From -250° F Temperature Change

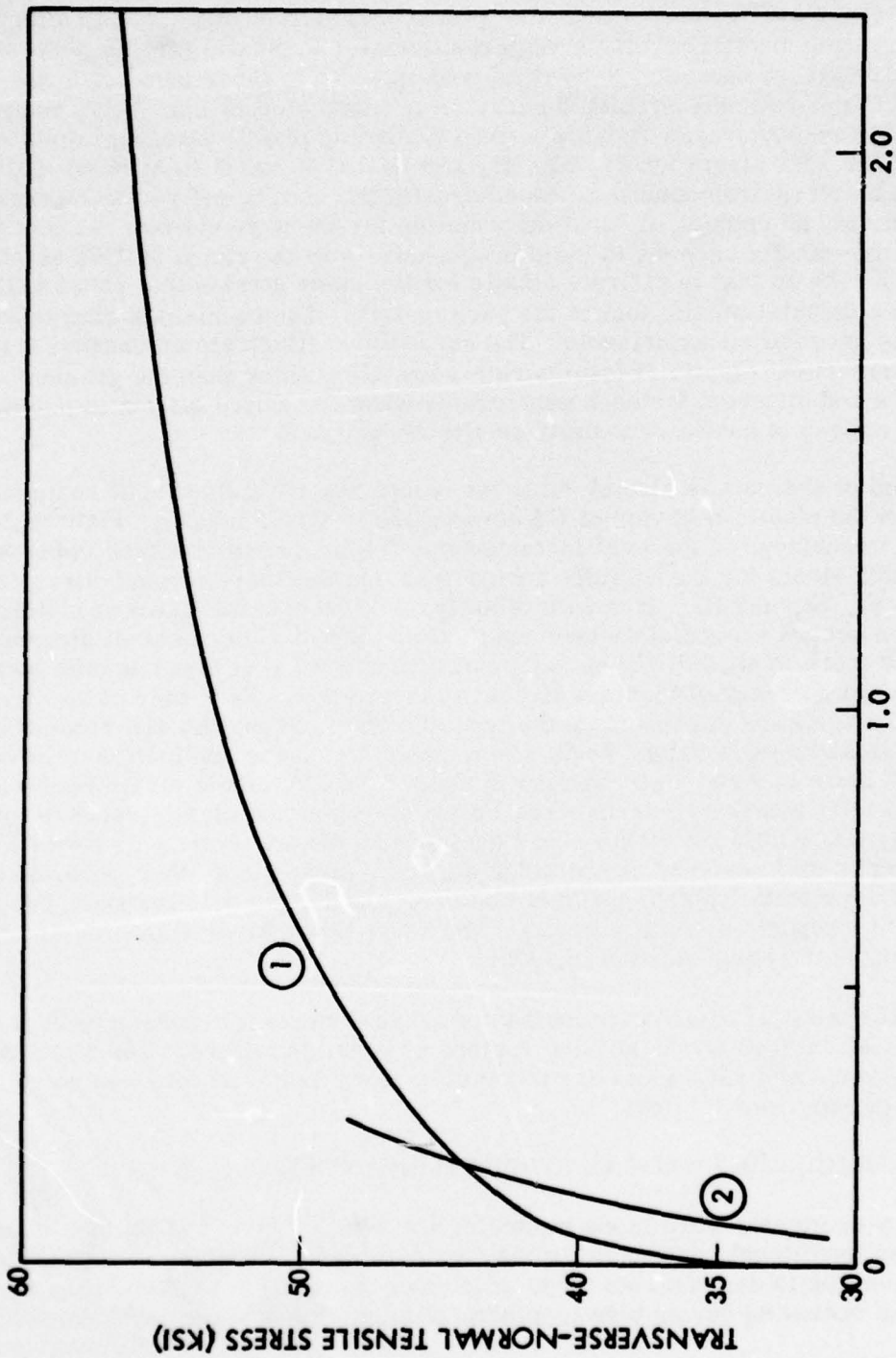

Fig. 3-26 Calculated PSTNT Stress-Strain Curves for UDH1 50 vol % B/Al(6061-T6) Composite; Initially ① Stress-Free and ② With Residual Stresses From -250°F Temperature Change

contribution of the reinforcement. The near unity value results from the longitudinal constraint of the stiff reinforcement that produces a virtual plane-strain situation such that conservation of matrix volume requires transverse plastic strains perpendicular to the applied stress direction to be equal and opposite to those parallel to the applied stress. The theoretically predicted behavior is illustrated in Fig. 3-27, where the total transverse-transverse Poisson's ratio (including plastic strains) is plotted as a function of the TNT strain for S1, S2, H1, and H2 UD 50 vol % B/Al (6061-T6) composites initially in a stress-free condition, together with the matrix and reinforcement Poisson ratio, assuming no necking or local deformation for the pure matrix. Except for case H1, the entire matrix appears to yield progressively in the range of TNT strain from 0.0015 to 0.0035 so that is entirely plastic for the same strains that cause uniform yielding in a uniaxial tensile test of the pure matrix. The anomalous character of the H1 curve is presently unexplainable. The curves also illustrate an unusual feature in that the composites' elastic Poisson's ratios are all greater than the greatest of the constituents and different for each case except when the entire matrix is plastic and the values appear to converge to unity or slightly greater.

This method of analysis is also of value for comparing the influence of residual thermal stresses on the plastic behavior of UD composites in UTNT loading. Figures 3-28 through 3-30 are comparisons of the total instantaneous transverse-transverse Poisson's ratios versus UTNT strain for the initially stress-free and thermal-residual-stress cases for arrays S1, S2, and H1. It is immediately apparent that the onset of matrix plastic deformation occurs immediately upon application of load when residual stresses are present, as there is essentially no region of constant ratio at lower tensile strains as observed when no residual thermal stresses are present. Each pair of curves has unique characteristics dependent on the type of array. S1 and H1 are similar in that the total Poisson's ratio values begin rising rapidly with the application of load, whereas for case S2 there is a region from zero to about 5×10^{-4} tensile strain where the increase of total transverse-transverse Poisson's above the elastic value is imperceptible. Also, array H1, within the strain range analyzed, does not produce as large a total Poisson's ratio difference as do the other arrays. Analysis of other differences, such as with the asymptotic values, could not be performed under this program but will be described in a report on similar work for the U.S. Naval Air Systems Command to be published by the same authors in 1975.

Figure 3-31 shows the alternative method of presenting plastic-zone growth data that has certain advantages for identifying regions of possible failure. The total transverse-transverse Poisson's ratio plots are potentially more useful as they can be compared directly with experimental data.

3.7 MICROMECHANICS – LOCAL STRESSES AND STRAINS

Introductory comments were made regarding the advantages of the finite-element method over traditional continuum mechanics methods. Additional data are presented in this subsection to demonstrate these advantages in addition to elucidating the mechanisms operating during elastic-plastic deformation of UD composites with and

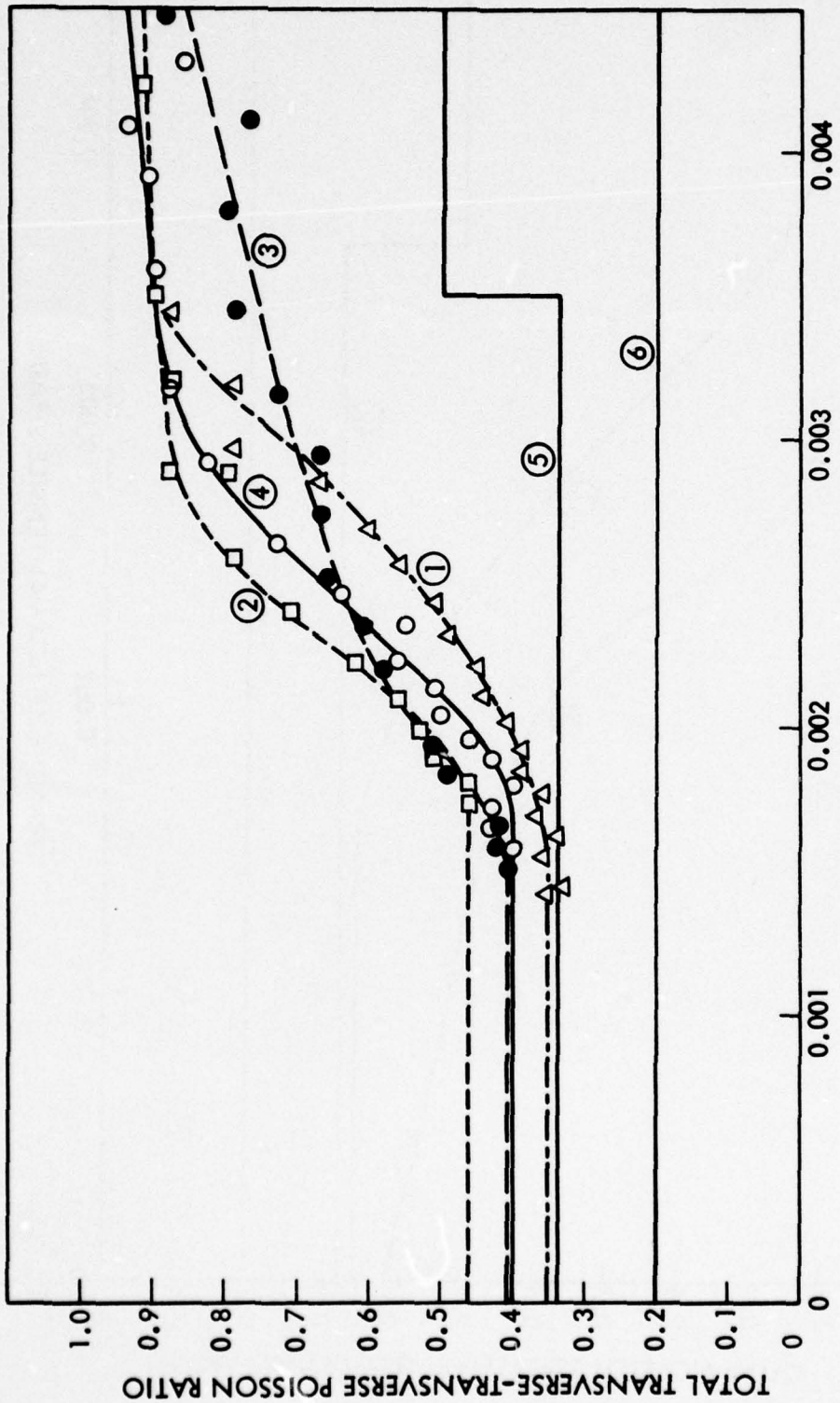

Fig. 3-27 Calculated Plane-Strain Total Transverse-Transverse Poisson Ratio Versus TNT Strain for UD 50 vol % B/Al(6061-T6) Composites Reinforcement Array as Follows: ① S1, ② S2, ③ H1, and ④ H2. Included for comparison are the curves for: ⑤ Al(6061-T6) and ⑥ boron

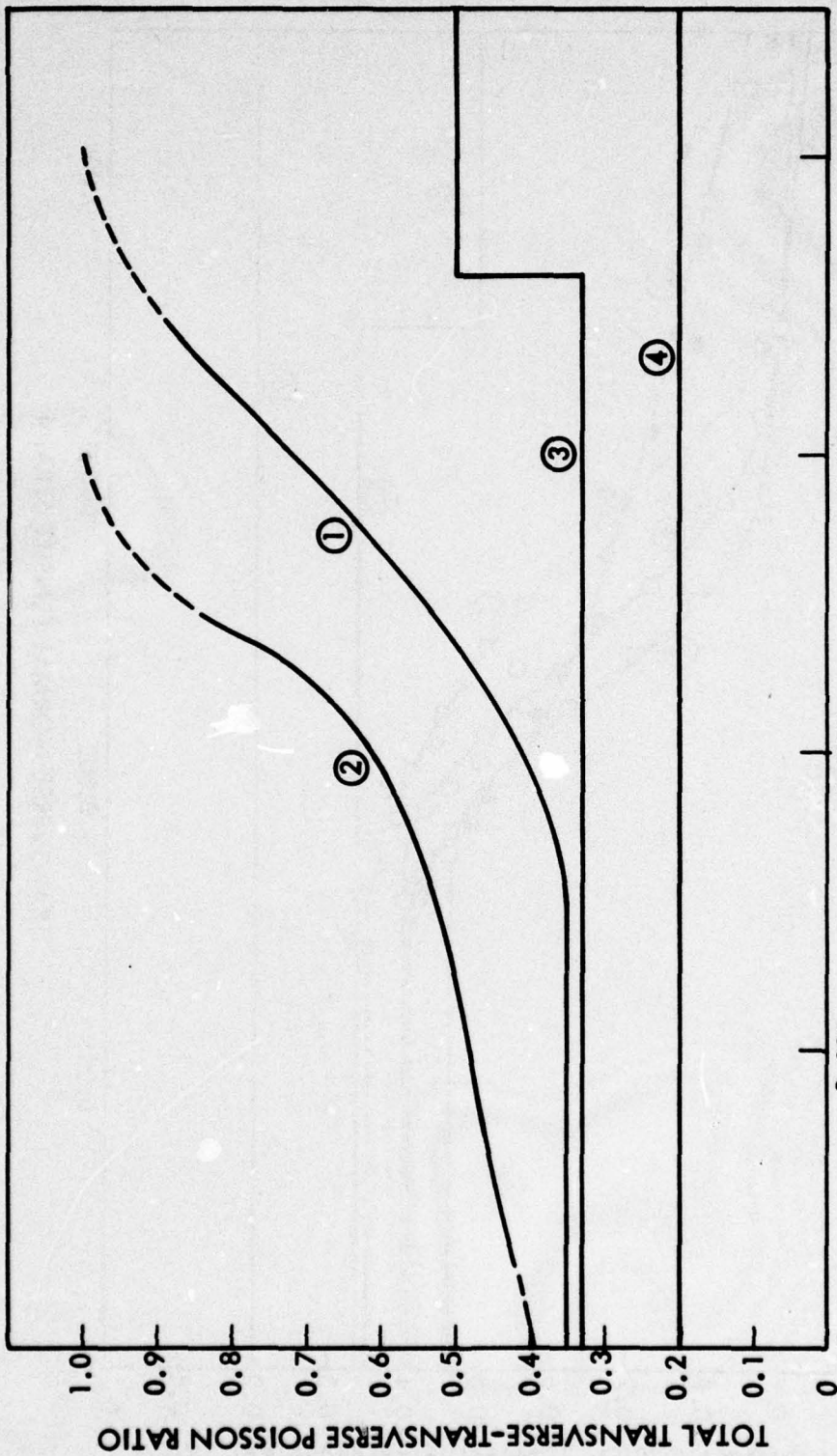

Fig. 3-28 Calculated Plane-Strain Total Transverse-Transverse Poisson Ratio Versus TNT Strain in UDSi 50 vol % B/Al(6061-T6) Composite; Initially ① Stress-Free and ② With Residual Stresses From -250°F Temperature Change. Included for comparison are curves for ③ Al(6061-T6) and ④ boron

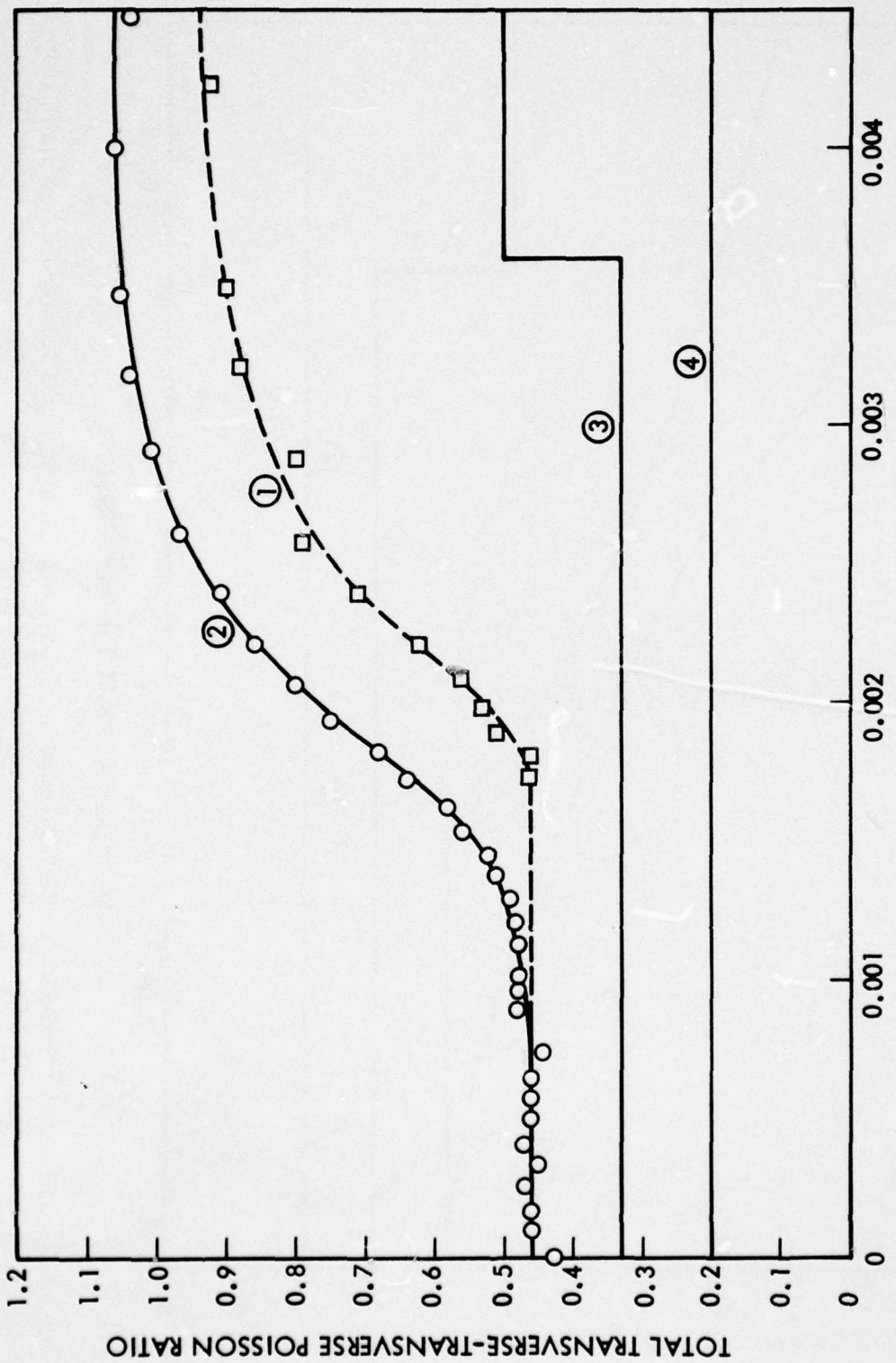

Fig. 3-29 Calculated Plane-Strain Total Transverse-Transverse Poisson Ratio Versus TNT Strain in UDS2 50 vol % B/Al(6061-T6) Composite; Initially ① Stress-Free, and ② With Residual Stresses From -250°F Temperature Change. Included for comparison arc curves for ③ Al(6061-T6) and ④ boron

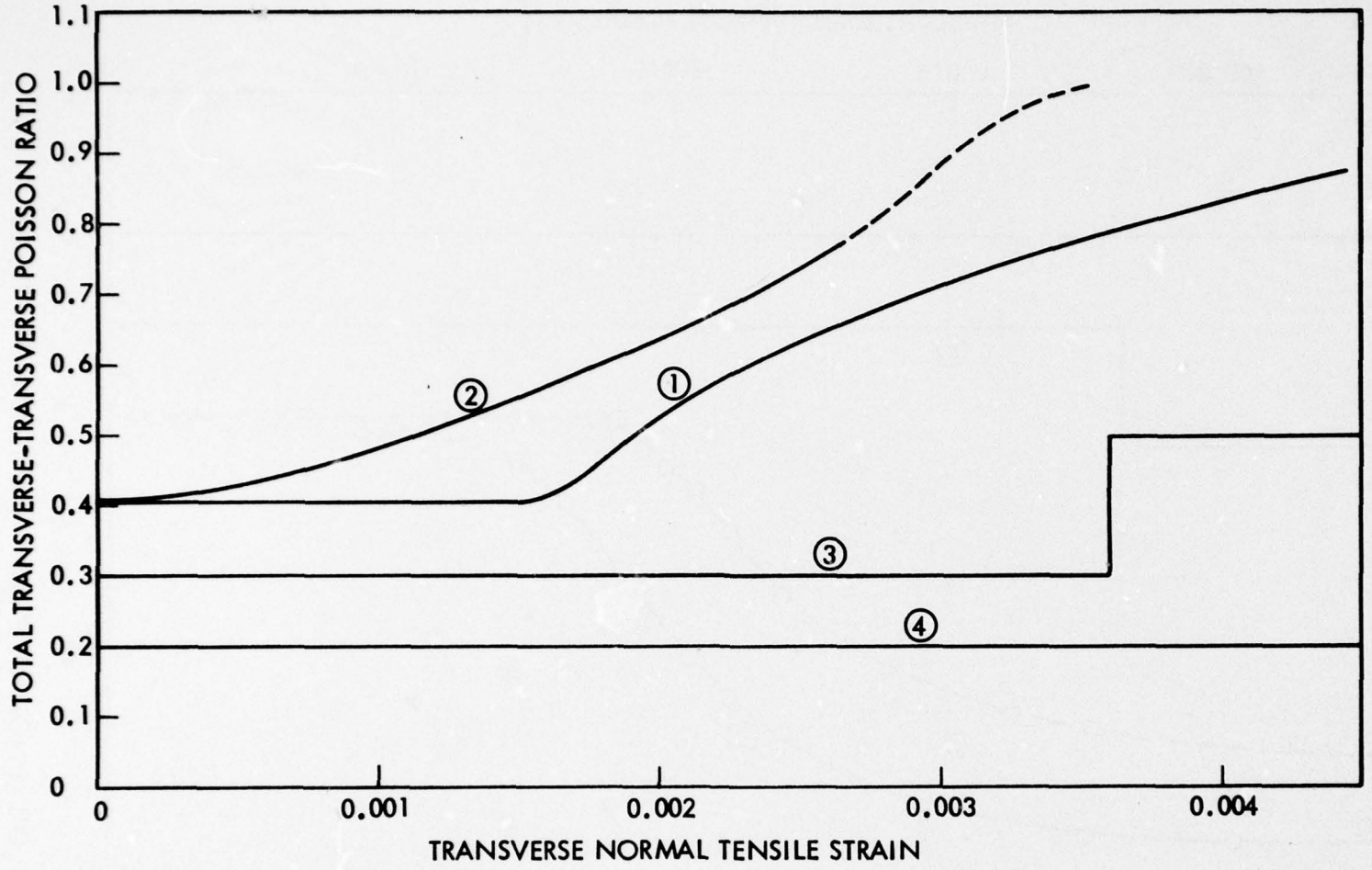

Fig. 3-30 Calculated Plane-Strain Total Transverse-Transverse Poisson Ratio Versus TNT Strain in UDH1 50 vol % B/Al(6061-T6) Composite; Initially (1) Stress-Free and (2) With Residual Stress From -250°F Temperature Change. Included for comparison are curves for (3) Al(6061-T6) and (4) boron

LOCKHEED PALO ALTO RESEARCH LABORATORY
LOCKHEED MISSILES & SPACE COMPANY, INC.
A SUBSIDIARY OF LOCKHEED AIRCRAFT CORPORATION

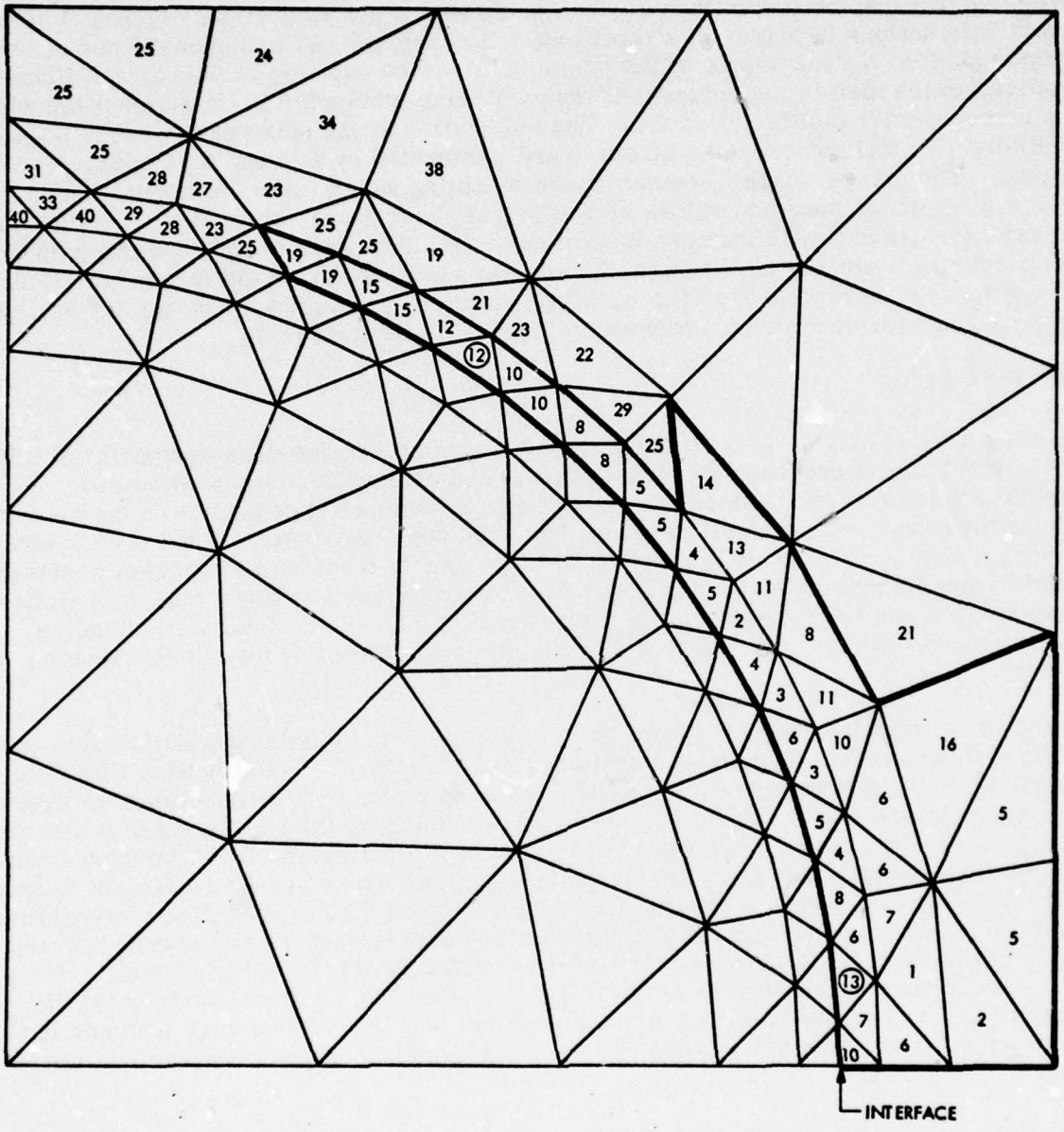

Fig. 3-31 Calculated Plastic Zone Growth With Applied PSTNT Stress for UDS1 50 vol % B/Al(6061-T6) Composite. Heavy outline is predicted zone at failure with 54,416-psi load when bilinear matrix stress-strain representation was used, and remainder is zone predicted for failure at 59,459 psi, using five-segment, piece-wise-linear matrix stress-strain representation. Each number indicates sequence of yielding. Failure was predicted at (13) for bilinear representation and (12) for piece-wise linear representation, and iterations 17 and 38, respectively

without residual thermal stresses. These are stress-vector plots with plastic-zone overlays that are available from any computer with a graphics link by appropriate program instructions to print, on a repeating cell chart, sets of orthogonal lines of lengths proportional to the magnitude of the principal stresses existing at the point of intersection, which also is the centroid of the particular triangular finite element for which the stress-vector plot is called for. The orientation of the principal stresses is plotted realistically, and compressive stresses are designated by a letter C at each end of the vector. The plastic zones were delineated by noting which finite elements, at the end of a computer run, had values of octahedral shear stress exceeding the value for a uniaxial tensile test with the pure matrix material, then smoothing a boundary through the bordering elements to eliminate the angular features that would otherwise results as can be seen in Fig. 3-31. The resulting plots are presented for cases S1, S2, and H1 with and without residual stresses in Figs. 3-32 through 3-37.

3.7.1 S1 Array

Loading a UDS1 50 vol % B/Al(6061) residual-thermal-stress-free composite in UTNT to the yield stress produces the internal principal stress distribution shown in Fig. 3-32(a). The reinforcement is in a fairly uniform state of tension in the applied stress direction, with a small compression at 90 deg. In constrast, the matrix stress is very nonuniform. There is a region of large double tension in the region where the reinforcements are closest along the applied stress direction, and a region of moderate compression and little tension in the corresponding region at 90 deg to the loading direction. As can be expected, yielding begins in the region of high double tension, as shown.

Doubling the UTNT produces little change in the uniform distribution that existed earlier in the reinforcement, though the magnitudes are increased. The situation within the matrix is changed significantly, however, with large principal stress rotations occurring near the reinforcement, double compression developing at the 90-deg position and the plastic zone now occupying the entire matrix except for a small region farthest from the reinforcements. Initially, the plastic zone exists very close to the matrix as was determined by duplicating a similar run using the same FEG with the interface shifted one band of elements toward the reinforcement center so that the two narrowest circular bands of elements were bounding the interface in the matrix [see Fig. 2-4(e)]. The plastic zone was nevertheless confined to the first band of matrix elements adjacent to the reinforcement as before although a steep gradient just beyond that region should have produced at least a partial broadening due to the presence of finer elements in the adjacent band.

The same composite when cooled 250°F to room temperature develops a plastic zone of size and shape almost equal to that for UTNT stressing to 68,930 psi. However, the principal stresses causing this flow are very different as are the reinforcement stresses shown in Fig. 3-33(a). The latter are compressive nearly everywhere while in the matrix near the reinforcement there are varying radial compressive stresses and quite uniform circumferential stresses that, in combination, produce the plastic flow. The region of the matrix farthest from the reinforcement is least stressed.

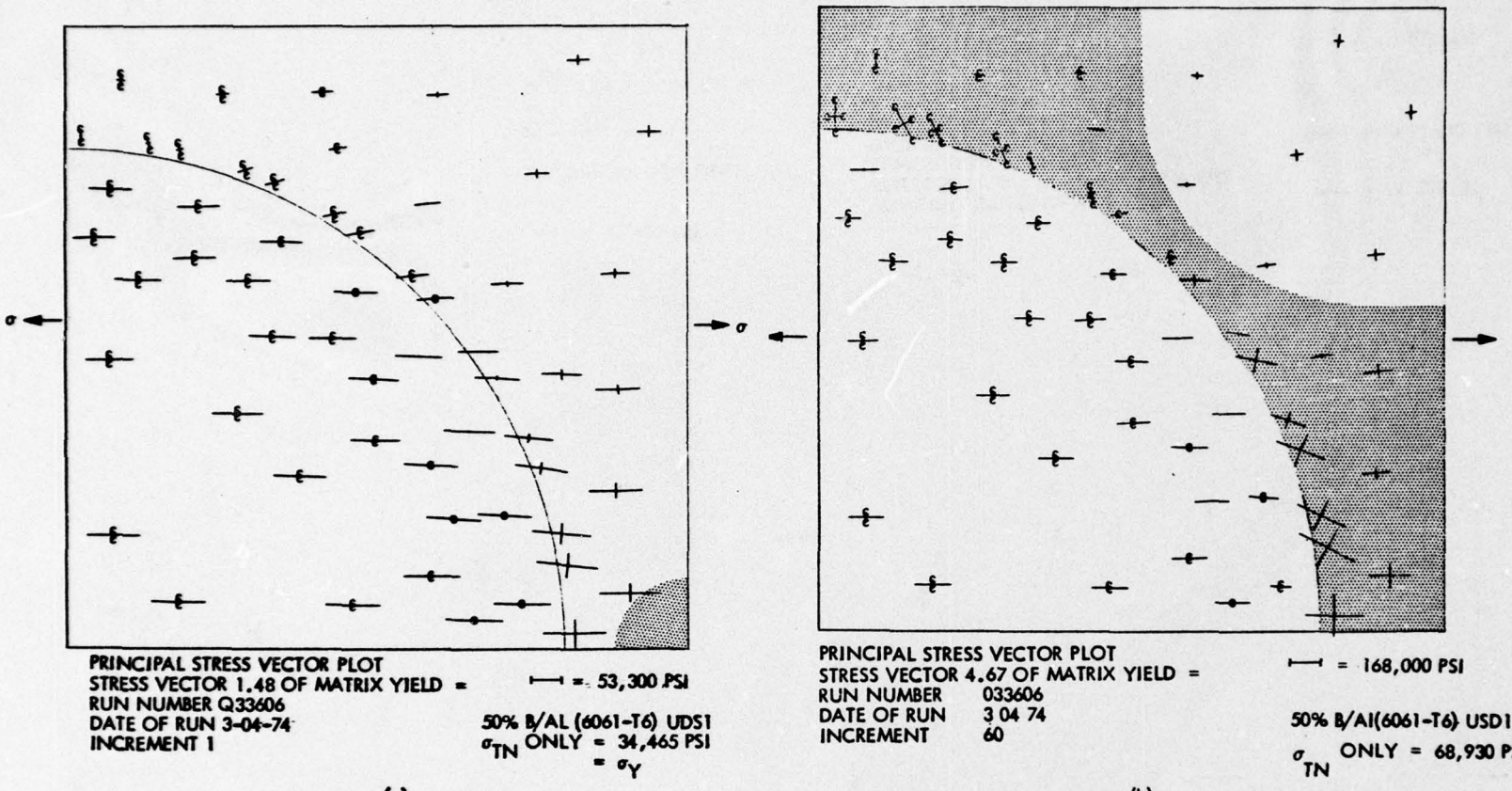

Fig. 3-32 Principal Stress-Vector Plots Showing Microstress Distribution in UDS1 50 vol % B/Al(6061-T6) Composites in PSTNT of (a) 34,465 psi (Yield) and (b) 68,930 psi. Shaded regions are approximate plastic zones

LOCKHEED PALO ALTO RESEARCH LABORATORY
LOCKHEED MISSILES & SPACE COMPANY, INC.
A SUBSIDIARY OF LOCKHEED AIRCRAFT CORPORATION

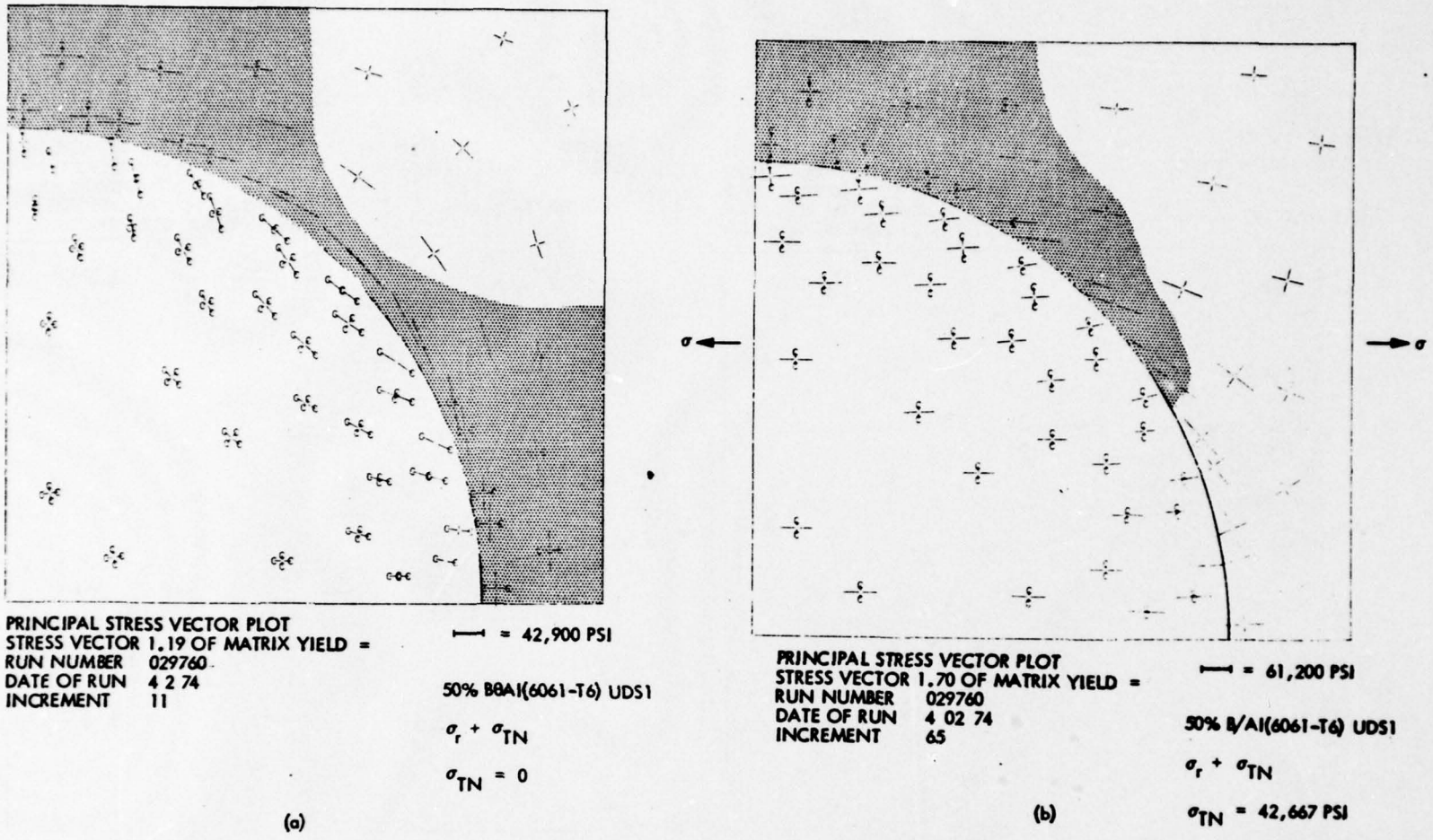

Fig. 3-33 Principal Stress-Vector Plots Showing Microstress Distribution in UDS1 50 vol % B/Al(6061-T6) Composite After: (a) -250°F Temperature Change and (b) Same With a PSTNT of 42,667 psi. Shaded regions are approximate plastic zone

LOCKHEED PALO ALTO RESEARCH LABORATORY
LOCKHEED MISSILES & SPACE COMPANY, INC.
A SUBSIDIARY OF LOCKHEED AIRCRAFT CORPORATION

Superimposition of a UTNT load of 42,667 psi onto the residual stress state [Fig. 3-33(b)] is sufficient to render uniform the stress field within the reinforcement and to modify the matrix distribution by cancelling out compressive components in the applied stress direction, among other things, in such a way that the size of the plastic zone is reduced to nearly half its original size. As a greater UTNT stress is applied, a new plastic zone should form as in the residual-thermal-stress-free case, and that zone should be attached to the other and grow to include eventually the entire matrix.

3.7.2 S2 Array

The microstress and yield behavior in this case is very different from the one just discussed. With no residual thermal stresses [Fig. 3-34(a)] the onset of yield occurs in regions most distant from the reinforcements and, with increasing load, virtually the entire matrix is plastic for a much lower applied stress than needed to produce only partial yielding in case S1. The stresses within the reinforcements are similar though somewhat less uniform at either load value. Although the matrix has almost entirely yielded at a 49,113 psi applied UTNT stress as is evident from Fig. 3-34(b), the orientations and distribution of the principal stresses are not changed significantly, and the magnitudes are increased about 50 percent above the values at yield.

Naturally, the residual thermal stresses induced on cooling 250° F to room temperature should be the same as case S1 as is seen on comparing Figs. 3-33(a) and 3-35(a). Subsequent application of a UTNT stress of 42,667 psi produces a much different situation, however, as can be seen on examining Fig. 3-35(b). Whereas stressing array S1 produced a decrease in the thermally induced plastic zone size, the same stress in this case causes yield to occur throughout nearly the entire matrix. This observation is entirely consistent with the stress/strain curves shown in Figs. 3-23, 3-24, and 3-25, which at 42,667 psi show much more tensile strain for case S2 than for case S1.

3.7.3 H1 Array

The evaluation of a plastic zone for the hexagonal array H1 would be expected to resemble that for the diagonally stressed square array S2 because of configurational similarities. Indeed, Fig. 3-36(a) shows the yield surface (elastic-plastic interface) originating in the vicinity of the midpoint of lines parallel to the applied stress connecting the centers of adjacent reinforcements. The differences between the exact shapes result from quantitative differences in the arrays and, to a lesser extent, from FEG differences.

Application of a larger UTNT stress (52,667 psi) causes nearly the entire matrix to flow plastically, with the exception of small regions about the reinforcement poles perpendicular to the stress direction where small compressive and tensile stresses develop that are too small to cause flow. The reinforcements have one set of principal stresses of nearly equal magnitude and nearly parallel to the applied stress, with the orthogonal principal stresses mostly compressive and small, a situation differing significantly from case S2.

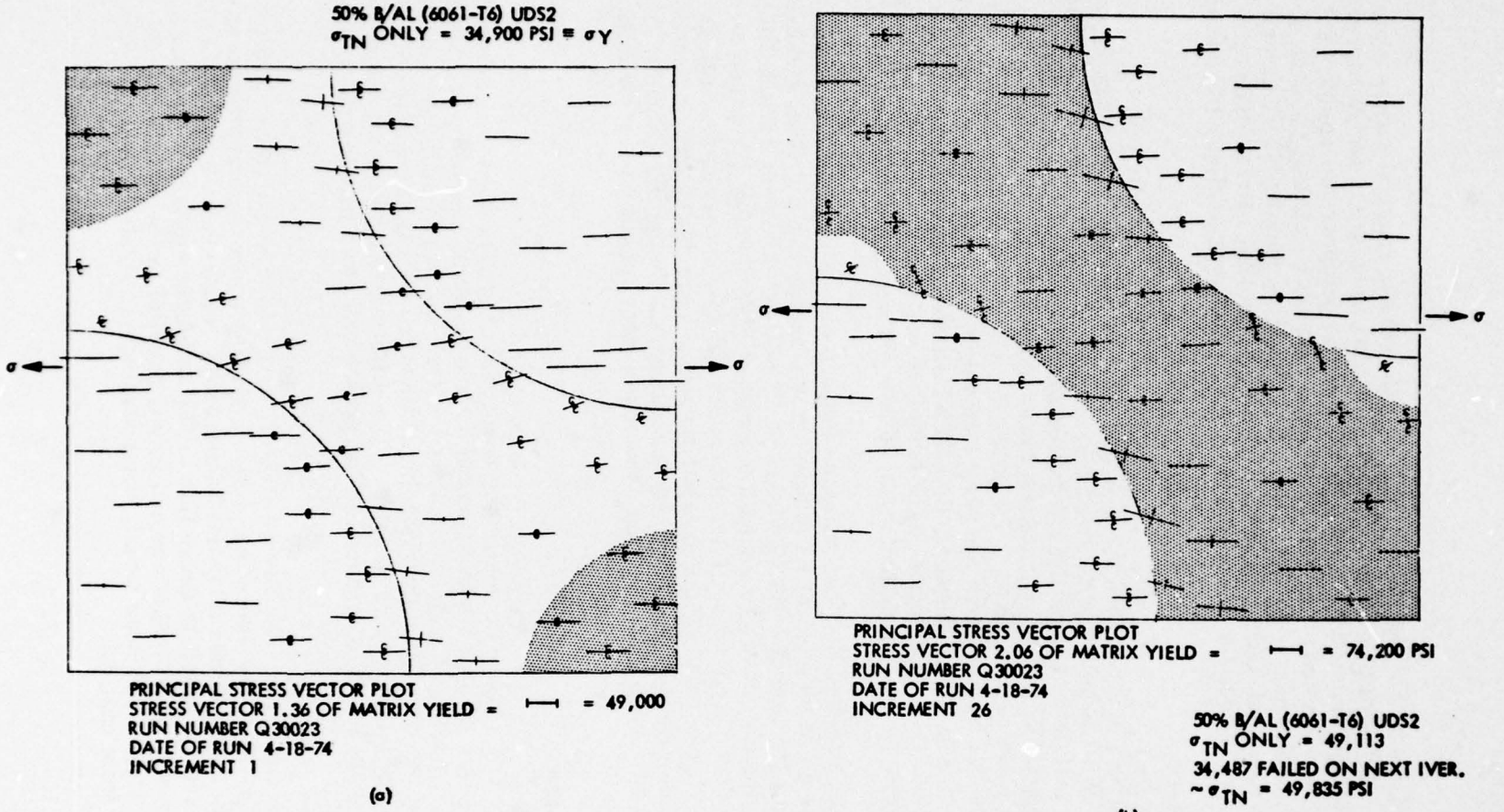

Fig. 3-34 Principal Stress-Vector Plots Showing Microstress Distribution in UDS2 50 vol % B/Al(6061-T6) Composite; Initially Stress-Free and Loaded in PSTNT to (a) 34,906 psi (Yield) and (b) 49,113 psi

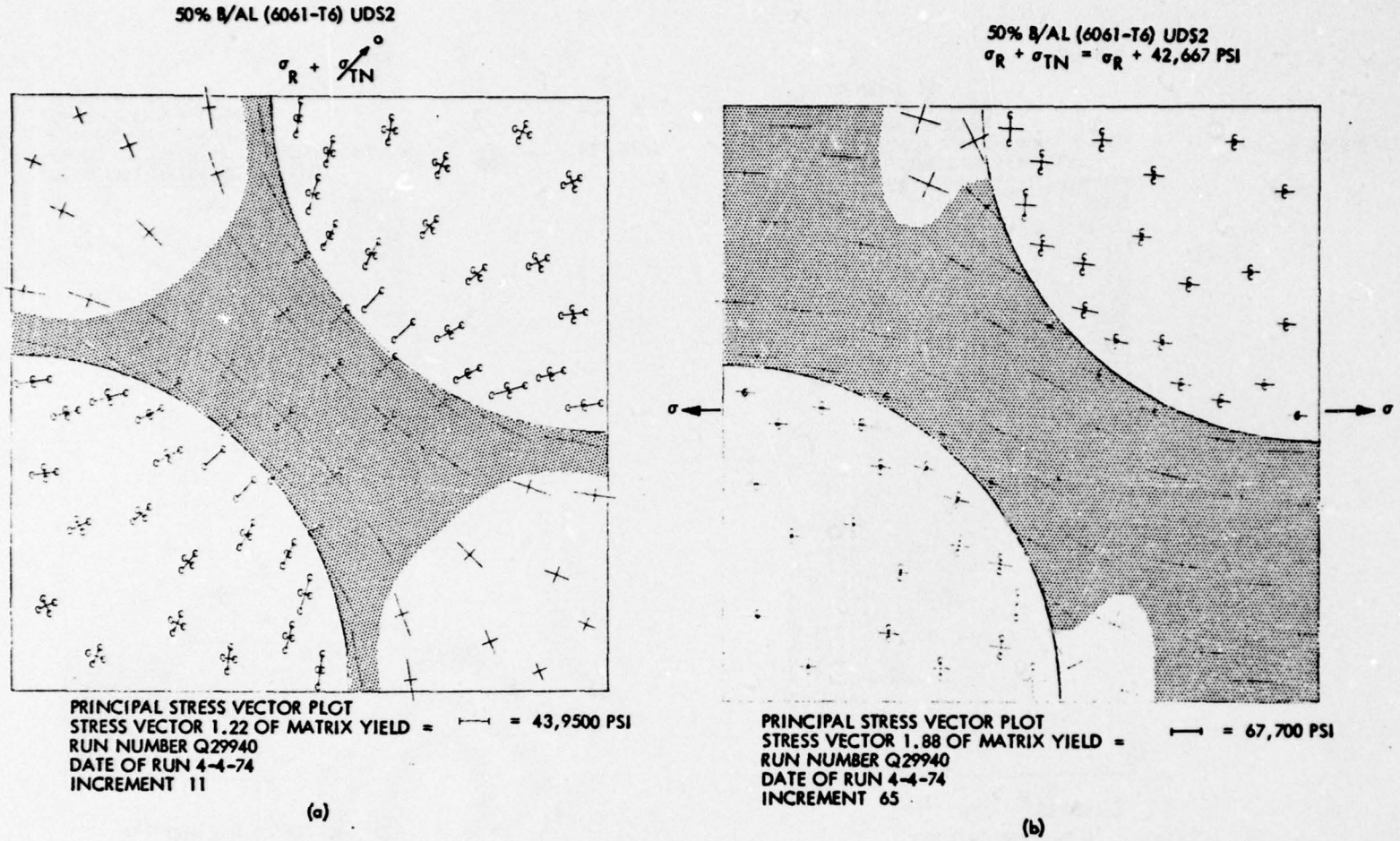

Fig. 3-35 Principal Stress-Vector Plots Showing Microstress Distribution in UDS2 50 vol % B/Al(6061-T6) Composite After: (a) -250°F Temperature Change and (b) Same With a PSTNT Stress of 42,667 psi. Shaded regions are approximate plastic zones

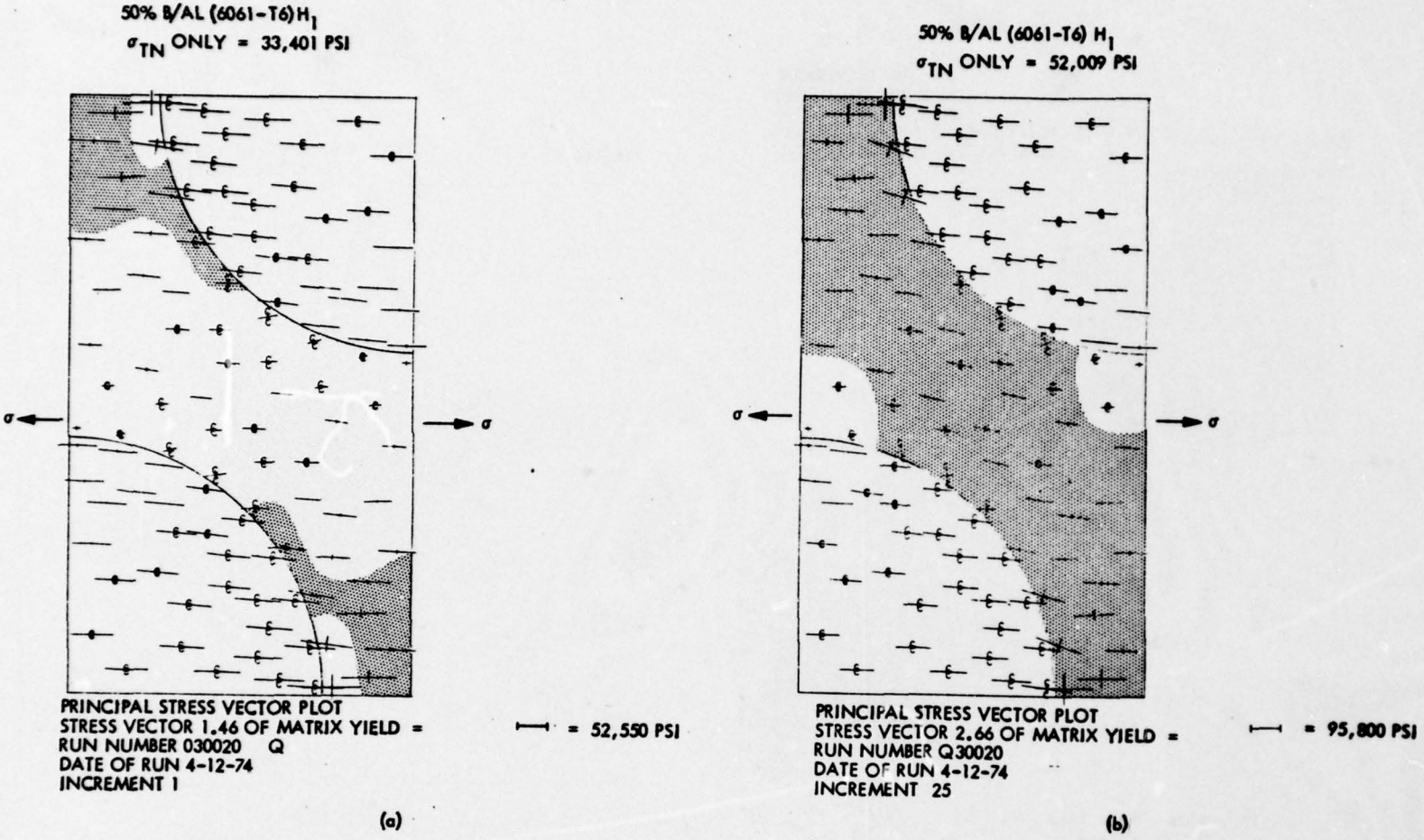

Fig. 3-36 Principal Stress-Vector Plots Showing Microstress Distribution in UDH1 50 vol % B/Al(6061-T6) Composite; Initially Stress-Free, Then Loaded in PSTNT to: (a) 33,401 psi (Yield) and (b) 52,009 psi. Shaded regions are approximate plastic zones

LOCKHEED PALO ALTO RESEARCH LABORATORY
LOCKHEED MISSILES & SPACE COMPANY, INC.
A SUBSIDIARY OF LOCKHEED AIRCRAFT CORPORATION

Thermal residual stresses in UD H1 50 vol % B/Al(6061) on cooling 250°F to room temperature after T6 annealing are shown in Fig. 3-37(a). Again the yielded region resembles that for the diagonally stressed square array except that the elastically stressed region is shifted upward from the lower boundary. This is actually a point-of-reference difference only easily realizable by noting that for each array (S2 and H1) the residual thermal matrix stresses are smallest at the centers of the large regions formed by groups of adjacent reinforcements. Thus, in array S2, the smallest stresses occur at the center of the matrix regions formed by four reinforcements at the corners of squares, while in array H1 the regions are at the centers of equilateral triangles with a reinforcement centered at each vertex.

Superimposition of a UTNT stress of 42,667 psi onto the residual stress state of H1 arrays has an effect intermediate to that for arrays S1 and S2. Specifically, the array of the yielded region neither expands nor contracts but merely changes slightly in shape by shifting the elastic regions perpendicular to the direction of the applied stress until each is symmetrically distributed about the centers of lines joining the centers of nearest neighbors parallel to the applied stress direction. The shape of the plastically deforming region varies too greatly with thermal excursions and applied stress to note a consistency with the behavior of the gross stress-strain curve, particularly the cross-over of the with and without residual stress curves at about 44,500 psi applied stress and the much slower growth of the transverse-transverse total Poisson's ratio shown in Fig. 3-27.

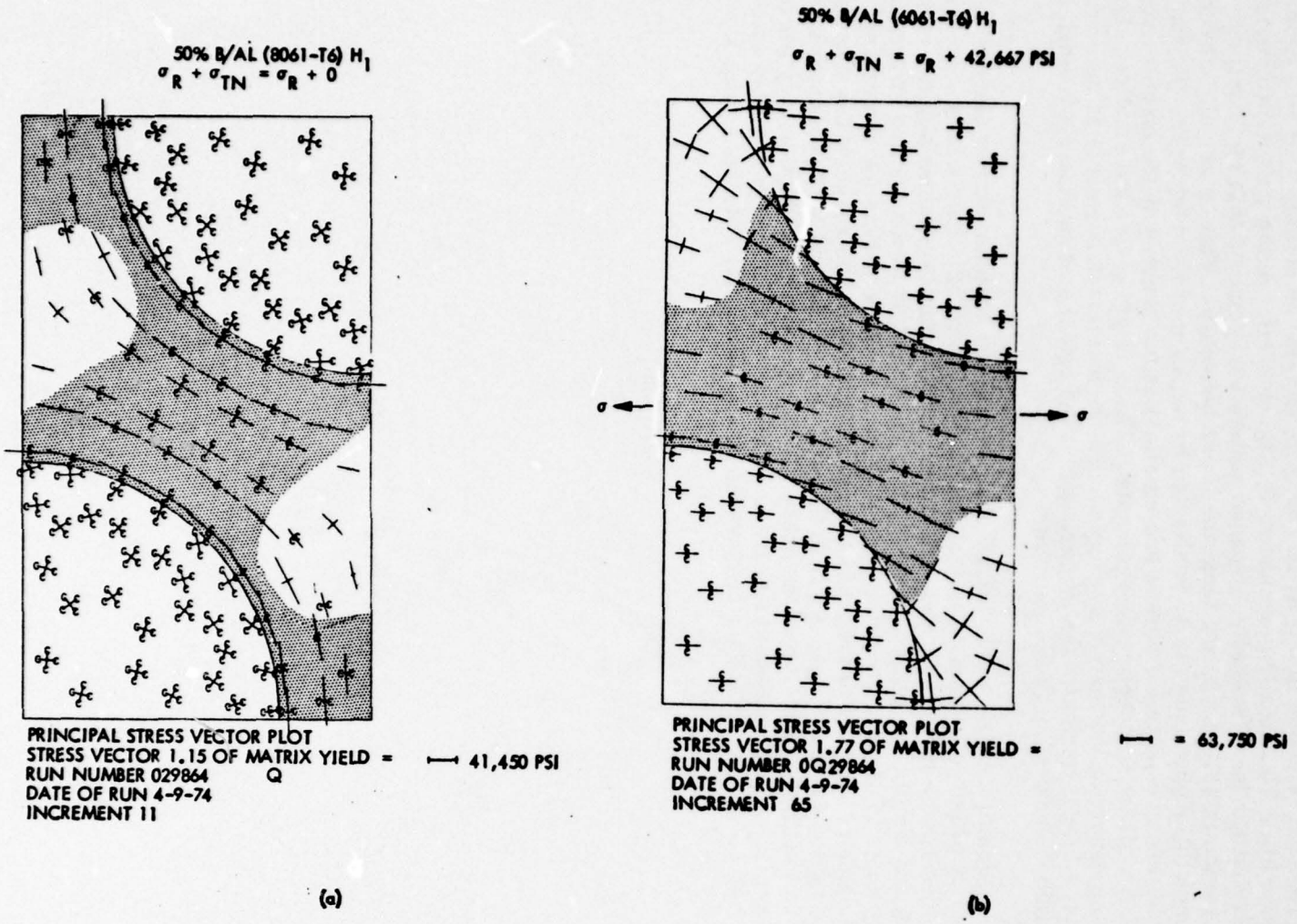

Fig. 3-37 Principal Stress-Vector Plots Showing Microstress Distribution in UDH1 50 vol % B/Al(6061-T6) Composite After: (a) -250°F Temperature Change and (b) Same With a PSTNT Stress of 42,667 psi. Shaded regions are approximate plastic zones

Section 4
EXPERIMENTAL DETERMINATIONS

Two "precision" UDS1 W/Al(6061) composites were prepared in the laboratory for tensile testing to provide data directly comparable to the theoretical predictions described in Section 3 of this report. These were identical in composition to the similar specimens described in Ref. 1, but fabrication was accomplished using additional precautions to ensure, as much as possible, the retention of the square-packing array throughout the pressing operation. Testing was also modified in an attempt to obtain more reliable results. Tungsten was selected as a reinforcement substitute for boron since the latter is not available in diameters sufficiently large to facilitate precise fabrication, and because the mechanical properties of tungsten are nearly the same as those of boron.

4.1 TEST-SPECIMEN PREPARATION

The composites were prepared from 0.040-in.-diameter centerless-ground tungsten rod and aluminum (6061-0) sheet with parallel, directly opposing, 90-deg grooves on both surfaces formed by hot-pressing the sheets in a specially designed die. Such grooves ensure proper initial alignment and distribution of the reinforcing rods, and minimize the amount of metal flow required to achieve full densification. The original thickness of the aluminum sheets was half of the interlayer spacing to ensure a 50 vol % concentration.

Four-layer stacks of alternating tungsten rods and aluminum sheets were initially bonded with a polystyrene solution to facilitate handling. Polystyrene is known as a fugitive binder that depolymerizes and evaporates leaving no char or residue at temperatures below that required for upset-forming and diffusion-bonding aluminum. It was demonstrated in previous work (Ref. 1) that a fully constrained die is necessary for the forming/bonding operation to prevent lateral flow of metal that drags along the reinforcements nonuniformly and destroys the desired double periodicity. To this end, a pressing die was made that consists essentially of a shallow closed rectangular cavity with a matching ram. The grooved matrix sheets and rods were cut to dimensions that just filled the length and width of the cavity such that only through-the-thickness deformation is possible.

Hot upsetting and diffusion bonding were performed within a large vacuum chamber that contains an inductively heated susceptor surrounding a fixed water-cooled anvil and a hydraulically actuated, water-cooled ram. Pressing was accomplished at approximately 950°F, and a pressure of 2000 psi applied for 60 min. The specimens produced are as shown in Fig. 4-1 after steel end tabs were installed to facilitate gripping. Each

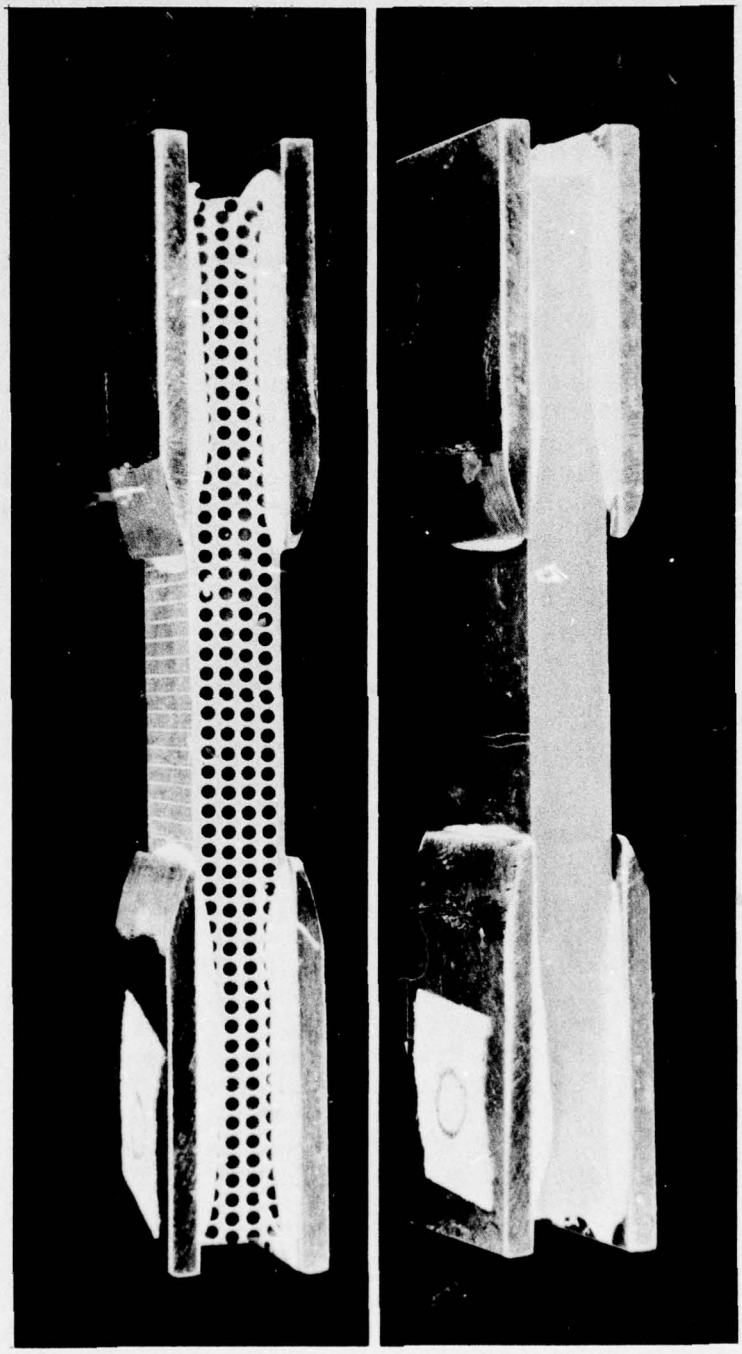

Fig. 4-1 Hot-Upset and Diffusion-Bonded Precision UDS1 50 vol % W/Al(6061) Tensile Tests Specimen (a) , and Pure Al(6061) Specimen Used to Verify Theoretical Predictions

specimen was 2.85 in. long by 0.60 in. wide by 0.25 in. thick. The reinforcement concentration is somewhat less than 50 vol % as the two face sheets were initially of the same thickness as the three intermediate sheets. This should have little effect on the properties that depend on the internal concentrations.

The uniformity of the distribution within the gage length was excellent, as can be seen in Fig. 4-2. Also, the densification was excellent as was the interface bonding, though interface strength was only good. The latter is more evident in Fig. 4-3(a) and (b), which shows metallographically polished cross sections at 500× magnification. The darker phase with a stringer texture is tungsten. The scattered small dark regions at the interface may be unbonded, as is the larger region in Fig. 4-3(b).

Two specimens were annealed to provide tests of the -0 and -T6 matrix condition. This was done according to conventional practice.

Steel end tabs were epoxy-cemented to each side of the test specimens to ensure as uniform a load transfer as possible from the serrated wedge-locking grips that had to be used with the specimen configuration. Each end had a bonded area of about 1.2 in., which was considered adequate to support the largest load expected for UD/UTNT-loaded composites if interface failure occurred.

4.2 EXPERIMENTAL RESULTS

The transverse tensile specimens were tested in an Instron Universal Testing machine at a cross-head rate of 5 mils/min. Elongation was measured with a 0.5-in. gage length clip-on extensometer working through an amplifier and other electronics to drive one axis of an X-Y plotter while the other axis was driven by a signal from the load cell. Preliminary tests with unreinforced aluminum (6061-0, and -T6) were made to verify the accuracy of the apparatus.

The UTNT stress-strain curves for the composite and unreinforced matrix, each in the -0 condition, are presented in Fig. 4-4, together with the predicted curves for the well-bonded composite and the nonbonded composite (modulus only). The experimental data are intermediate to that for the two extremes of bonding, suggesting that partial (local) debonding had occurred early in the loading cycle. If the modulus follows the rule of mixtures, for the effective volume fraction of composite that is well-bonded at the interface, the measured 10×10^6 psi elastic modulus would occur if a good bond existed over about 27 percent of the composite. The elastic-plastic portion of the curve would progressively approach the debonded case if interface failure occurred locally on increasing load whereas catastropic interface failure would cause the curve to fall immediately to the no-bond level with leveling out of the curve at about 6-ksi applied stress.

Evidence supporting the failure mode is clearly present in Fig. 4-6(a), which shows a combination of interface debonding and transverse reinforcement splitting at the fracture surface. As there are four layers in the composite, the fractured reinforcement that

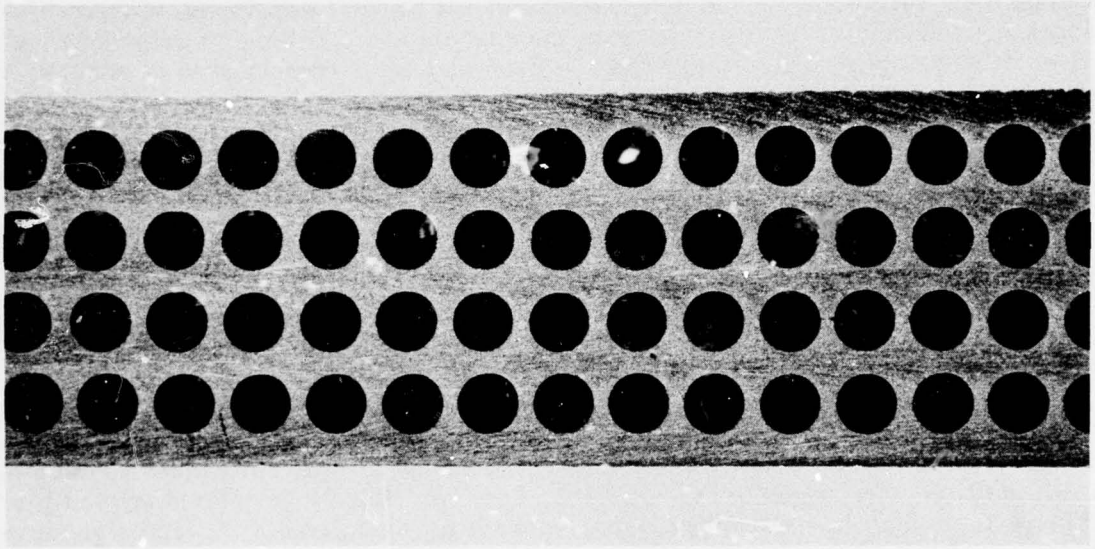

Fig. 4-2 Micrograph of Gage Section From Precision UDS1 50 vol % W/Al(6061) Composite Showing Uniformity of Reinforcement Distribution 8×

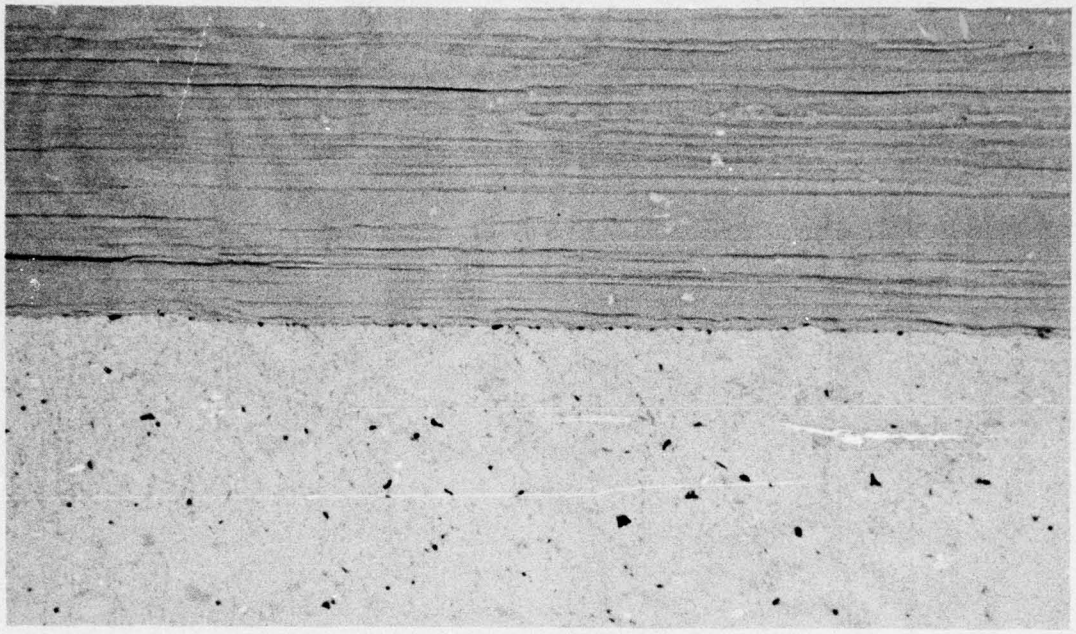

(a)

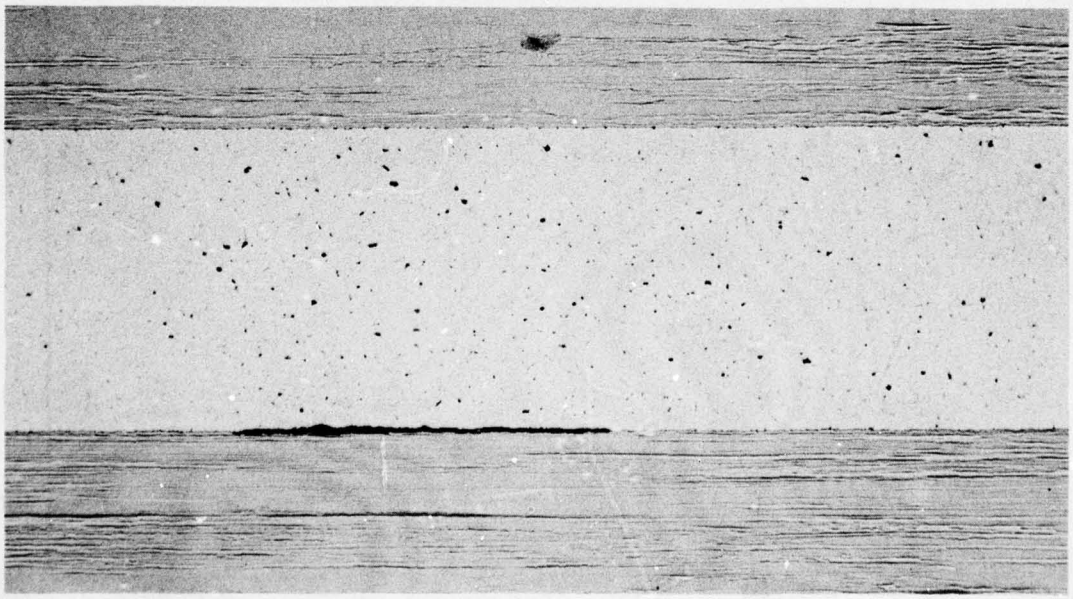

(b)

Fig. 4-3 Micrograph of W/Al Interface in Precision Test Composite Showing: (a) Characteristically Good Bond (500×) and (b) Isolated Region With No Bond (100×)

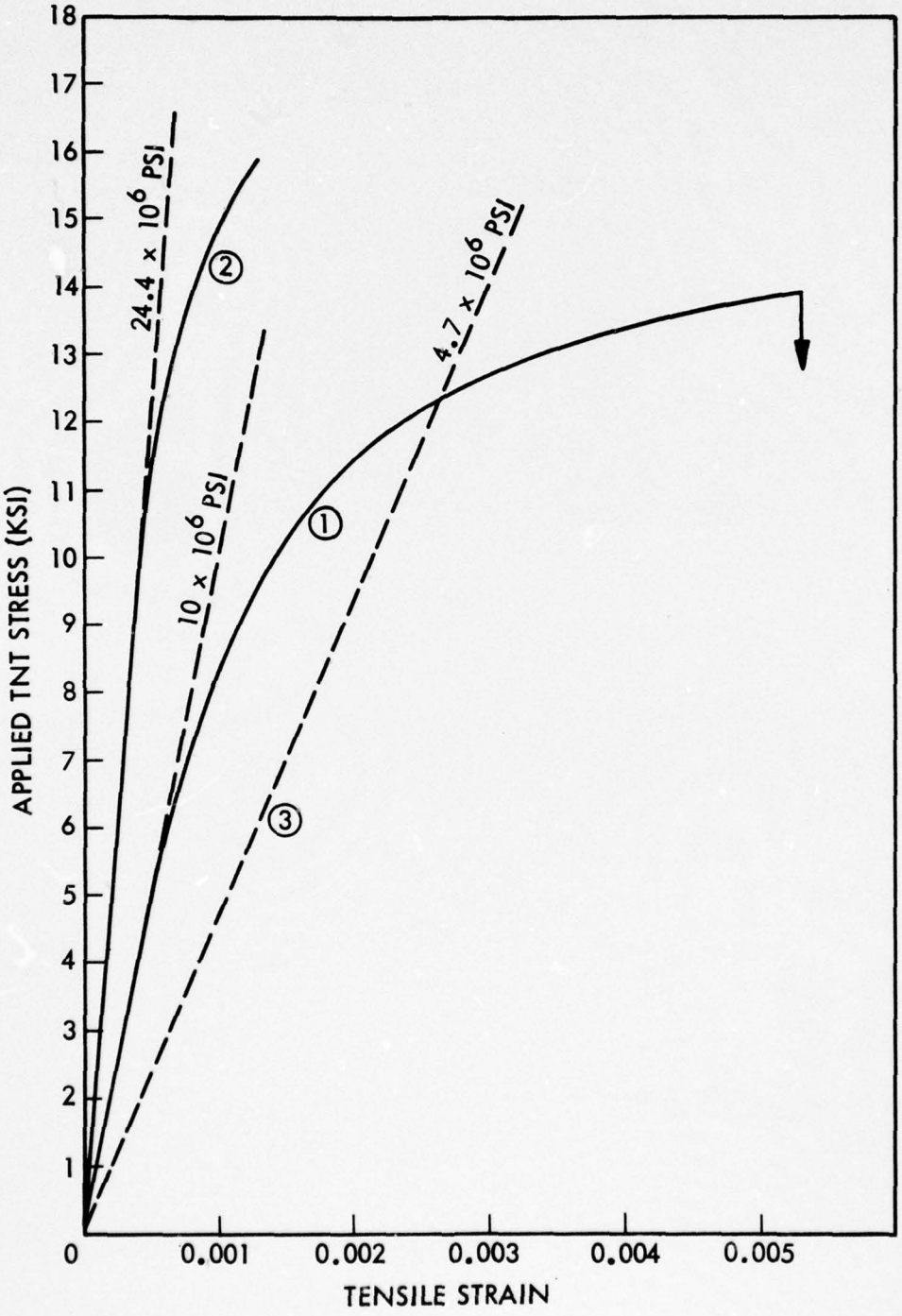

Fig. 4-4 Comparison of Measure Transverse-Normal Tensile Stress-Strain Curve for (1) UDS1 50 vol % W/Al(6061-0) Composite, (2) With Predicted Theoretical Behavior of B/Al(6061-0) Composite With Good Bond, and (3) Modulus of Same With no Bond

apparently was well-bonded comprises 25 percent of the break – in excellent agreement with the prediction based on the modulus of the experimental stress-strain curve as accounted for by the rate of mixtures. The -T6 condition results are presented in Fig. 4-5, together with various relevant theoretical predictions. The composite modulus is much higher than for the -0 condition, suggesting 81 percent interface bonding at least during the initial loading and about 29 percent debonding leading to failure. The fracture macrograph [Fig. 4-6(b)] shows no filament breakage in this case, suggesting that the sudden change of slope in the stress-strain data was the onset of progressive debonding that resulted in ultimate failure.

Examination of reinforcement and exposed interface surfaces of the fracture suggests that a minute reaction layer had formed or that a good, though weak, bond had formed between the tungsten and aluminum. The markings on both surfaces were identical, resembling the centerless-grinding marks on the rods and the appearances of both bright metallic.

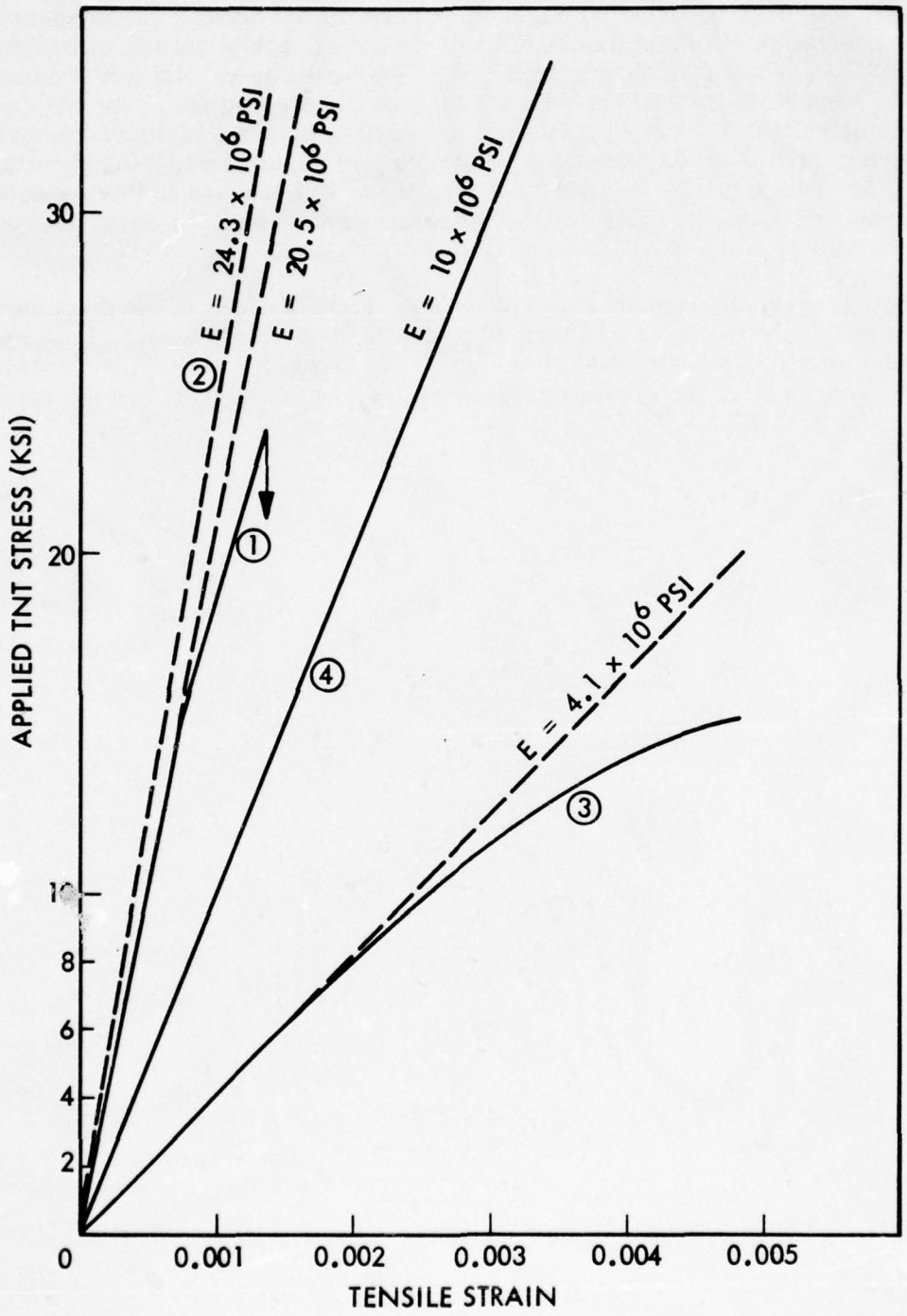

Fig. 4-5 Comparison of Measure Transverse-Normal Tensile Stress-Strain Curve for (1) UDS1 50 vol % W/Al(6061-T6) Composite With (2) Predicted Theoretical Behavior of Similar Boron Reinforced Composite With Good Bond, (3) Fully Debonded and (4) Measured Al(6061-T6)

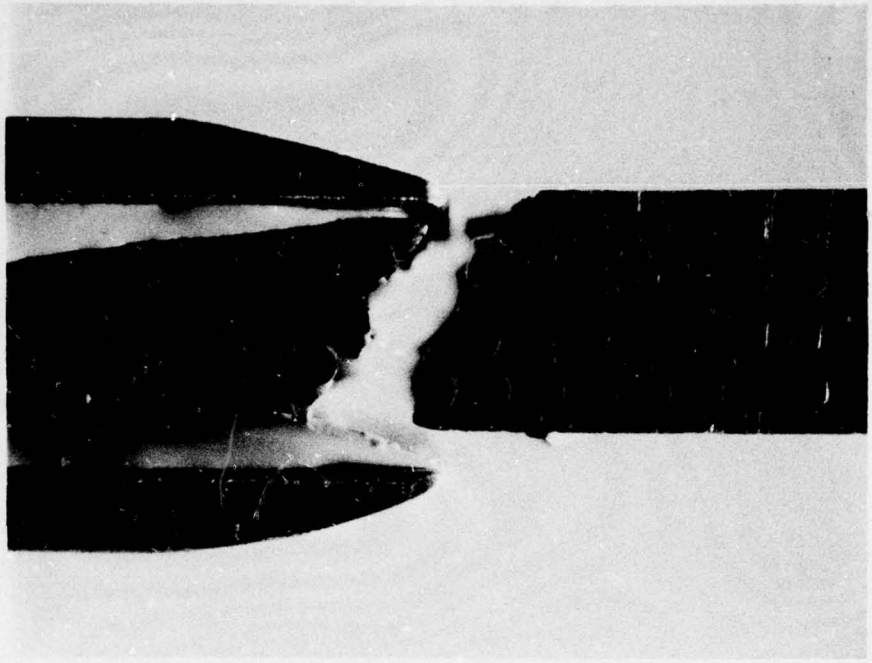

(a)

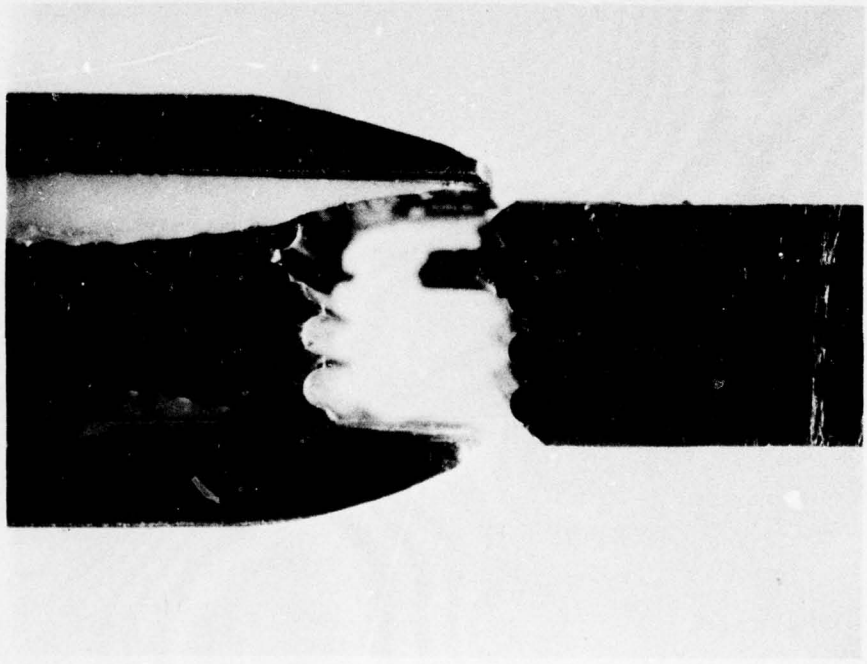

(b)

Fig. 4-6 Fracture in Precision UDS1 50 vol % W/Al(6061) Tensile Specimens: (a) 0 Condition and (b) T6 Condition ~ 6×

Section 5
CONCLUSIONS AN DISCUSSION

5.1 CONCLUSIONS

From this work it can be concluded generally that the finite-element method provides an unequaled analytical tool for studying the micro- and macro-mechanics of unidirectionally reinforced composites with different combinations of packing arrays and applied uniaxial transverse-normal loading direction, with or without the presence of residual thermal stresses. It can be concluded further that the method is amenable to the analysis of more complicated configurations and interactions by suitable modification. Specific conclusions, regarding the reinforcement mechanisms in metal-matrix composites, can be drawn from the calculations performed. For UD B/Al(6061-T6) the most significant are as follows:

- Catastrophic interface failure by tensile-normal debonding can occur for any reinforcement concentration in the range of 20 to 60 vol % and for square or hexagonal reinforcement arrays.
- The maximum interface-normal tensile stress leading to debonding failure, increases monotonically with reinforcement concentration for a square-array composite.
- The maximum interface-normal stress concentration factor varies from 0.9 for a 50 vol % hexagonal array stressed in tension parallel to lines connecting the center of next-nearest neighbors, to approximately 1.5 for square or hexagonal arrays stressed in tension parallel to lines joining the center of nearest-neighbor reinforcements.
- Residual thermal stresses developed on cooling from the -T6 condition modify the interface-normal tensions to retard debonding failure.
- For square-array composites elastic modulus increases with reinforcement concentration from about 14.8×10^6 psi at 20 vol % to nearly 35.5×10^6 psi at 70 vol %.
- The dependence of transverse-transverse elastic modulus on reinforcement concentration is less for a square array stressed parallel to lines connecting the centers of next-nearest neighbors than it is for the same array stressed parallel to connectors of nearest-neighbors, with values increasing monotonically from $\sim 15 \times 10^6$ psi at 20 vol % to $\sim 27 \times 10^6$ psi at 70 vol %.
- For 50 vol % composites, the transverse elastic modulus is greater for square arrays stressed parallel to lines connecting the centers of nearest neighbors than it is for uniaxial stressing parallel to lines connecting the centers of next-nearest neighbors with hexagonal packing being intermediate.
- Residual thermal stresses developed on cooling to room temperature from a -T6 anneal, produce a decrease of about 10 percent in the apparent elastic

modulus for the 50 vol % hexagonal independent of transverse loading direction, and square arrays stressed parallel to lines of nearest neighbors.

- Residual thermal stresses developed on cooling to room temperature, after a -T6 anneal, are sufficient to cause extensive yielding of the matrix for all arrays studied.
- The residual stress state and amount of plastic flow that occurs on cooling to room temperature after a -T6 anneal, modifies the subsequent transverse stress-strain behavior such that local plastic flow occurs on the first increment of stress and the composite exhibits a somewhat larger amount of work-hardening.
- Measurement of the instantaneous total (elastic plus plastic) transverse-transverse Poisson's ratio, under uniaxial transverse normal tensile stressing, is an effective method of following the growth of the plastic zone size.
- The instantaneous transverse-transverse plastic Poisson's ratio in UD B/Al(6061) composites, attains a limiting value of 1.0 because of the constraining influence of the reinforcements in their longitudinal direction.
- The instantaneous total transverse-transverse Poisson's ratio can be used effectively to ascertain the amount of plastic flow the matrix has experienced because of residual thermal stresses.

The following conclusions were reached from the experimental results:

- It is possible to fabricate square array composites with good precision by using hot-upset/diffusion bonding under vacuum in a die that effectively constrains all flow and associated displacements in a direction normal to the specimen or in the direction of pressing.
- The interface normal tensile strength of a W/Al(6061) couple can exceed the transverse tensile strength of a centerless-ground tungsten rod of 40 mils diameter.
- The gross transverse tensile behavior of UD 50 vol % W/Al(6061-T6, or -0) can be reconciled in terms of the preceding theoretical analysis.

5.2 DISCUSSION

The quantity of information that can be generated from a computer-programed finite-element analysis of composites appears to exceed that available with comparable effort utilizing other methods. While certain quantitative aspects of the results are not as accurate as might be desired, there is adequate evidence indicating that improvements will come in this area as the result of continuing research. For example, as seen in Appendix A, a considerable extension of the elastic-plastic stress-strain curve and consequently improvement, matrix failure prediction capability was achieved by relatively modest refinements of the original computer program.

In its present state, the computer program used in the preceding study is very adequate for predicting relative, semiqualitative, micro behavior, and fully qualitative gross mechanical properties by further refinement to include, for example, generalized plane

strain, as it more exactly represents the true state of stress in unidirectional composites under transverse-normal applied stress. Such a program would permit also a determination of the effect on longitudinal properties of variations in the parameter that have been examined already for the transverse case.

The FEGs employed for analyzing the various volume fractions, arrays, and loading geometries should be standardized to provide a uniform element size in the regions of highest stresses. This would render the results more comparable, relatively, as the significant processes would be occurring over regions of the same dimensions. One could also employ non-linear interpolation functions to the same end but possibly only with an increase in program complexity that would require special justification.

There is no question regarding the extreme usefulness of FEM analysis to provide a basic understanding of how composites function. It will continue to be used as a source of generating data essential to the materials developed as a basis for analyzing results and determining how improvements might best be brought about within the inherent constraints revealed by the method.

Appendix A
COMPUTER PROGRAM MODIFICATIONS

This section is included as an appendix since it is concerned with the investigation and solution of a problem related to the computer program used to perform the theoretical analyses described in the text. The finite element program is too complicated to describe in detail here. Certain of its features will be described as necessary to illustrate the material to follow. For additional details the reader may consult Refs. 15 and 16 of this report.

A.1 PREMATURE FAILURE PREDICTIONS

As a result of approximating the stress-strain behavior of the matrix Al (6061-T6) by a bilinear curve during the early stages of this study, failure was indicated prematurely because of local unloading of elements that have yielded plastically. This is illustrated in Fig. A-1 where the octahedral shear stress developed within three elements is plotted versus the number of 1.2-ksi load increments beyond initial yield. The octahedral stress in the first element to yield (No. 67) slowly increases in the plastic range as the elastic octahedral stress in each of two other remote elements (Nos. 36 and 116) rapidly increases to a value slightly above yield, then continuously decreases at a slower rate until it falls below yield. The program then assigns elastic properties to the elements, which results, in the next iteration, in an octahedral stress in excess of the value designated as that required for fracture, and the element is designated as having failed.

A.2 STRESS-STRAIN CURVE REPRESENTATION

Attempts to obviate the difficulty were made by substituting for the bilinear curve a least-squares curve-fitting routine, and a cubic spline function routine, each requiring only tabular input data points from an experimental stress-strain curve. Neither of these modifications solved the problem, though for different reasons, however. In the case of the least-squares method, the available program could not adequately represent the data just beyond yield without considerable difficulty to ensure monotonicity. The spline function routine failed in the same region by introducing inflections between input data points that produced poorer results than the bilinear approximation.

Since no computer interpolation routines were available to adequately represent the data in smooth form, a polygonal approximation was adopted wherein the stress is a unique linear function of strain between adjacent input data points. Such a representation has the advantage of allowing a large number of points in regions of rapid slope change. Indeed, the most practical piece-wise-linear curve for 6061-T6 aluminum was found to consist of the yield point, four points equal-spaced with respect to stress on the knee of the curve and the point of failure.

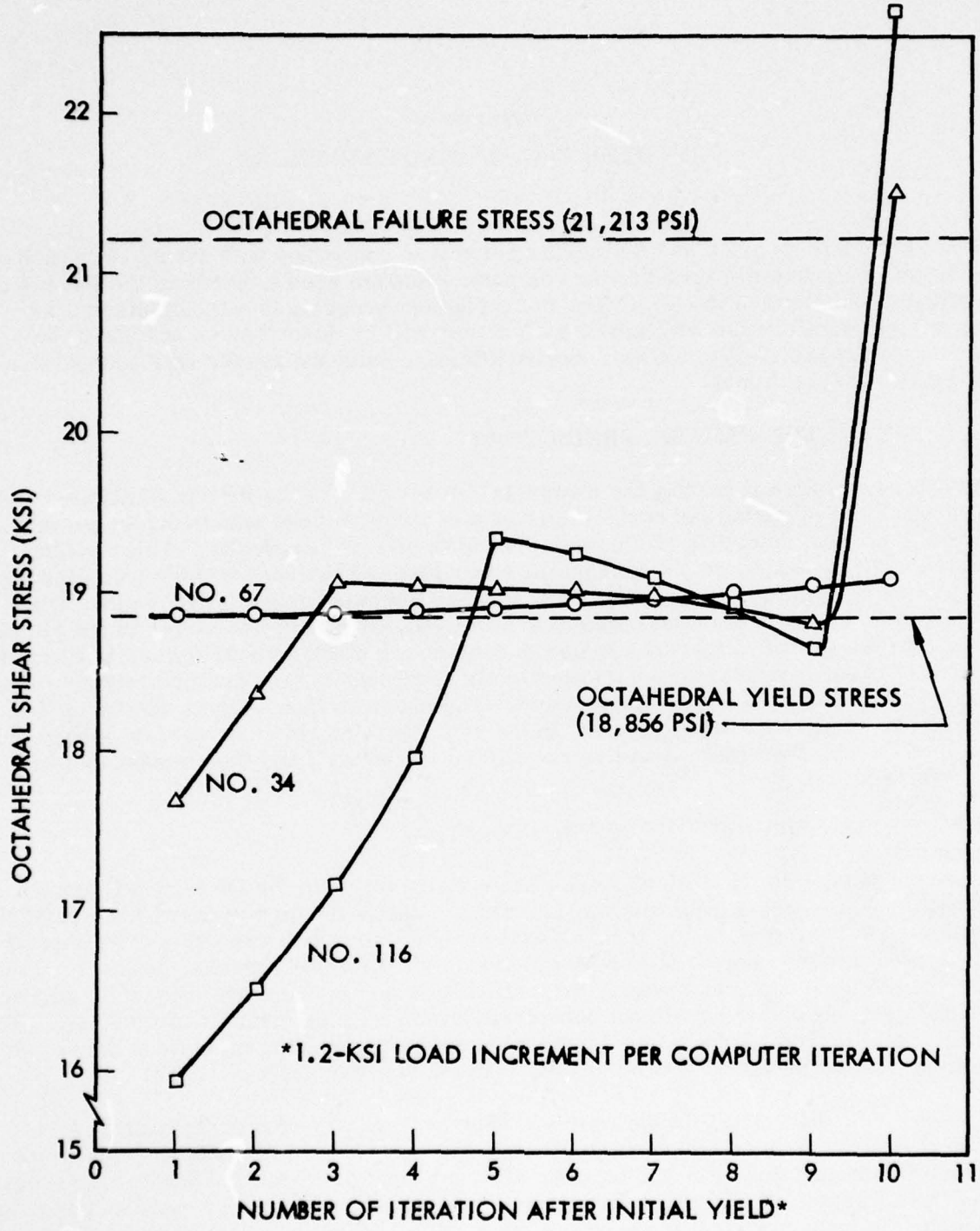

Fig. A-1 Calculated Octahedral Shear Stress Versus Applied Load for First Element to Yield (No. 67) and Two Elements That Failed Anomalously (Nos. 34 and 116) Because of Assumed Bilinear Stress-Strain Curve of the Matrix Al (6061-T6)

A.3 STRESS-INCREMENT RESTRICTION

An additional computer program change was made as an additional precaution to ensure anomalous early-failure predictions. Since load increments of arbitrary size are prescribed at the beginning of the computation, these may be selected to be large enough to produce an erroneous result as described above. Also, the load increment cannot be made arbitrarily small as inordinate computation times may result. A compromise measure was adopted wherein a rather large increment is prescribed, but a check is made after each incremental computation to determine which finite-elements, if any, are experiencing an octahedral shear stress exceeding a given value beyond the linear stress-strain interval used at the start of the iteration. When such are detected, the incremental load for that iteration is reduced to bring within bounds the octahedral shear-stress of the element with the greatest deviation beyond the bound.

The stress increment restriction and the number of intervals selected for the piece-wise linear representation of the matrix stress-strain curve each contribute not only to mitigating the anomalous stress excursions leading to premature failure predictions, but also to reducing the computation time required to reach a given composite strain.

Results of three runs with the modified program are compared with the previous bilinear results in Fig. A-2. The elastic part of the calculations are not affected and the curves coincide exactly. Beyond yield the new method predicts a slightly different stress-strain but, more important, with optimized parameters it is possible to analyze the behavior of a 50 vol % B/Al (6061-T6) composite to a plastic strain 2.88 times greater. The bilinear yield strength specified in the earlier method was higher (42,000 psi) than the current value (36,177 psi) to most closely approximate the stress-strain curve over its entire range. The difference in the resulting composite stress-strain behavior is imperceptible.

The influence of the program modifications on the micromechanical stress analysis is also very pronounced. Figure A-3 shows the progression of yield through the matrix for the original unrestricted bilinear computation and for the five-segment piece-wise-linear stress-strain representation computation with the restriction that no applied stress increment would load any finite element to an octahedral shear stress beyond the upper limit of the next higher interval from the one containing the octahedral shear stress at the start of a particular stress-increment computation. The bilinear calculations, made with 1100-psi applied-load increments starting at 42,000 psi yield, give the dark-outlined region of yield to failure at about 55,000 psi. The failure sequence is essentially as indicated by the numbers. The remainder of the figure gives the yield sequence predicted by the modified program. In this case the last element to yield (indicated by number 38) did so with an applied load of 59,459 psi, nearly 7.5 percent greater than the previous failure load. Actually, the calculation was continued without additional yielding until at 62,075 psi, an 11.4 percent higher sustaining load than previously predicted, the computation was terminated by apparent failure of the element inscribed with the circled number 13.

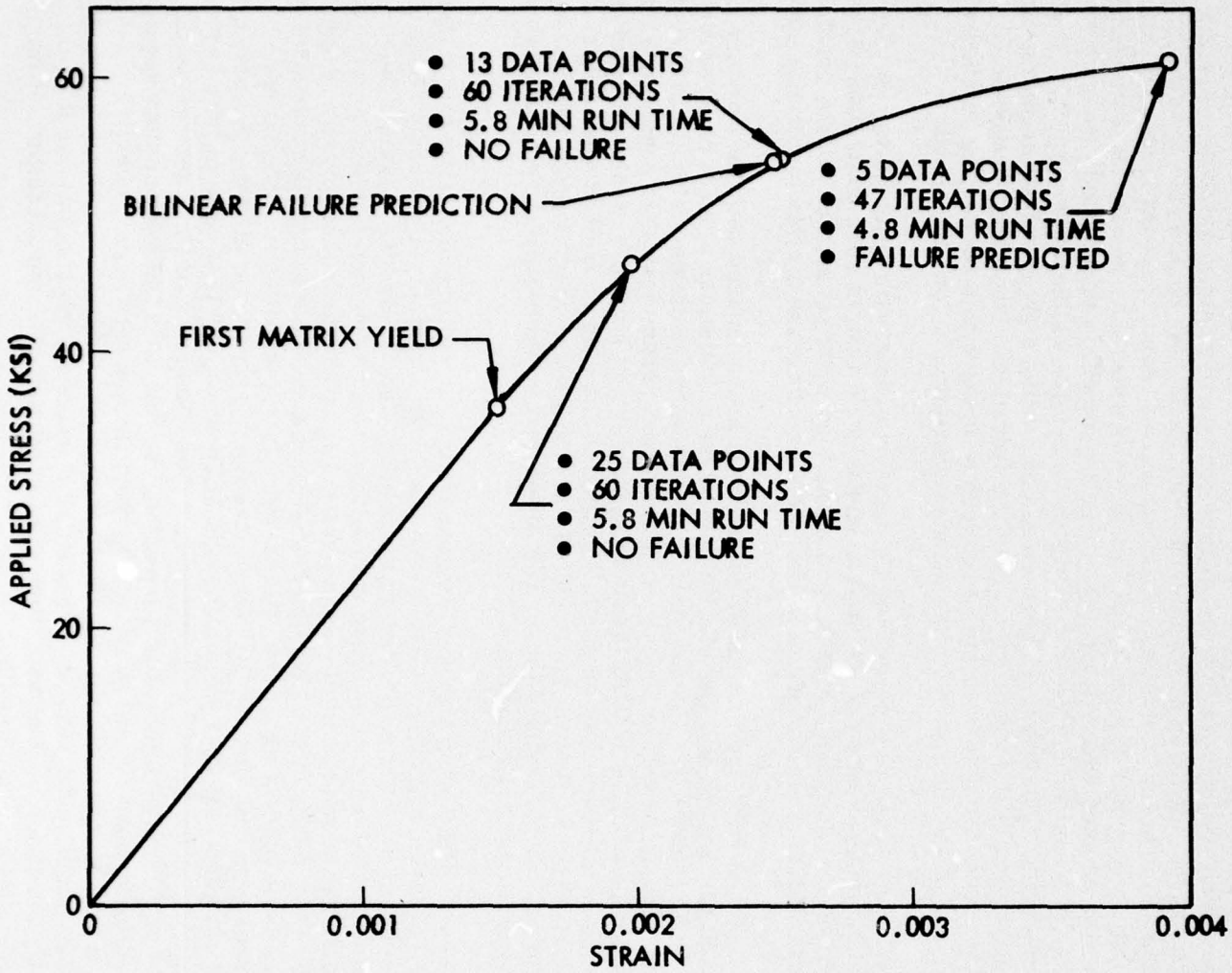

Fig. A-2 Predicted Transverse-Normal Stress-Strain Curve for a 50 vol % B/Al (6061-T6) Unidirectional Square-Array Composite, Calculated With a Bilinear Matrix Stress-Strain Curve and No Local Stress Increment Limit, and With Three Piece-Wise-Linear Stress-Strain Representations Each With Different Number of Data Points and Internal Local-Stress-Increment Limiter

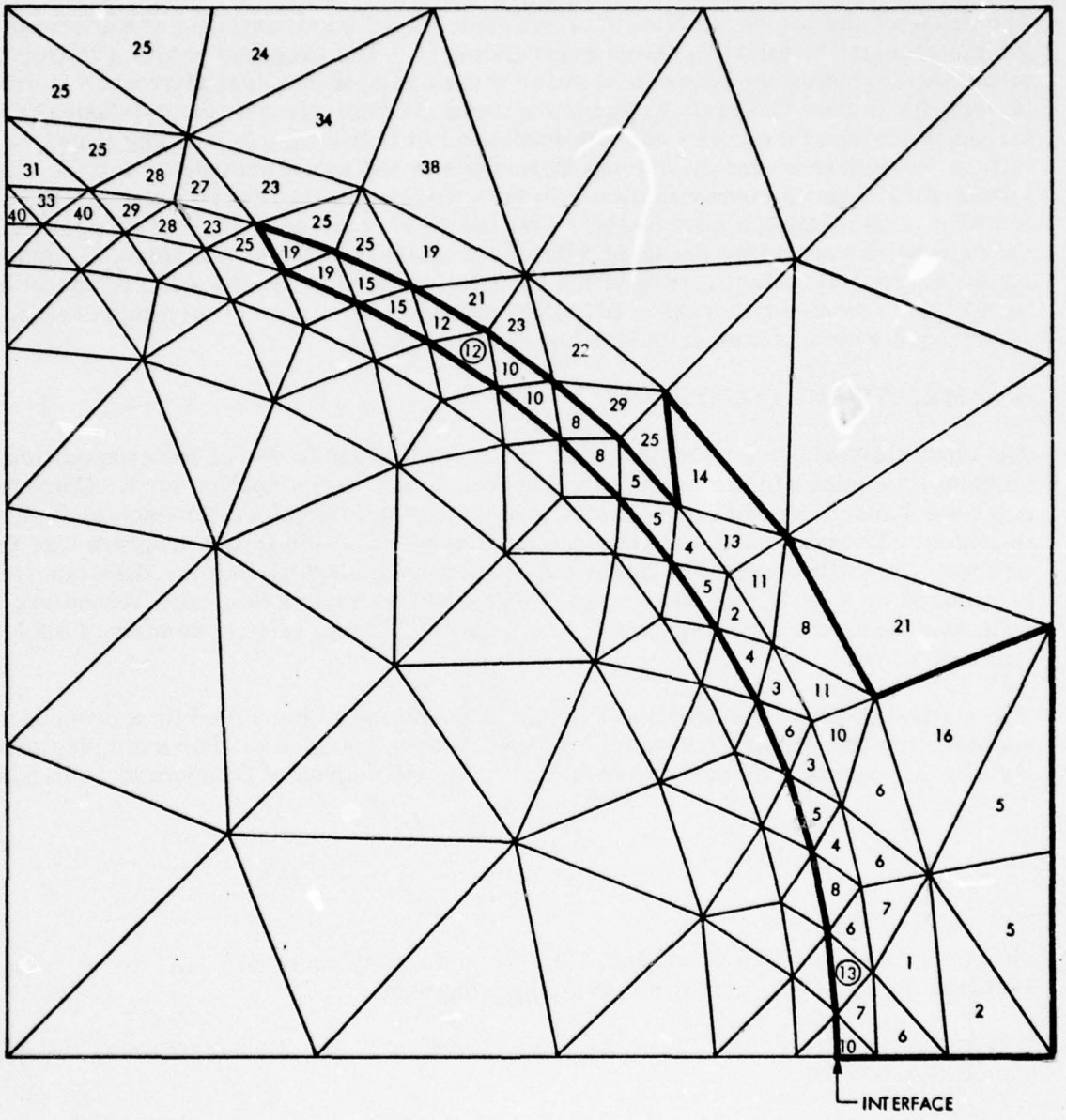

Fig. A-3 Schematic Representation of Yield-Zone Growth With Increasing Applied Transverse-Normal Load Predicted for a Unidirectional Square-Array Composite of 50 vol % B/Al (6061-T6). Outlined region is for loading to anomalous failure at 54,416 psi, assuming a bilinear matrix stress-strain curve. Remainder is for a five-segment piece-wise-linear representation and loading to predicted failure at 59,459 psi. Numbers correspond to load-increment (800 psi) at which elements yielded. Failure was predicted at circled 12 for bilinear curve and at circled 13 for segmented curve

AD-A032 407 LOCKHEED MISSILES AND SPACE CO INC PALO ALTO CALIF PA--ETC F/G 11/4
REINFORCEMENT MECHANISMS IN METAL-MATRIX COMPOSITES.(U)
JUL 74 R F KARLAK, F W CROSSMAN, J GRANT N62269-73-C-0576

UNCLASSIFIED LMSC-D403435 NL

2 OF 2
AD-A
032 407

END
DATE
FILMED
11-3-77
NTIS

The cause of the predicted failure is not clear based on an analysis of the stress history for the element in point, or those surrounding it. The program prints a listing of all stresses, including the octahedral shear stress in each element after each iteration (stress-increment calculation) and from these it is certain that the octahedral shear stress in the element to fail had not decreased to below the yield at any time, so the failure prediction certainly was not anomalous in the same manner as for the bilinear stress-strain curve approximation. In fact, the octahedral shear stress in the element to fail was oscillating approximately ± 81 psi (± 15.7 percent of stress/segment) around the data point separating the third and fourth interval of the seven segment input stress-strain curve. The significance of the calculation is being questioned primarily because it involved a sudden reversal of principal stresses from tensile to compressive, an occurrence which has never before been observed.

A.4 MULTIPOINT CONSTRAINT

The computer program used until this report period made use of a superposition technique to calculate the proper strains transverse to the applied load. Consequently, two time-consuming stiffness-matrix inversions were required for each load-increment iteration. To reduce the computation time, a modification in the program was made whereby the stiffness matrix bandwidth is increased slightly, but the time per iteration is reduced by as much as 25 percent. The stiffness matrix non-zero values are concentrated about the main diagonal. The bandwidth is the largest number of such values from all rows.

The method in effect reduces the number of equations to be solved by a procedure analogous to the algebraic solution of simultaneous equations. For example, given the simple case of a three-node structure with one degree of freedom at each node;

$$(r_i) = (k_{ij})\,(\Delta_j)$$

$$i, j = 1, 2, 3$$

where r_i are the nodal reactions, Δ_j the nodal displacements, and the k_{ij} the stiffness coefficients, analogous to spring constants.

It is known, a priori, that $\Delta_1 = \Delta_3$ and $r_1 + r_3 = F$ are the constraints, the equation can be reduced to:

$$\begin{bmatrix} R_1 \\ R_2 \end{bmatrix} = \begin{bmatrix} K_{11} & K_{12} \\ K_{21} & K_{22} \end{bmatrix} \begin{bmatrix} \Delta_2 \\ \Delta_3 \end{bmatrix}$$

or

$$(R_i) = (K_{ij})\,(\Delta_i)$$

$$i, j = 1, 2$$

where $K_{11} = k_{22}$, $K_{12} = k_{21} + k_{23}$, $K_{21} = k_{12} + k_{32}$, and $K_{22} = k_{11} + k_{13} + k_{31} + k_{33}$, $R_1 = r_1$, and $R_2 = F$.

A sample calculation was made with a 73-node model having an original stiffness-matrix bandwidth of 22. With the multipoint constraint, the bandwidth was increased to 30, increasing the computation time, but the need for only a single inversion reduced the time sufficiently to give a net gain of 25 percent.

There is an additional advantage in solving for thermal residual stresses partially relaxed by creep where the representation cell is required to expand without distortion.

Appendix B

REFERENCES

1. R. F. Karlak, F. W. Crossman, and J. Grant, Reinforcement Mechanisms in Metal-Matrix Composites, LMSC-D313101, Final Report on Contract N00019-71-C-0289, Dec 1972

2. I. J. Toth and G. D. Menke, The Time Dependent Mechanical Behavior of Composite Materials, AFML/AFC Technical Report, AFML-TR-70-174, Jun 1970

3. S. T. Scheirer, I. J. Toth, and G. D. Menke, The Time Dependent Behavior of Metal Matrix Composites, AFML/AFSC Technical Report AFML-TR-72-149, Sep 1972

4. S. T. Scheirer and I. J. Toth, The Mechanical Behavior of Metal-Matrix Composites, AFML/AFC Technical Report AFML-TR-73-178, May 1973

5. G. D. Swanson and J. R. Hancock, Effect of Interfaces on Off-Axis and Transverse Tensile Properties of Boron-Reinforced Aluminum Alloys, ONR Technical Report No. 2, NR 031-743, Sep 1970

6. J. E. Alexander and R. G. Carlson, Failure Processes in Metal-Matrix Composites, AFML/AFSC Technical Report AFML-TR-73-290, Phase I, 21 Dec 1973

7. R. E. Allred et al., "Elastic Plastic Ratio of Borsic-Aluminum," J. Composite Materials, Vol. 8, Jan 1974, pp. 15–28

8. T. H. Lin et al., "Elastic-Plastic Analysis of Unidirectional Composites," J. Composite Materials, Vol. 6, 1972, p. 48

9. D. F. Adams, "Elastoplastic Crack Propagation in Transversely Loaded Composites," J. Composite Materials, Vol. 8, Jan 1974, pp. 38–54

10. O. Buyukozturk et al., "Deformation and Fracture of Particulate Composite," J. Engineering Mechanics Division, Proceeding of the ASCE, EM3, Jun 1972, pp. 581–593

11. Ing-Wu Yu and G. P. Sendeckyj, "Multiple Circular Inclusion Problems in Plane Elastostatics," J. Applied Mechanics, Transactions ASME, Mar 1974, pp. 215–221

12. G. P. Sendeckyj and Ing-Wu Yu, "Multiple Circular Inclusions Problems in Plane Elastostatics," Interface and Mechanics Research in Fiber Reinforced Composites, H. R. Nara, ed., AFML/AFSC Technical Report AFML-TR-71-260, Mar 1972

13. G. J. Dvorak et al., "Generalized Initial Yield Surfaces in Unidirectional Composites," J. Applied Mechanics, Transactions ASME, Mar 1974, pp. 249–253

14. C. A. Hoffman, Effect of Thermal Loading on Composites With Constituents of Differing Thermal Expansion, NASA TN-D-5926, Aug 1970

15. O. C. Zienkiewicz, The Finite Element Method in Structural and Continuum Mechanics, McGraw-Hill, New York, 1967

16. C. S. Desai and J. F. Abel, Introduction to the Finite Element Method, Van Nostrand Reinhold Co., New York, 1972

17. W. C. Paulsen, "Finite Element Analysis," Parts 1–3, Machine Design, 30 Sep, 14 Oct, and 28 Oct 1971

18. D. F. Adams and S. W. Tsai, "The Influence of Random Filament Packing on the Transverse Stiffness of Unidirectional Composites," J. Comp. Mat., Vol. 3, 1969, p. 368